THESIS FOR THE DEGREE OF DOCTOR OF PHILOSOPHY

Singlet Fission and Exciton Coupling Design Principles for Efficient Photon Harvesting

Rasmus Ringström

Department of Chemistry and Chemical Engineering
CHALMERS UNIVERSITY OF TECHNOLOGY
Gothenburg, Sweden 2024

Singlet Fission and Exciton Coupling Design Principles for Efficient Photon Harvesting
RASMUS RINGSTRÖM
ISBN: 978-91-8103-016-7

Doktorsavhandlingar vid Chalmers Tekniska Högskola
Ny serie nr 5474
ISSN: 0346-718X

Department of Chemistry and Chemical Engineering
Chalmers University of Technology
SE-412 96 Gothenburg
Sweden
Telephone +46 31 772 1000

Cover: Illustration of a light pulse and a sample containing some of the molecules investigated in this thesis.

Printed by Chalmers digitaltryck
Gothenburg, Sweden 2024

Singlet Fission and Exciton Coupling Design Principles for Efficient Photon Harvesting

RASMUS RINGSTRÖM

Department of Chemistry and Chemical Engineering

Chalmers University of Technology

Abstract

Extensive research efforts have been dedicated to unravelling the diverse array of processes triggered by the interaction of light with matter. Harnessing and comprehending some of these phenomena holds immense potential in humanity's transition towards renewable energy sources. At the heart of this transition lies the Sun, which provides the Earth with an abundance of energy in the form of light. In addition to generating electricity through solar cells, sunlight can also drive photochemical reactions to produce fuels such as hydrogen gas. Despite significant strides in utilizing solar energy, there remain numerous processes that are not fully understood, presenting opportunities for refinement and enhancement. This thesis embarks on an exploration of the photophysical processes singlet fission (SF) and exciton coupling, aimed at maximizing the efficient utilization of the energy of light, particularly from the Sun.

Both SF and exciton coupling rely heavily on the relative orientation and distance between the interacting molecules. Therefore, the essence of the research presented in this thesis revolves around the complex interplay between molecular structure and photophysical properties. This thesis underscores how various configurations of identical molecules can result in diverse photophysical outcomes. Furthermore, it showcases the importance of considering both the interconnectivity of molecules from a Lewis structure and optimal energy configuration standpoint, as well as their capacity to assume different conformations dynamically.

SF has been explored in three systems. The initial investigation, focused on pentacene derivatives, aimed at elucidating the impact of rotational conformations in intramolecular SF systems. The second study aimed to expand the limited library of photostable, intramolecularly capable SF molecules by investigating an anthracene derivative. However, this study revealed additional processes that hindered SF efficiency, underscoring the delicate balance required between energetics, molecular interconnectivity, and solvent polarity for efficient SF. In the final SF study, strides were made towards integrating SF into dye-sensitized solar cells, utilizing a derivative of diphenylisobenzofuran attached to semiconductor thin films. The study highlights the importance of substrate energetics and solvent polarity in dictating the dominant photophysical processes on the surface, with highly polar solvents impeding SF by stabilizing charge-separated states. In the exciton coupling study, alignment of molecular systems comprising boron dipyrromethene and anthracene in a covalent J-aggregate-like configuration demonstrated a novel method of selectively modulating the energy of the singlet excited state while leaving the triplet excited state energy unaffected. This work shows how photophysical properties can be tuned *via* molecular design, with potential applications in various fields of optoelectronics.

Keywords: Singlet fission, exciton coupling, electron transfer, transient absorption spectroscopy.

List of Appended Papers

This thesis is based on the appended papers listed below:

Paper I

Molecular Rotational Conformation Controls the Rate of Singlet Fission and Triplet Decay in Pentacene Dimers. Rasmus Ringström[§], Fredrik Edhborg[§], Zachary W. Schroeder, Lan Chen, Michael J. Ferguson, Rik R. Tykwinski and Bo Albinsson. *Chem. Sci., 2022, 13, 4944-4954*.

Paper II

Triplet Formation in a 9,10-Bis(phenylethynyl)anthracene Dimer and Trimer Occurs by Charge Recombination Rather than Singlet Fission. Rasmus Ringström, Zachary W. Schroeder, Letizia Mencaroni, Pavel Chabera, Rik R. Tykwinski and Bo Albinsson. *Journal of Physical Chemistry Letters, 2023, 14, 35, 7897-7902*.

Paper III

Singlet Fission and Electron Injection from the Triplet Excited State in Diphenylisobenzofuran–Semiconductor Assemblies: Effects of Solvent Polarity and Driving Force. Elin Sundin, Rasmus Ringström, Fredrik Johansson, Betül Küçüköz, Andreas Ekebergh, Victor Gray, Bo Albinsson, Jerker Mårtensson and Maria Abrahamsson. *The Journal of Physical Chemistry C, 2020, 124, 38, 20794–20805*.

Paper IV

Selective Lowering of the Singlet Excited State Energy to Decrease the Singlet-Triplet Gap *via* Intramolecular Exciton-Exciton Coupling. Clara Schäfer[§], Rasmus Ringström[§], Jörg Hanrieder, Martin Rahm, Bo Albinsson and Karl Börjesson. *Manuscript*.

[§] These authors contributed equally

Contribution Report

The author's contribution to the appended papers are summarized below:

Paper I
Planned, designed and evaluated all photophysical characterization together with F.E. and B.A. Wrote most of the manuscript. DFT calculations were performed by F.E. Synthesis and related characterization were performed by Z.W.S and L.C. First authorship shared with F.E.

Paper II
Conceived the project together with B.A. Planned, designed and evaluated all photophysical characterization together with B.A. Wrote the manuscript. Synthesis and related characterization were performed by Z.W.S.

Paper III
Designed and performed the spectroscopic experiments and analyzed the data together with E.S. and B.K. Wrote parts of the manuscript. Synthesis and characterization were done by F.J., A.E. and V.G.

Paper IV
Designed and performed the spectroscopic experiments and analyzed the data together with C.S., K.B. and B.A. Wrote parts of the manuscript. Synthesis and related characterization were done by C.S. First authorship shared with C.S.

Papers not Included in the Thesis

Paper A
Optically Switchable NIR Photoluminescence of PbS Semiconducting Nanocrystals using Diarylethene Photoswitches. Lili Hou, Rasmus Ringström, Andrew B. Maurer, Maria Abrahamsson, Joakim Andréasson and Bo Albinsson. *J. Am. Chem. Soc. 2022, 144, 39, 17758–17762.*

List of Abbreviations

ACN	Acetonitrile
AO	Atomic orbital
BODIPY	Boron dipyrromethene
BPEA	9,10-Bis(phenylethynyl)anthracene
CB	Conduction band
CCD	Charge coupled device
CR	Charge recombination
CS	Charge separated
CT	Charge transfer
CV	Cyclic voltammetry
DCM	Dichloromethane
DFT	Density functional theory
DPH	Diphenylhexatriene
DPIBF	1,3-diphenylisobenzofuran
DSSC	Dye-sensitized solar cell
EAS	Evolution associated spectra
EPR	Electron paramagnetic resonance
ES	Excited-state
ESA	Excited state absorption
ET	Electron transfer
fsTA	Femtosecond transient absorption
GS	Ground state
GSB	Ground state bleach
H_{DA}	Electronic coupling term
HOMO	Highest occupied molecular orbital
HRI	High refractive index
IC	Internal conversion
IRF	Instrument response function
ISC	Intersystem-crossing
J_c	Coulumb coupling
LUMO	Lowest unoccupied molecular orbital
MO	Molecular orbital
MTHF	2-Methyltetrahydrofuran
nsTA	Nanosecond transient absorption
OLED	Organic light-emitting diode
OPA	Optical parametric amplifier
PM	6,13-Bis(triisopropylsilylethynyl)pentacene
PMT	Photomultiplier tube

PV	Photovoltaic
RP-ISC	Radical-pair inter-system crossing
S_1	Lowest singlet excited state
SAS	Species associated spectra
SE	Stimulated emission
SF	Singlet fission
SO	Spin-orbit
SOCT-ISC	Spin orbit charge transfer inter-system crossing
SVD	Singular value decomposition
PDI	Perylene diimide
PtOEP	Platinum-octaethylporphyrin
T_1	Lowest triplet excited state
^{1}(TT)	Triplet-pair of singlet multiplicity
TA	Transient absorption
TADF	Thermally activated delayed fluorescence
TCSPC	Time correlated single photon counting
TD-DFT	Time-dependent density functional theory
TDM	Transition dipole moment
THF	Tetrahydrofuran
TIR	Total internal reflection
TTA-UC	Triplet-triplet annihilation upconversion
UV-vis	Ultraviolet and visible
VR	Vibrational relaxation

Acknowledgements

I am deeply grateful to a multitude of individuals whose support, both within and beyond the realm of academia, have been instrumental in my completion of this thesis. First, I want to thank my supervisor, Bo Albinsson. Your unwavering positivity and dedication to cultivating a culture of learning have made my journey towards my degree more enjoyable than I could have ever imagined. I have greatly appreciated your guidance and consistent assistance throughout my time as a PhD-student and I am very thankful that you gave me this opportunity.

A huge thank you also to my co-supervisor Maria Abrahamsson for your support and guidance. Without your influence, I might never have ventured into this captivating realm of research. I am particularly grateful for your efforts in organizing the journal club meetings, which have been instrumental in my development as a PhD-student. Moreover, I am forever thankful to you for unknowingly employing - and thereby making me cross paths with - the person who turned out to be the love of my life. Additionally, my thanks extend to my examiner, Joakim Andréasson, for always offering assistance whenever required.

I want to thank all the wonderful people at the department for making me enjoy coming to work everyday. A special acknowledgement is reserved for both past and present members of the esteemed spectroscopy group – Fredrik, Betül, Elin, Axel, Wera, Jessica, Hassan, Hanna, Deise, Pauline, Alma, Long, Gerard, Sean, Carlos, Gaowa, Letizia, Lili, and Cassandra. Thank you for all the fun and interesting discussions we have had and for always being helpful in the lab. A special thank you to Fredrik for our work together on shared projects and for always being happy to answer any question I have. You have taught me so much and I am very grateful for all the fun we have had in the lab together. To Elin and Betül, I extend gratitude for your collaboration and patience in guiding a novice master's student through the intricacies of spectroscopy. Thank you Deise for your endless kindness and for a great collaboration with the OTHO-gels. To my office mates Liam and Andrew - thank you so much for all your help and interesting discussions and for creating a wonderful work atmosphere. Thank you Wera, Hassan, Hanna, Andrew, Liam and Jessica for proofreading parts of the thesis.

I want to acknowledge and thank all collaborators involved in the papers presented herein, with special appreciation for Zack and Clara, whose insightful discussions and exceptional synthesis skills have been integral to the realization of this thesis.

I want to thank Karl Börjesson for involving me in the BODIPY-oligomer investigation and generously granting me access to your instruments. I am deeply grateful for the wealth of knowledge I have gained under your guidance.

I would also like to express my gratitude to my friends, who have been a source of support throughout this journey. A special acknowledgment goes to my Blender guru, Robin, whose expertise and help has been invaluable for the design of many figures in this thesis.

I want to thank my parents, Bosse and Gisela, for their continuous support for me throughout my entire life and educational journey. Even though I know it is difficult to understand exactly what it is I am doing at work you have always shown interest and supported me wholeheartedly. Thank you for being the best parents anyone could ever ask for. Thank you also to my sister, Hannah, and her family, Johan and Olle, and all of my relatives for always supporting me. I love you all.

Lastly, I want to thank Wilma for always being there for me and making the happiest I have ever been. Of all the things I have done and accomplished at Chalmers during all these years, meeting and getting to know you has undoubtedly been the most important. I love you so very much.

Contents

Chapter 1

Introduction

The development of techniques utilizing sunlight for fuel and energy production is of central importance in mitigating the adverse effects of climate change while maintaining our high standards of living. Photovoltaic (PV) devices, converting light into electricity, stand out as a promising option to address escalating global energy demands and transition away from fossil-fuel based energy generation. However, despite the Earth receiving an abundance of sunlight, less than 1 % of 2021's energy production came from PV solar sources.[1,2] Despite seeing major advancements in terms of cost and efficiency in the past two decades, economic viability remains a challenge for PVs.[3] And, as with many things in today's society, short-term economical gains with potential long-term disastrous consequences will in most cases be prioritized over long-term sustainable and slightly more expensive options. Consequently, it is of paramount importance to increase the efficiency and/or reduce the cost of PVs even more to make them competitive with our current means of energy production. However, PVs are fundamentally limited in their efficiency due to spectral losses, stemming from a mismatch between photon energies in the solar spectrum and the energy input required for semiconductor materials in conventional PVs. Figure 1.1 illustrates the solar spectrum alongside silicon's band gap (1.1 eV),[4] the predominant semiconductor in use today.[5]

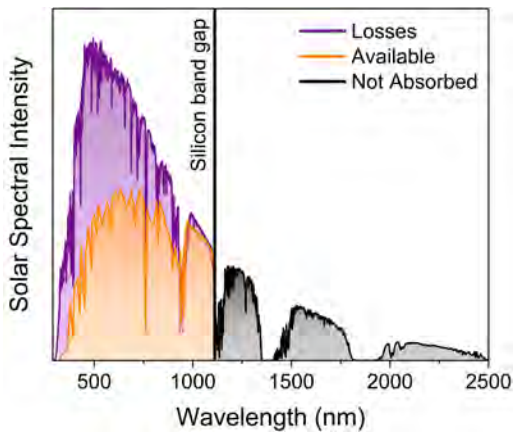

Figure 1.1: The solar spectrum at sea level.[6] The orange region represents the part of the solar spectrum that can be effectively harnessed by silicon. Below band gap photons can not be absorbed, leading to the losses marked as grey. The purple region represents the thermalization losses.[7]

Photons with energy exceeding the band gap (wavelengths shorter than approximately 1150 nm) can be absorbed. However, each absorbed photon can only generate a single electron-hole pair, with the excess energy lost as heat. These losses, known as thermalization losses, are the dominating losses for single-junction silicon solar cells. When combined with losses from photons with insufficient energy for absorption, these contribute to the Shockley-Queisser limit. Named after William Shockley and Hans J. Queisser, who calculated the thermodynamic energy conversion limit in 1961, the limit caps the theoretical efficiency of single-junction cells at around 33 %, with Si-based PVs reaching approximately 30 %.[8] Several technologies are currently being investigated to increase the efficiency of PVs beyond the Shockley-Queisser limit. The technology most relevant to this thesis is a photon energy conversion technique that aims to change the energy of the incoming photons from the Sun so that they match better with the band gap of the PVs. The technique is called singlet fission (SF) and it is a photophysical process in which an excited state, formed by absorption of a single photon, can share its excited state energy with a neighboring molecule to form two separate excited states of roughly half the energy of the initial state.[9] If the energy of both generated lower energy excited states can be transferred to a PV device the Shockley-Queisser limit can be increased from ~33 % to ~45 %.[10–12] This may at first appear to be a very modest increase. However, an increase of only a few percentage units can still have a large impact considering the abundance of sunlight that is received by the Earth every day.[13] Furthermore, the SF material could in principle be integrated directly with existing solar cells as an extra layer as illustrated in Figure 1.2 and would thus not require extensive engineering in an ideal scenario.

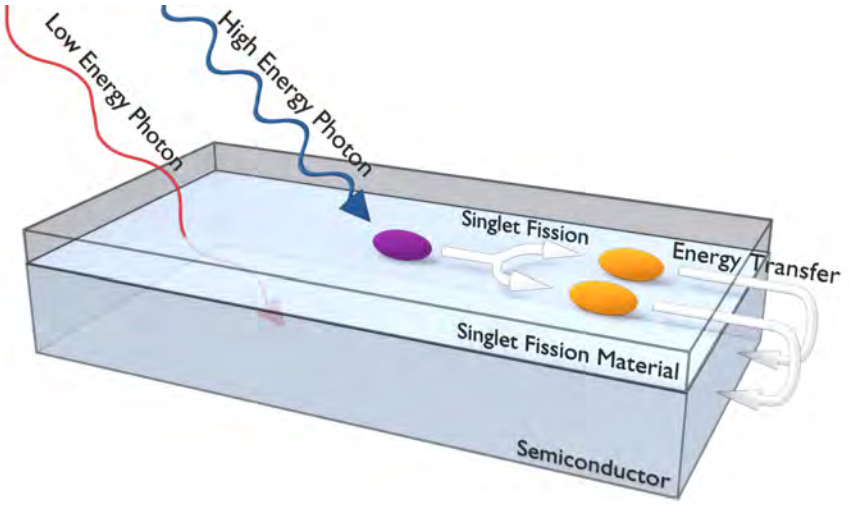

Figure 1.2: Illustration of the theoretical implementation of SF in a PV device.

While SF would be useful for the efficient utilization of high energy photons, there is another technology relevant to this thesis that can also be used to manipulate the composition of the incoming light called triplet-triplet annihilation upconversion (TTA-UC).[14,15] This method offers a solution to mitigate losses associated with photons in the grey area in Figure 1.1a that lack sufficient energy for absorption. In essence, TTA-UC operates in a manner opposite to SF, com-

bining the energy of two low-energy excited states to produce one high-energy photon. Notably, unlike other upconversion mechanisms like two-photon absorption[16] and second harmonic generation,[17] TTA-UC can function with non-coherent and low-intensity light, making it particularly advantageous for applications using solar energy.

As a final note, it should be emphasized that while the pursuit for improved PV efficiencies remains a paramount motivation in the realm of SF and TTA-UC research, their applications extend beyond solar energy harvesting optimization. TTA-UC has emerged as a promising contender for driving demanding photochemical reactions.[18,19] Additionally, its ability to convert visible light into UV-light holds significant potential, not least in the context of photocatalytic water splitting,[20] where many systems rely on UV-absorbing catalysts like TiO_2.[21,22] Moreover, recent investigations have unveiled the expansive possibilities of SF across various fields. In quantum computing, for instance, the multiexciton quintet state, generated as an intermediate in SF between pairs of molecular chromophores, holds promise as a qubit.[23,24] Application can also be found in photodynamic therapy, leveraging the formed triplet excited states' ability to generate singlet molecular oxygen.[25] Additionally, a relatively underexplored avenue for SF lies in its potential application for photocatalysis where SF holds substantial promise in addressing prevalent challenges within the field of accumulative charge separation.

1.1 Purpose and Objective

Although both SF and TTA-UC show promise in addressing the limitations of conventional PVs and exhibit potential for various applications, these technologies are not currently ready for integration into commercial systems. This thesis aims to contribute to the advancement of knowledge regarding both TTA-UC and SF-capable systems, with the ultimate goal of understanding the optimal ways to apply them in future devices. Specifically, the thesis focuses on the photophysical characterization of organic molecules capable of SF and the optimization of a component involved in TTA-UC known as a triplet photosensitizer. Through case studies of specific molecular systems, the goal is to elucidate how chemical structure and intermolecular geometry influence the behavior of molecular materials after photoexcitation.

1.2 Thesis Outline

The thesis is structured as follows: Chapter 2 provides a review of the relevant background and theory behind the concepts used in this work. In Chapter 3, the experimental techniques used are briefly described. Chapter 4 presents the results of **Paper I**, investigating how the dynamics in the excited state of pentacene dimers govern the rate of SF and the subsequent lifetime of the formed excited states. In Chapter 5, the findings of **Paper II** are presented, aiming to expand the limited library of SF-capable molecules in solution by characterizing the photophysics of an anthracene derivative both inter- and intramolecularly. In Chapter 6 the focus is more oriented towards applications of SF. The initial segment delves into the outcomes detailed in **Paper III**, wherein a

derivative of diphenylisobenzofuran was attached to the surface of different semiconductor thin films. This study sought to understand if the photoinduced processes that occur on the surface, for example SF or charge separation, can be controlled by varying the substrate or surrounding environment. Moreover, Chapter 6 extends its exploration into the potential of SF materials acting as dual electron donors for the specific aim of photocatalysis, employing supramolecular coordination complexes. In Chapter 7, we take a slight departure from the SF theme while remaining consistent with the primary thesis theme — efficient utilization of light. The chapter presents the findings of **Paper IV**, where exciton coupling was applied to specifically reduce the energy of the singlet excited state in boron-dipyrromethene oligomers, while keeping the triplet excited state energy unaffected.

Chapter 2

Fundamentals

The primary objective of this chapter is to familiarize the reader with key photophysical concepts integral to the papers presented in this thesis. It commences with a concise overview of interactions between light and matter at the quantum level. Subsequent sections offer more detailed insights into processes such as singlet fission, exciton coupling and photoinduced electron-transfer. A solid understanding of these processes is crucial for comprehending the following chapters.

2.1 Light-Matter Interactions

Light can be described as an electric field that oscillates perpendicularly to an oscillating magnetic fields as illustrated in Figure 2.1. The two fields propagate in the same direction and the distance between corresponding points of two consecutive waves on either field is called the wavelength (λ).[26]

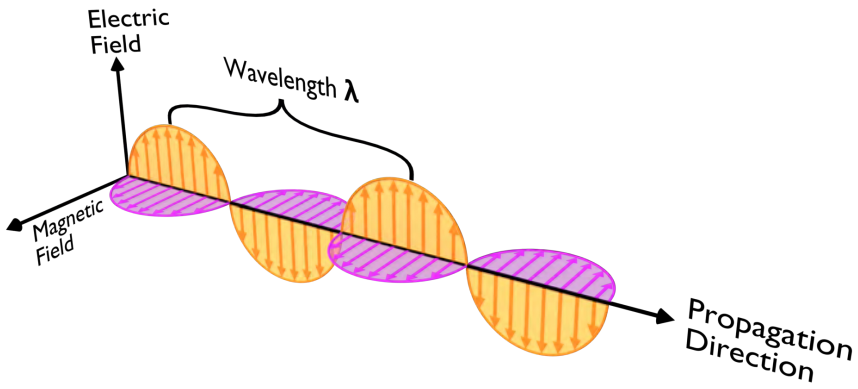

Figure 2.1: Illustration of the propagation of an electromagnetic wave with perpendicularly oscillating electric and magnetic fields.

In addition to being described as a wave, light can also be seen as particles referred to as photons. The energy of photons (E_{photon}) is quantized and is related to the wavelength, or frequency (ν),

of the electromagnetic field together with the speed of light in vacuum (c, 299 792 458 m s^{-1}) and Planck's constant (h, 6.62607015·10^{-34} J s^{-1}) according to Equation 2.1.[27]

$$E_{photon} = \frac{hc}{\lambda} = h\nu \tag{2.1}$$

In order to understand how and in what ways light can interact with matter we must also briefly describe the nature of matter itself. The smallest constituents of matter that will be considered for the contents of this thesis are protons, neutrons, and electrons that together form atoms. Atoms in turn constitute the foundation of all materials and objects around us. In an analogous fashion to light, atoms too exhibit quantization in energy. As a consequence of this, electrons within atoms are confined to distinct so called atomic orbitals (AO) of specific energies. AOs can, in turn, be combined to form molecular orbitals (MO). The concept of orbitals arises from the quantum mechanical description of electrons and is a measure of their nuclei-centered probability distributions. The configuration of electrons in orbitals follows a strict set of quantum mechanical rules by which we understand the properties of atoms and molecules and predict in what ways they can interact with each other and with light. According to *Pauli's exclusion principle* electrons cannot occupy the same quantum state simultaneously. As a consequence of this, MOs can be occupied by a maximum of two electrons and if two electrons do occupy one orbital the spin of the electrons must be oriented in an anti-parallel fashion. Here, spin refers to the intrinsic angular momentum of electrons, which is a quantum mechanical property. The magnitude of the spin of an electron is always 1/2 and the orientation is given by the spin quantum number m_s which can be +1/2 or -1/2, often referred to as "up/↑" and "down/↓". Two electrons that share an orbital will thus have oppositely oriented spins as illustrated in Figure 2.2 where the electrons are symbolized as arrows pointing up or down in orbitals represented as lines.[28]

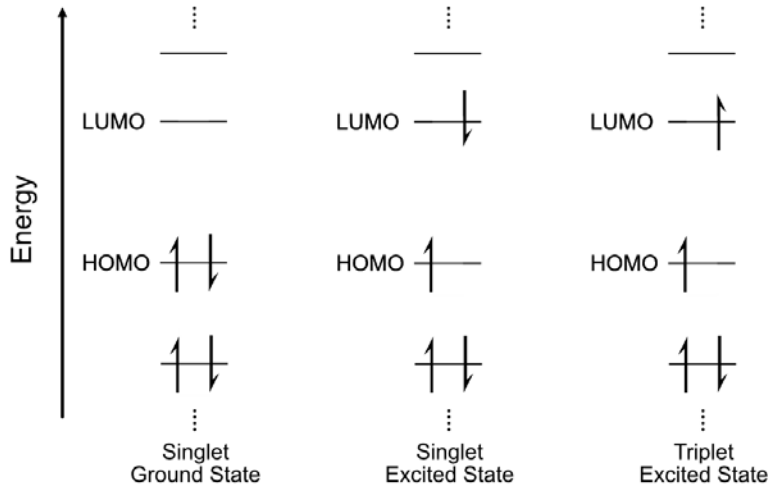

Figure 2.2: Orbital energy diagram with electrons symbolized as half-arrows illustrating the different spin configurations of singlet and triplet states.

Figure 2.2 further shows that electrons occupy lower energy orbitals before filling higher energy ones according to the *Aufbau principle* under conditions of non-degeneracy and where the pair-

ing energy is lower than the orbital energy difference. The highest occupied molecular orbital (HOMO) and lowest unoccupied molecular orbital (LUMO) are of considerable interest to photochemists because even if there are a multitude of filled molecular orbitals lower in energy, most photophysical properties in molecules are based on these *frontier orbital* electrons that are more energetically accessible. As indicated in Figure 2.2, a molecule is in a so called *singlet ground state* when the HOMO is filled with two electrons forming a closed shell with net zero spin (one up and one down). Here, ground state refers to the lowest energy electronic configuration of the molecule and the word singlet refers to the *spin multiplicity* of the molecule. Spin multiplicity describes the number of possible orientations the net spin S of a multi-electron system can assume. In a two-electron system, S can assume a value of 0 or 1 as given from the coupling of the electrons individual spin angular momentum in a Clebsch-Gordan series. The spin-multiplicity, defined as $2S+1$, can thus, in a two electron system, be one or three. A spin multiplicity of one signifies that it is a singlet state with anti-parallel spins of the electrons and three means that it is a triplet state with parallel spins. In addition to the singlet ground state, Figure 2.2 also shows two other electron configurations called singlet excited state and triplet excited state. An electronically excited state can be formed if a molecule or atom absorbs energy, for instance in the form of a photon. This may raise the molecule to a temporary higher energy state by moving an electron from a lower energy orbital to a higher energy orbital. This can occur if the incoming photon energy matches the energy gap between the initial (i) and final (f) state and is known as Bohr's frequency condition.[26,29]

$$E_f - E_i = E_{photon} \tag{2.2}$$

In the excited state the two electrons are separated in different orbitals and consequently, Pauli's exclusion principle no longer demands that the two electrons have paired spin. As a result, an initial singlet ground state (which the vast majority of organic molecules are in) can have a different spin multiplicity in the excited state. However, there are also some molecules that have a triplet ground state. One such example is molecular oxygen (O_2) which has two degenerate (same energy) highest lying orbitals each occupied by one electron, in accordance with *Hund's rule*,[30] that allows for parallel spins of the electron pair even in the ground state.[31]

2.1.1 Radiative and Non-Radiative Transitions

Once formed, excited states are inherently energetically unstable and atoms and molecules will decay back to the ground state after a certain time period that is highly system dependent. The processes that can occur subsequent to absorption of a photon are commonly depicted in a Jablonski state diagram such as the one in Figure 2.3. Here, electronic levels are represented as solid thick horizontal lines and the singlet ground state is denoted as S_0. The first singlet excited state is denoted as S_1 and so on for higher energy excited states whereas triplet excited states are denoted as T_n. The electronic levels all contain numerous vibrational and rotational energy levels spaced between them that are also quantized in energy. The vibrational levels are shown as horizontal thin solid lines and are separated by energies that range from approximately

0.1 to 0.15 eV which in wavelength scale is around 8-10 μm. This can be compared to the energy spacing between electronic energy levels which, for a typical organic molecule, is on the order of 1.5 to 3.5 eV corresponding to transitions in the ultraviolet-visible region (UV-vis, 350-750 nm). The energy separating the rotational energy levels are almost two orders of magnitude smaller than the energy separation of vibrational energy levels and have thus been omitted in the diagram for visual clarity.[32]

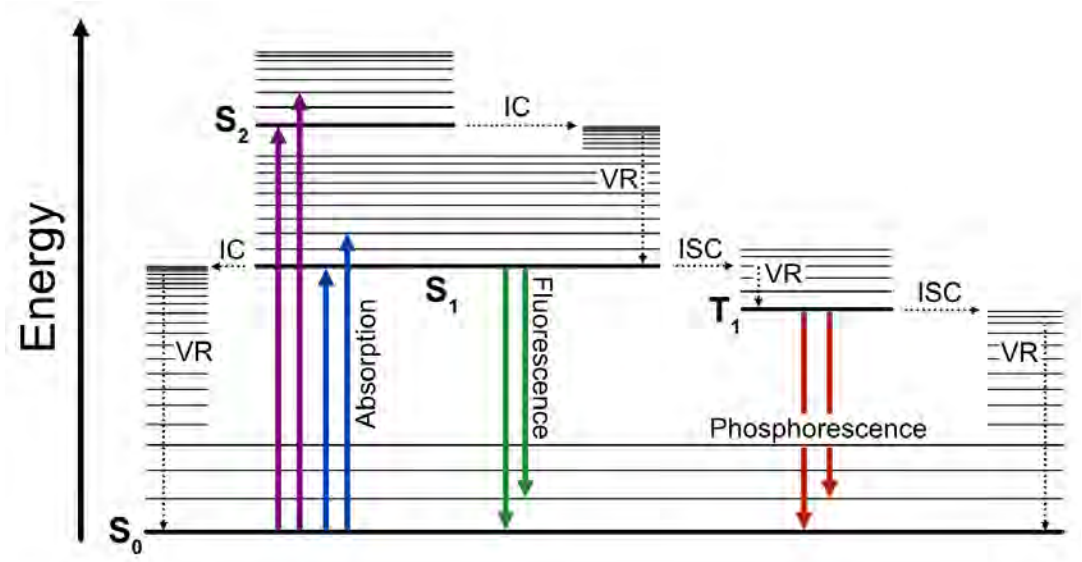

Figure 2.3: Jablonski diagram with singlet (S) and triplet (T) energy levels shown as horizontal lines. Thick lines depict the electronic levels and thinner horizontal lines are the vibrational levels. The diagram illustrates a selection of common photophysical processes such as absorption, fluorescence, phosphorescence, internal conversion (IC), vibrational relaxation (VR) and intersystem-crossing (ISC). Photoexcitation and radiative decay processes are marked as solid lines and non-radiative processes are marked as dotted lines.

Photoexcitation typically occurs from the ground state S_0 to excited states of the same multiplicity S_n. Transitions directly to triplet states T_n are *spin forbidden* since they would require a spin change and transitions must, in addition to satisfying the law of energy conservation, also conserve the total angular momentum. However, as will be described shortly, even formally forbidden processes can in fact sometimes still occur, albeit generally with very low probability. The probability of a radiative transition is related to the transition dipole moment (TDM), a molecule- and transition-specific parameter whose magnitude can be experimentally determined by measuring the absorption intensity or emission rate of a given transition. The concept of TDMs is central to spectroscopy and can be interpreted as a vector pointing in the direction of the net electron flow as a molecule is excited. Consequently, when molecules encounter polarized light, those with TDMs oriented along the electric field vector of the light are preferentially excited. This principle underpins fluorescence anisotropy techniques and holds significant importance across various spectroscopic methodologies. Moreover, the vectorial nature of TDMs forms the foundation for modeling the Coulombic interaction between atoms and molecules, an aspect elaborated upon in greater detail in Section 2.3 within the context of exciton coupling. Turning

our attention back to the Jablonski diagram, it can be seen that after population of a singlet excited state S_n the molecule will quickly relax to different electronic levels of the same multiplicity via internal conversion (IC) and via vibrational relaxation (VR) to different vibrational levels. These non-radiative processes are marked as dotted arrows in the Jablonski diagram. IC and VR can occur on the sub picosecond (10^{-12} s) time scale between states where the energy difference is small such as for transitions from S_n to S_1 (or from T_n to T_1). The correlation of increased rate of non-radiative decay the smaller the energy gap is between the states has been demonstrated for many molecular systems and is known as the *energy gap law*.[33,34] As a result of the rapid IC and VR from higher excited states, most photophysical processes in condensed phase occur predominantly from S_1 or T_1 since these states are generally more long-lived. This is known as Kasha's and Vavilov's rules.[35] From S_1 the molecule can return to the ground state via radiative or non-radiative processes that typically occur on the nanosecond time scale (10^{-9} s). The radiative relaxation from S_1 to S_0 is called fluorescence and involves the emission of a photon. S_1 can also decay non-radiatively to a triplet state T_n in a process called intersystem crossing (ISC). As mentioned previously, a transition involving a spin change is quantum mechanically forbidden and consequently this process typically occurs slowly due to its low probability. The rate can however vary from the microsecond (10^{-6} s) to the picosecond timescale since it can be heavily influenced by the magnitude of spin-orbit (SO) coupling in the molecule. SO coupling refers to the interaction between the spin- and orbital angular momentum. The magnitude of SO coupling is related to the nuclear charge and is larger for molecules containing heavy atoms. This is called the *heavy-atom effect* and it is known to enhance the rate of spin-forbidden processes such as ISC.[29] Radiative decay between states of different spin multiplicities is called phosphorescence. Since both ISC and phosphoresence from T_1 to S_0 require a change of spin, triplet excited states are typically much longer lived than singlet excited states and can have lifetimes on the micro- or millisecond timescales (or even seconds).[36]

2.1.2 Singlet and Triplet Energy Gap

At this point, a comment regarding the discrepancy of the relative energies of the singlet- and triplet excited states in the orbital energy diagram in Figure 2.2 compared to the state diagram in Figure 2.3 is perhaps warranted. The discrepancy originates from the omission of electron-electron interactions in the orbital energy diagram. Specifically, the interaction between the two electrons in the now singly occupied MOs in the excited state must be accounted for. In essence, the degree of orbital overlap between these two singly occupied MOs directly influences the magnitude of the *exchange interaction* term, determining the energy difference between S_1 and T_1, denoted as ΔE_{ST}. This exchange interaction elevates the energy of the singlet state while simultaneously diminishing the energy of the triplet excited state by an equivalent amount.[36,37] To grasp this qualitatively, one can envision it as an extension of Pauli's exclusion principle. The electrons with parallel spins in the triplet excited state 'avoid' each other to a larger degree than the electrons in the singlet excited state, ensuring compliance with the exclusion principle and, consequently, reducing electron-electron repulsion. The existence of an energy gap between

singlet and triplet excited states forms the cornerstone of all the work presented in this thesis. Notably, some projects rely on molecules exhibiting an unusually large energy gap between S_1 and T_1. In contrast, the final project explores a novel approach to actively reduce this energy gap.

2.1.3 Quantum Yield and Excited State Lifetime

Spectroscopists use several different parameters to characterize and quantify processes that occur in systems under investigation. One frequently encountered and important parameter when dealing with photophysical processes is the quantum yield (ϕ). Quantum yield is defined as the number of events that occur per photon absorbed in a given system according to Equation 2.3.

$$\phi = \frac{\#events}{\#absorbed\ photons} \tag{2.3}$$

The quantum yield can refer to any photoinduced process such as fluorescence (ϕ_f), ISC (ϕ_{ISC}) or even SF (ϕ_{SF}). It is also possible to express quantum yields in terms of the rate constant of the process in question (k_i) divided by the sum of all the rate constants (k_j) that can deactivate the state according to Equation 2.4.

$$\phi = \frac{k_i}{\sum_j k_j} \tag{2.4}$$

The inverse sum of all the rate constants, *i.e.* the denominator in Equation 2.4, is another important parameter called the lifetime (τ) of a state. The lifetime is thus inversely proportional to all rate constants that depopulate the state as described in Equation 2.5 and is the average time a molecule spends in its excited state. Lifetimes and methods to experimentally determine them will be explained in more detail in Chapter 3.

$$\tau = \frac{1}{\sum_j k_j} \tag{2.5}$$

2.1.4 Inter- and Intramolecular Interactions

The description of the photophysical properties so far has been limited to that of single molecules. However, many useful and interesting processes in photochemistry relies on *inter*molecular interactions. When two or more molecules are covalently linked, the interactions among the individual chromophore units within the molecule are termed *intra*molecular interactions. This thesis will delve into instances of both types of interactions and the theoretical background of the processes most relevant to this thesis will be presented in the following sections.

2.2 Singlet Fission

Singlet fission (SF) is a photophysical process in which a singlet excited-state, formed by absorption of a single photon, can share its excited state energy with a neighboring molecule to eventually form two separate triplet excited-states.[9,38] Since the product of SF is two triplet

excited-states for each absorbed photon the maximum quantum yield, as defined in Equation 2.3, is 200 %. SF has been known since the 1960s, initially discovered in crystals of anthracene[39] and soon after in tetracene crystals.[40–43] Initial evidence was largely based on the magnetic field effect on the prompt fluorescence, as documented by Merrifield.[44] Magnetic field dependent measurements such as the above mentioned and new techniques, remain of paramount importance in the characterization of SF materials to date .[45–47] After an initial flurry of SF reports in the 1960s and 1970s, research interest in the field declined, and SF was seen more as a curiosity than something useful. However, reports emerged on its potential uses such as in 1979 when Dexter proposed for the first time that SF could theoretically be used to increase the efficiency of PVs if both created charges from one photon could be utilized.[48] Nonetheless, probably due to the infancy of PV technology at this point in history, it would take until 2006 when Hanna and Nozik revived Dexter's idea for the SF field to truly set off.[11] Following this seminal work, research on SF materials was reinvigorated, and a flood of research ensued. SF remains a hot topic even today since there are still many unanswered questions and unexplored applications.

2.2.1 Singlet Fission Mechanism

In its simplest description, SF can be delineated into three distinct steps, as illustrated in Figure 2.4.

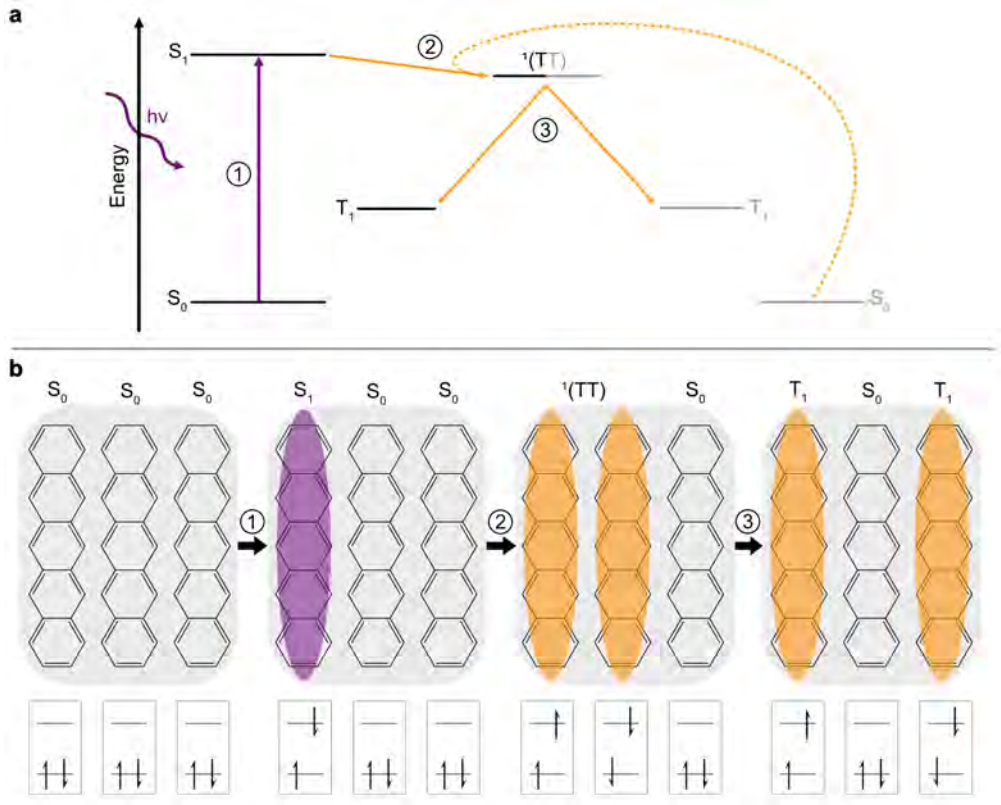

Figure 2.4: a) Jablonski diagram illustrating the SF process: (1) Excitation of a single molecule, (2) formation of correlated triplet ^{1}(TT), (3) generation of independent triplet states. b) Schematic of the SF process with pentacene as a model SF molecule. The arrows indicate the spin of the involved states.

Following photoexcitation to a singlet excited state, the initial phase of the SF process involves the formation of a correlated triplet pair, denoted as ^{1}(TT), with an overall singlet multiplicity. Subsequently, this correlated pair undergoes decorrelation and separates into two fully independent triplet excited states. As the total spin angular momentum is conserved during the formation of the triplet pair, SF is a spin-allowed process that can occur on a sub-picosecond timescale. To satisfy the law of energy conservation, there exists a general energetic condition wherein the energy of the singlet excited state ($E(S_1)$) must be greater than or equal to twice the energy of the triplet excited state ($E(T_1)$) for SF to occur. However, although this condition approximately holds true, SF has been demonstrated to proceed in systems that are slightly endothermic.[49] SF is a relatively uncommon process, primarily due to the stringent energetic prerequisites and the necessity for short intermolecular distances to facilitate electronic communication between molecules. Additionally, the relative orientation of the molecules undergoing SF also significantly influences the rate and feasibility of the process. SF has been extensively investigated in crystalline environments where molecules are densely packed and well-ordered, ensuring the required proximity for efficient SF. However, researchers have also explored SF in highly concentrated solutions,[50–52] representing another form of intermolecular SF, albeit with less control over molecular order and orientation. A third approach to satisfying the distance criterion involves designing systems capable of intramolecular SF, achieved by covalently linking two or more SF-capable molecules. However, intramolecular SF often encounters challenges, particularly in sustaining long triplet-pair lifetimes, as the tightly coupled molecules hinder triplet diffusion, leading to rapid recombination.[53] Designing an efficient SF dimer necessitates striking a delicate balance between achieving strong electronic coupling to promote SF while avoiding excessively strong coupling that deactivates the triplet-pair immediately after formation. This delicate balance is crucial for ensuring both quantitative triplet formation and prolonged triplet lifetimes, essential for practical applications. Strategies incorporating various bridging units and using larger oligomers to facilitate triplet separation have emerged as promising avenues for extending triplet lifetimes.[54] Another challenge in intramolecular systems, which is particularly evident in systems where the energetics of SF are finely balanced, is to ensure that dimerization does not lower the S_1 energy more than the T_1 since this may render SF endothermic.[55]

SF has been observed and confirmed in various molecular systems. Among the canonical SF systems are the linear polyacenes tetracene[56–58] and pentacene[59,60] which exhibit endothermic and exothermic SF, respectively. In the case of pentacene, SF can quantitatively occur in the solid state, leading to the total quenching of singlet excited states as fast as 200 fs.[61] Close to 200 % has also been demonstrated for intramolecular systems in solution.[62,63] Despite the endothermic nature of tetracene, SF rates remain substantial, with triplet yields approaching 200 % and triplet excited state formation occurring on the picosecond timescale.[64] Other molecular classes have also been shown to undergo SF and have been studied in detail. Examples include molecules such as 1,3-diphenylisobenzofuran (DPIBF),[65–67] diphenylhexatriene (DPH)[68,69] and the rylene family[70,71] which include for instance perylene diimide (PDI)[72,73] and terrylene diimide.[74]

It is essential to recognize that the kinetic scheme of SF often surpasses the simplicity depicted in Figure 2.4. In the conversion from S_1 to the ^{1}(TT) state there is some debate regarding direct[75,76] and non-direct[77,78] pathways, each of which has been demonstrated to be operational in different systems. The non-direct pathways are believed to involve virtual and/or real charge transfer (CT) intermediate states,[60,79] and even the intermediate formation of excimer states has been proposed.[50] However, disagreements persist in the literature, particularly regarding the role of the excimer intermediate and arguments have been proposed to support both its role as a trap state and as an intermediate.[80–83] A comprehensive understanding of the ^{1}(TT) formation mechanism remains elusive, partly due to the challenge of identifying a unified mechanism across all SF-capable systems. Thus, it is crucial to emphasize that the presented scheme represents a generalized process, while the actual mechanism is inherently system-dependent, varying across different classes of SF-capable molecules, as well as different molecular assemblies and geometries of the same type of molecule.[62,63,78] Moreover, during the transition from the initial ^{1}(TT) state to free independent triplets, evidence suggests that the triplet pair can assume states of different spin multiplicities, particularly over longer timescales. Quintet states (^{5}(TT)), in particular, are believed to play a pivotal role in the formation of free triplets. Spectroscopic techniques involving magnetic fields, such as time-resolved electron paramagnetic resonance (EPR), have been instrumental in elucidating the spin evolution of the triplet pair.[84–86] However, magnetic field effects are beyond the scope of the works presented in this thesis.

2.2.2 Triplet Harvesting

In the introduction of this thesis, it was highlighted that one of the primary motivations for SF research is its potential integration into PV applications. For this integration to occur, the generated triplet excited states need to be effectively harvested and several strategies on how to achieve this have been explored in the literature. One approach involves direct energy transfer from individual triplets. This strategy could allow for SF to be integrated with the already well-established and efficient silicon-based PV devices. Efforts have been made in this direction with some degree of success,[87] yet engineering the interface between the SF material and silicon remains a formidable challenge for achieving optimal performance. Another strategy is to transfer the energy from the individual triplets to an emissive specie that can emit photons which in turn may be absorbed by the solar cell material.[88] A third strategy involves charge transfer to an electron acceptor, such as for instance in the setting of organic PV devices or in a dye-sensitized solar cell (DSSC).[89] While this thesis does not delve into actual device implementation, Chapter 6 explores initial strides toward SF applications, focusing on the third strategy.

2.3 Exciton Coupling

Similar to SF, exciton coupling theory was discovered more than 50 years ago. However, unlike SF, the comprehension of the exciton coupling theory was significantly advanced and well-established from its early days,[90] with subsequent expansions of the initial concepts over the years.[91] Exciton coupling is a through space Coulumbic interaction between the TDMs of atoms and molecules. One of the pioneering models that articulated these theories was proposed by Kasha, who directed his efforts towards unraveling the photophysical properties of molecular aggregates.[90,92] Employing the point-dipole approximation to describe the Coulombic interaction between two molecules, Kasha's work laid a foundational understanding for the subsequent developments in exciton coupling theory. The theory is perhaps most easily comprehended when considering a pair of TDMs as illustrated in Figure 2.5 in combination with the expression for the Couloumb coupling (J_c) between the two TDMs which is defined according to Equation 2.6.

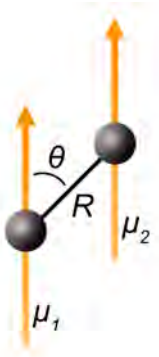

Figure 2.5: Illustration of the relative orientation of two TDMs in a J-aggregate θ<54.7° and H-aggregate 54.7°<θ<90°.

$$J_c = \frac{\mu^2(1 - 3cos^2\theta)}{4\pi\epsilon R^3} \tag{2.6}$$

In Equation 2.6, the TDMs μ_1 and μ_2 from Figure 2.5 are assumed to be of equal magnitude (μ). θ is the relative orientation of the TDMs, ϵ is the dielectric constant of the medium and R is the distance between each molecule's center of mass. At angles less than 54.7° the TDMs are aligned in a head-to-tail configuration in what is commonly referred to as a J-aggregate. In this case the Couloumb coupling J_c assumes a negative value. On the contrary, for angles larger than 54.7° the TDMs are kept in a side-by-side configuration with $J_c > 0$ and are instead called H-aggregates. Coulumb coupling can have a profound effect on the photophysical properties of the interacting molecules and the interaction can lead to the formation of new exciton states that are shifted in energy relative to the individual monomer excited states. Figure 2.6 present the two extreme cases of θ equal to zero (full head-to-tail configuration) and 90° (side-by-side).

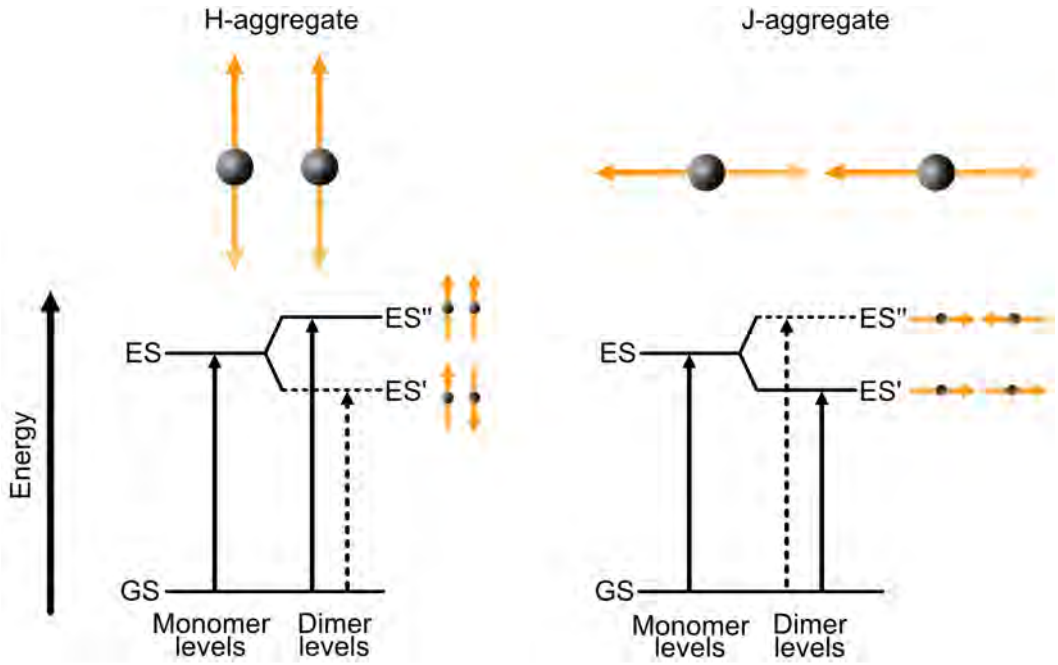

Figure 2.6: Energy diagram for the energy levels of the individual monomers and exciton bands formed for the dimer in an H-aggregate and J-aggregate. GS is an abbreviation for ground state and ES stands for excited state. In an H-aggregate the lowest energy transition is forbidden due to cancellation of the TDMs and conversely the highest energy transition in a J-aggregate is forbidden (dashed arrows).

In both cases two new exciton states are formed as a consequence of in-phase and out-of-phase dipole interactions. Arrangements of in-phase dipoles are allowed and will have an enhanced TDM relative to the monomer. In the case of J-aggregates the TDM increases by a factor of $\sqrt{N}$ where N is the number of coupled molecules, which in the example in Figure 2.6 is two. In contrast, for out-of-phase arrangements the TDMs cancel each other rendering these states optically dark. The energetic arrangement of the dark and optically allowed exciton states which ultimately leads to a bathochromic (red) shift in the case of J-aggregates and hypsochromic (blue) shift in the case of H-aggregates is a consequence of the sign of J_c, as previously described, which dictates if the interaction is repulsive or attractive. Notably, the application of the exciton coupling model presented herein is not limited to the simple dimer case that has been presented thus far. Its applicability transcends to more complex molecular configurations, as will be demonstrated in subsequent chapters. When dealing with intricate molecular arrangements, the matrix notation proposed by Yoon et al.[93] proves to be particularly valuable. The methodology involves first defining a square matrix V:

$$V = \begin{bmatrix} v_{11} & v_{12} & v_{13} & \dots & v_{1n} \\ v_{21} & v_{22} & v_{23} & \dots & v_{2n} \\ v_{31} & v_{32} & v_{33} & \dots & v_{3n} \\ \vdots & \vdots & \vdots & \ddots & \vdots \\ v_{n1} & v_{n2} & v_{n3} & \dots & v_{nn} \end{bmatrix}$$

consisting of the TDM coupling energy, v_{ij}, between any molecule i and j in a multimolecular

system. The individual values of v_{ij} (in cm^{-1}) can be calculated according to Equation 2.7[94]

$$v_{ij} = \frac{5.04 f_L^2 |\mu_i||\mu_j| k_{ij}^2}{\epsilon R_{TS}^3} \tag{2.7}$$

where f_L^2 is a unitless correction factor $f_L^2 = ((\epsilon + 2)/3)$, μ_i and μ_j are the TDMs in Debye, R_{TS}^3 is the center to center through space distance in nm and finally, k_{ij}^2 is the orientation factor defined according to Equation 2.8 where the angles are illustrated in Figure 2.7.

$$k_{ij}^2 = (cos\theta_T - 3cos\theta_i cos\theta_j)^2 \tag{2.8}$$

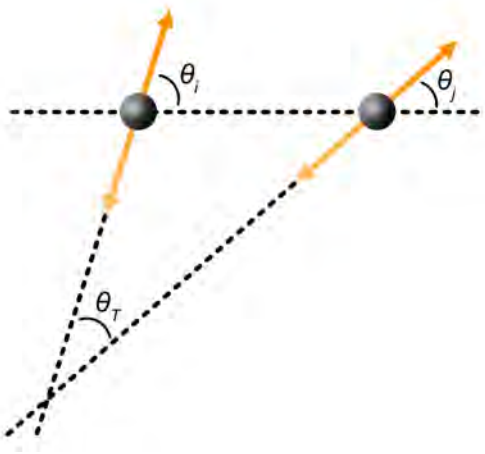

Figure 2.7: Illustration of the relative orientation of the TDMs and definition of the angles in Equation 2.8.

The magnitude of the TDM in Debye can be determined from the molar absorptivity $\epsilon(\nu)$ spectra using Equation 2.9 where *n* is the refractive index of the solvent and ν represents wavenumber in cm^{-1}.[95]

$$\mu = 9.58 \cdot 10^{-2} \left(\frac{(2n^2+1)^2}{9n^3} \int \frac{\epsilon(\nu)}{\nu} \right)^{1/2} \tag{2.9}$$

In the matrix *V* all diagonal elements v_{ij} (i = j) are zero (no self-coupling) and $v_{ij} = v_{ji}$ when $i \neq j$. The key part of the analysis is to now diagonalize *V*. Matrix diagonalization is a mathematical operation in which a square matrix is converted into a product of matrices $V = CEC^{-1}$. *E* is a so-called diagonal matrix which contains the *n* eigenvalues of the system and *C* contains linearly independent column eigenvectors where each eigenvector is associated with a particular eigenvalue. For instance, (c_{11}, c_{21}, c_{31}, . . ., c_{n1}) corresponds to e_{11} and so forth.

$$E = \begin{bmatrix} e_{11} & 0 & 0 & \dots & 0 \\ 0 & e_{22} & 0 & \dots & 0 \\ 0 & 0 & e_{33} & \dots & 0 \\ \vdots & \vdots & \vdots & \ddots & \vdots \\ 0 & 0 & 0 & \dots & e_{nn} \end{bmatrix} \qquad C = \begin{bmatrix} c_{11} & c_{12} & c_{13} & \dots & c_{1n} \\ c_{21} & c_{22} & c_{23} & \dots & c_{2n} \\ c_{31} & c_{32} & c_{33} & \dots & c_{3n} \\ \vdots & \vdots & \vdots & \ddots & \vdots \\ c_{n1} & c_{n2} & c_{n3} & \dots & c_{nn} \end{bmatrix}$$

The extracted eigenvalues represent the energy shift of the exciton hybrid states relative to the individual monomers that are formed due to exciton coupling. By considering the geometry of the specific molecular assembly under investigation and correlating it with the summation of the eigenvectors, one can further ascertain the oscillator strength of transitions to the exciton energy states. This enables the determination of whether these transitions are allowed or forbidden, providing valuable insights into the system's electronic structure and optical properties.

2.4 Photoinduced Electron Transfer

Electron transfer (ET) plays a pivotal role in chemical transformations and photochemistry. This thesis focuses primarily on photoinduced ET, where the transfer occurs between two reactants, with one or both being in an excited state prior to the ET event. To assess the feasibility of ET between a donor (D) and acceptor (A), the most direct approach is to estimate the energy of the charge-separated (CS) state. This state comprises a radical anion $A^{\cdot -}$ and a cation $D^{\cdot +}$, and its energy can be determined using Equation 2.10.[96,97]

$$E(D^{\cdot +} - A^{\cdot -}) = E_{ox}(D) - E_{red}(A) - G_s \tag{2.10}$$

Here, E_{ox}(D) represents the oxidation potential of the donor, E_{red}(A) signifies the reduction potential of the acceptor, and G_s denotes the Coulombic interaction energy between the two charges. This parameter is contingent upon various factors, including the distance between the charges R_{DA}, the solvent dielectric constant ϵ_s, vacuum permeability ϵ_0, and the elementary charge *e*, as delineated in the initial term of Equation 2.11.

$$G_s = \frac{e^2}{4\pi\epsilon_0\epsilon_s R_{DA}} - \frac{e^2}{2}\left(\frac{1}{r_D} + \frac{1}{r_A}\right)\left(\frac{1}{4\pi\epsilon_0\epsilon_s} - \frac{1}{4\pi\epsilon_0\epsilon_{ref}}\right) \tag{2.11}$$

The second term in Equation 2.11, where r_A and r_D represent the radii of the acceptor and donor, respectively, can be further employed to estimate the energy of the CS state in a solvent with a different polarity (ϵ_{ref}) from the one in which the oxidation and reduction potentials were measured.[98] However, caution should be exercised when using this expression, as it provides a somewhat rough approximation. Generally, Equation 2.10 and 2.11 holds true predominantly in polar solvents. Once the CS state energy is determined, the Gibbs free energy change, ΔG^0, or commonly referred to as the driving force for the reaction, can be estimated by comparing the CS state energy with the energy of the state from or to which the electron transfer occurs. Figure 2.8a illustrates the significance of the excited state energy's contribution to the driving force using potential energy surfaces for the reactants and products. In this context, the product and reactant surfaces are functions of a *nuclear configuration*, representing the spatial arrangement of solvent molecules as well as the D-A molecules with respect to equilibrium configurations.

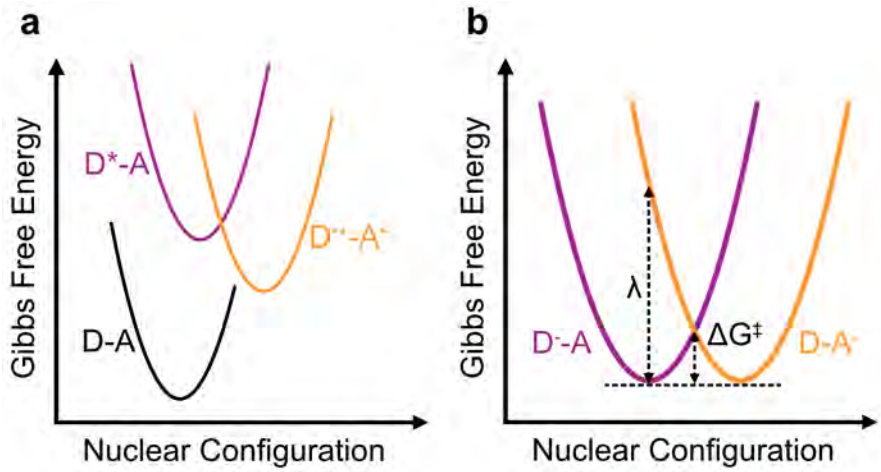

Figure 2.8: a) Potential energy surface diagram showing photoinduced ET. The diagram includes the ground state (D-A), the initially photoexcited state (D*-A) and the charge separated state $D^{\cdot+}$-$A^{\cdot-}$. The activation energy $\Delta G^{\ddagger}$ and reorganization energy λ are depicted for a self-exchange reaction in b).

R. A. Marcus pioneered the utilization of potential energy surfaces for describing ET reactions, and his theory constitutes the foundation upon which the kinetics of ET is comprehended.[99–102] Marcus Theory provides a framework that allows the calculation of ET reaction rates through the semi-classical expression presented in Equation 2.12.

$$k_{ET} = \frac{2\pi}{\hbar}\frac{H_{DA}^2}{\sqrt{4\pi\lambda k_b T}} exp\left(-\frac{(\lambda + \Delta G^0)^2}{4\lambda k_b T}\right) \tag{2.12}$$

In the expression, k_b denotes Boltzmann's constant, and T represents temperature. However, the more crucial parameters that govern the kinetics of ET reactions, that can be either computed or experimentally determined, include the reorganization energy λ, the extent of wavefunction overlap between the donor and acceptor (H_{DA}), often termed electronic coupling), and the driving force ΔG^0, as introduced earlier. The reorganization energy λ is defined as the energy difference between the product surface and the reactant surface, both in the equilibrium configuration of the reactants, as illustrated in Figure 2.8b. It can be conceptualized as the energy needed for solvent rearrangement and structural changes associated with the ET event. The overall reorganization energy is typically dissected into two components: an "outer-sphere" component λ_0 and an "inner-sphere" component λ_i representing solvent rearrangement and structural change contributions, respectively. However, outer-sphere contributions generally dominate the total reorganization energy, except in cases involving substantial structural changes. The outer-sphere component, λ_0, can be determined using Equation 2.13, where the only unmentioned parameter is the solvent optical dielectric constant ϵ_{op} (approximated as the square of the refractive index in the visible region).[103]

$$\lambda_0 = \frac{e^2}{4\pi\epsilon_0}\left(\frac{1}{2r_D} - \frac{1}{2r_A} + \frac{1}{R_{DA}}\right)\left(\frac{1}{\epsilon_{op}} - \frac{1}{\epsilon_s}\right) \tag{2.13}$$

To estimate the value of λ_i, one can utilize Hooke's law and with it determine the displacement of bond lengths from their equilibrium positions. The principal contribution to λ_i is the combina-

tion of all *n* involved bond displacements (j) with associated force constants f_j and equilibrium bond lengths d_p and d_r for products and reactants, respectively. This relationship is expressed by Equation 2.14.

$$\lambda_i = n\left[\frac{1}{2}\sum_j f_j(d_p - d_r)^2\right] \tag{2.14}$$

Equation 2.12 has been demonstrated to be applicable in scenarios involving diabatic and weakly adiabatic ET reactions, which is essentially when the electronic coupling ($\mathbf{H}_{DA}$) is relatively small. For strongly interacting donor and acceptor systems, where tunneling through the barrier is more substantial, additional considerations become pertinent. In such cases, ET can be viewed as occurring on a combined potential energy surface, with a barrier smaller than the crossing of the individual surfaces for the reactants and products.[104]

Upon closer examination of Equation 2.12, the Arrhenius-like expression in the exponent draws attention to the activation energy, $\Delta G^{\ddagger}$, governing an ET reaction. This energy can be expressed in terms of the driving force and reorganization energy, as outlined in Equation 2.15.

$$\Delta G^{\ddagger} = \frac{(\Delta G^0 + \lambda)^2}{4\lambda} \tag{2.15}$$

From Equation 2.15, one of the notable outcomes of Marcus theory emerges - a revelation of three distinct kinetic regimes governing ET. These regimes are commonly known as the normal region (where -ΔG^0<λ), the barrierless region (where -ΔG^0=λ), and the inverted region (where -ΔG^0>λ). In other words, a parabolic relationship between the barrier height, and consequently the ET rate, and the driving force is observed. As the driving force increases, the barrier initially decreases, reaches its minimum, and then subsequently increases for large driving forces, as depicted in Figure 2.9.

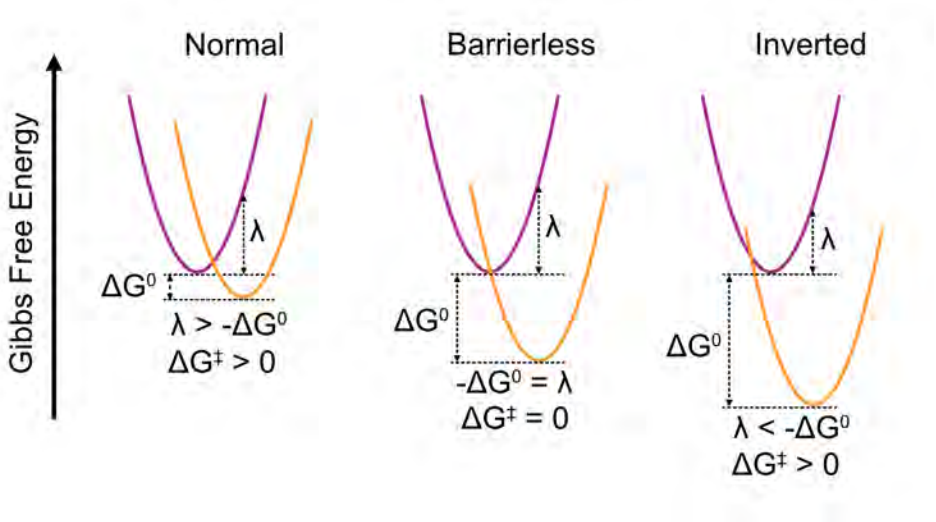

Figure 2.9: The different regimes of ET. From left to right we have the "Normal" electron transfer reactions, λ > -ΔG^0. "Barrierless" reactions when λ = -ΔG^0, which corresponds to a rate maximum. "Inverted" electron transfer when λ < -ΔG^0 which is predicted to result in a decrease in rate of ET.

It is crucial to note that particularly in the inverted region, there is a significant impact of nuclear tunneling, leading to a less quadratic fall-off than predicted in many cases in the literature. This is attributed to the utilization of high-frequency modes of the acceptor below the surface intersection point. In this context, inverted ET kinetics share similarities with the non-radiative decay of excited states.[104–106] Nevertheless, instances exist in the literature where experimental data exhibit remarkably good agreement with the parabolic inverted region predicted by Equation 2.12.[107]

2.5 Charge Transfer Mediated Triplet Formation

The formation of CS states subsequent to photoexcitation, as detailed in the preceding section, serves multiple functions within the realm of photochemistry. Of particular significance to this thesis is its role in mediating and facilitating the formation of triplet excited states in organic molecules. As described earlier in Section 2.2 and 2.1 the rate of triplet formation in systems incapable of SF or without involvement of heavy atoms to enhance SO-coupling is typically very low. However, research have shown that through CS states, the yield of triplet formation can approach unity.[108] Triplet formation via CS states commonly ensues through one of two distinct mechanisms: Spin–Orbit Charge Transfer Intersystem Crossing (SOCT-ISC) and/or Radical-Pair Intersystem Crossing (RP-ISC).[109,110] SOCT-ISC entails a direct conversion of the initial ^{1}CS state into the T_1 state, involving ET and a simultaneous spin inversion. This phenomenon is notably amplified when the constituent subunits assume a nearly perpendicular alignment. Such an orientation facilitates compensation for changes in electron spin angular momentum during ISC through adjustments in molecular orbit angular momentum which satisfies the condition of conserved total angular momentum. This molecular alignment is particularly evident in closely spaced dyads, where steric hindrance between the subunits enforces an orthogonal arrangement, as observed in dyads linked by a single C–C bond.[111–113] The SOCT-ISC process can thus be seen as an analogue to the El-Sayed's rules which states that ISC is more efficient when a change in orbital occupancy occurs.[114] El-Sayed's rules can for instance explain the efficient ISC in ketone compounds due to the orthogonality and separation of the orbitals in the transition from for instance S_n(n,π*) to T_n(π,π*). In contrast, the RP-ISC mechanism involves the emergence of an intermediate triplet charge-transfer state ^{3}CS prior to charge recombination (CR), leading either to the triplet state or the ground state. This mechanism, at times referred to as hyperfine interactions, depends on the interplay between nuclear spin and electron spin, causing spin dephasing and conversion to ^{3}CS. RP-ISC is more prevalent in electron donor-acceptor dyads characterized by weak electronic coupling between their donor and acceptor subunits due to considerable spatial separation (e.g., >10-15 Å).[115] This separation results in a small energy difference between ^{1}CS and ^{3}CS. In general, triplet formation based on SOCT-ISC occur with rate constants in the range of 10^9-10^{10} s^{-1} or faster compared to the relatively slow rates for RP-ISC (10^8 s^{-1} or slower). Notably, certain studies posit the coexistence of both mechanisms.[116]

Chapter 3
Experimental Techniques

This chapter aims to provide an overview and explanation of the spectroscopic and electrochemical techniques, along with the fitting procedures employed in this thesis. The descriptions intentionally maintain brevity, directing the reader to consult the cited references within the text for a more comprehensive understanding of these techniques.

3.1 Steady-State Absorption Spectroscopy

The initial step in most photophysical processes involves the absorption of light, promoting a molecule to an excited state. As will become clear during the course of this chapter there are many methods by which one can investigate both the formation and decay of excited states. Among these methods, steady-state absorption spectroscopy stands out as a straightforward yet profoundly important measurement technique. Typically, it yields valuable insights into the ground state absorption characteristics of a substance. This technique can be used to identify the composition of a sample and allow for quantification of substance concentrations within it. Figure 3.1 shows the main components of an absorption spectrometer.

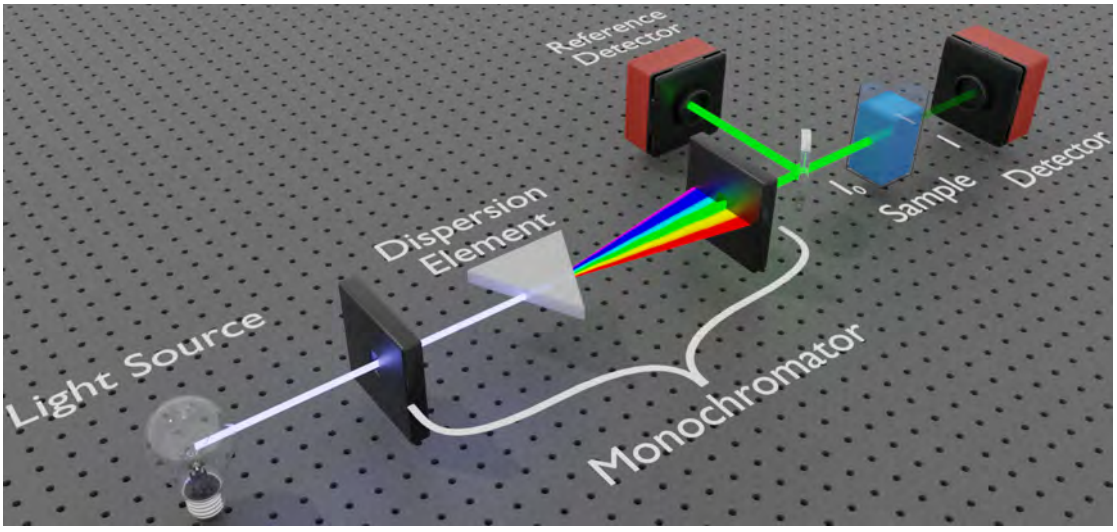

Figure 3.1: A 3D schematic model illustrating a typical absorption spectrometer.

The monochromator consists of a dispersive element, usually a diffraction grating, that spreads the light in different angles as a function of the wavelength, and a thin slit which is used to select the desired wavelength. The intensity before the sample ($I_0(\lambda)$) is measured by a reference detector and the intensity of the light having passed through the sample ($I(\lambda)$) is measured by a separate detector. The absorbance ($A(\lambda)$) can then be calculated according to Equation 3.1 and an absorption spectrum can be constructed by scanning through a range of wavelengths with the monochromator.[26]

$$A(\lambda) = \log_{10} \frac{I_0(\lambda)}{I(\lambda)} \tag{3.1}$$

The absorbance of a sample is proportional to the concentration (C), the pathlength (l) and the molar absorptivity at a particular wavelength ($\epsilon(\lambda)$) according to Equation 3.2 which is commonly referred to as the Beer-Lambert law.

$$A(\lambda) = \epsilon(\lambda) C l \tag{3.2}$$

The molar absorptivity is a measure of the probability for a molecule or a material to absorb a photon of a certain wavelength.[27]

3.2 Steady-State Emission Spectroscopy

The emission of a sample can be measured in a similar manner to absorption as illustrated in Figure 3.2. In steady state emission spectroscopy the sample is exposed to constant or pulsed illumination while the intensity of the emission is recorded by integrating over a certain time period. In contrast to steady state absorption, the emission spectrometer requires the use of a monochromator for both the excitation light and a second monochromator for the emission light.

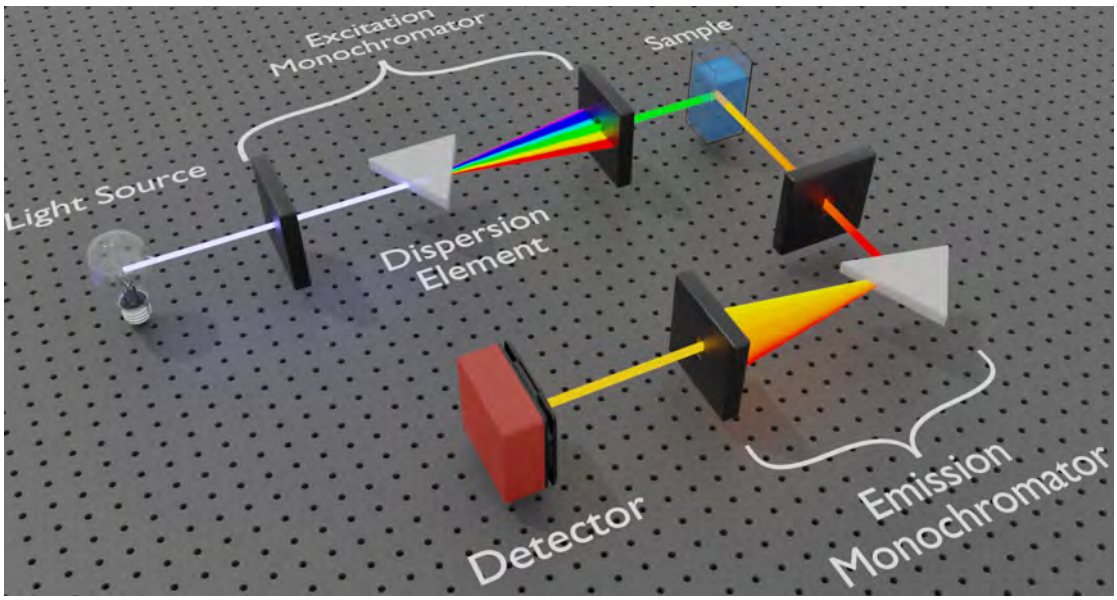

Figure 3.2: A 3D schematic model illustrating a typical emission spectrometer.

The detector is placed perpendicular to the light source to avoid as much scattered excitation light as possible. An emission spectrum can be obtained by adjusting the emission monochromator and monitor the emission at different wavelengths while keeping the excitation light locked at a particular wavelength. It is also possible to monitor the emission wavelength while scanning over a range of excitation wavelengths. The spectrum acquired in this case is called an excitation spectrum and will closely resembles the absorption spectrum if the sample follows Kasha's Rule and Vavilov's Rule.[117]

3.2.1 Total Internal Reflection Emission Spectroscopy

Performing emission measurements on highly concentrated samples is problematic, primarily due to the so called second-order inner-filter effect. This phenomenon arises from the inherent overlap between the absorption and emission spectra of most molecules in solution. This overlap can result in the re-absorption of emitted light, distorting the shape of the emission spectrum. To mitigate this issue, conventional emission measurements typically maintain low sample concentrations, with a commonly followed guideline of keeping the absorbance below 0.05. However, in situations where there is a need to characterize the emission spectrum of a highly concentrated solution, a viable approach is to conduct emission measurements under conditions of total internal reflection (TIR). TIR conditions effectively minimize the impact of the second-order inner-filter effect by restricting the penetration depth of the excitation light into the sample solution. This concept becomes clear when considering how TIR reflection functions. To establish TIR conditions at the interface between two mediums with refractive indices denoted as n_1 and n_2, two conditions must be met: *i)* The refractive index of the first medium (n_1) should be greater than that of the second (n_2) and *ii)* the angle of incidence of the light (θ_i) with a wavelength λ must exceed the critical angle (θ_c), as determined by Snell's law:

$$sin(\theta_c) = \frac{n_1}{n_2} \tag{3.3}$$

Under these conditions, a minute portion of the incident light can traverse the interface, giving rise to what is known as the evanescent wave. The intensity of this evanescent wave, denoted as I(z), follows an exponential decay pattern as described by Equation 3.4.

$$I(z) = I_0 e^{(-z/d)} \tag{3.4}$$

where z is the distance and d is the penetration depth defined according to Equation 3.5.

$$d = \frac{\lambda}{4\pi\sqrt{n_1^2 sin^2(\theta_i) - n_2^2}} \tag{3.5}$$

The experimental setup employed in this thesis is outlined in Figure 3.3. It entails the use of a high refractive index (HRI) half-sphere (with $n_1 = 2.0$), placed in direct contact with the solution under examination. To harness the TIR phenomenon, the angle of incident light is adjusted to surpass the critical angle, which can vary slightly based on the refractive index of the solvent. The emitted TIR fluorescence, generated by exciting the sample with the evanescent wave, is

collected by an optical fiber linked to a spectrometer. As an example using tetrahydrofuran with $n_2 = 1.4072$ and θ_i=59° (significantly exceeding the critical angle θ_c of 45°) the calculated penetration depth amounts to 32.9 nm. Consequently, the intensity has decreased to 1/e of the original value at 32.9 nm according to Equation 3.4. After only 100 nm the intensity has dropped by more than 95 % which ensures that the second order inner-filter effects are minimized.

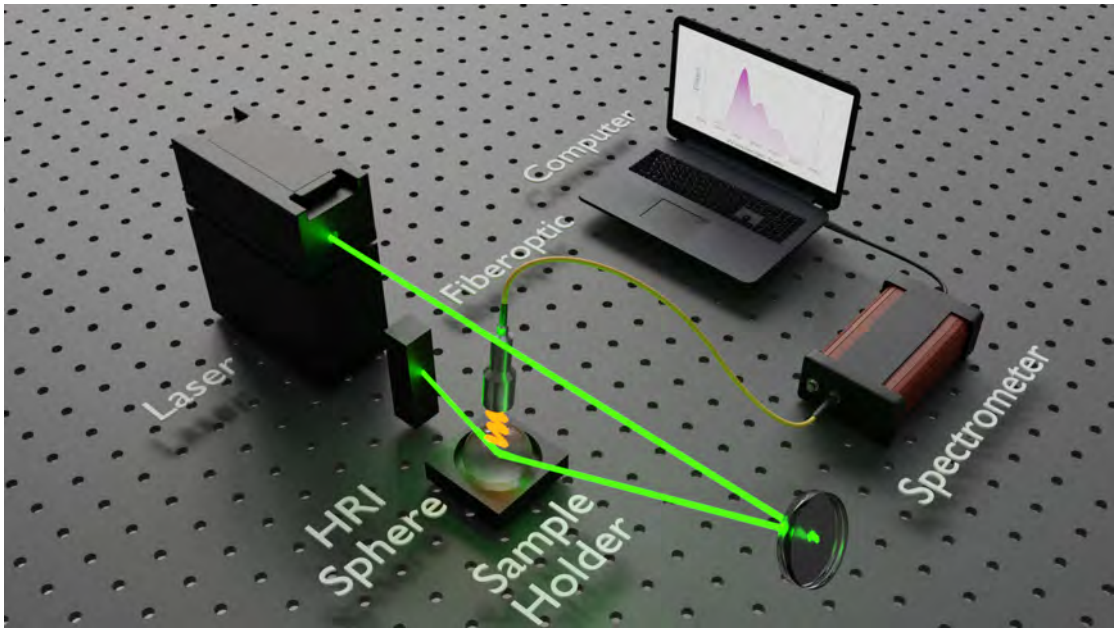

Figure 3.3: A 3D schematic model illustrating a total internal reflection (TIR) emission experimental setup. HRI is an abbreviation for high-refractive index.

3.3 Time Resolved Emission Spectroscopy

Steady state emission spectroscopy is limited in the sense that it gives no information of how or when an excited state is deactivated. To remedy this issue, time resolved emission is utilized. The method which is used in this thesis to measure emission lifetimes is called time correlated single photon counting (TCSPC). With this technique the sample is excited with a laser pulse that is typically much shorter than the emission lifetime under investigation. The overall time resolution of the measurement depends on the excitation pulse width in conjunction with the response time of the detector. The instrumental setup used for the experiments presented herein utilizes a pulsed laser diode and a micro-channel plate photomultiplier tube (MCP-PMT) resulting in a combined time resolution down to 70 ps. The operating principle of a TCSPC instrument revolves around recording the time elapsed between the excitation pulse and the arrival of the first photon at the detector using specialized electronics. This process is repeated for numerous excitation pulses, eventually enabling the construction of a histogram with time plotted on the x-axis and the number of detected photons on the y-axis. Since only the first photon of each excitation event is detected, TCSPC instruments are engineered so that approximately 1 photon is detected for every 100 excitation pulses. This deliberate design choice is due to the inherent randomness of photon emission. In essence, following an excitation pulse more photons are

emitted at early times than late times. Consequently, if many photons are sent out, but only the first is detected the measurement will be biased towards shorter times. This is referred to as pile-up and can be avoided by following the principle outlined above. The probabilistic nature of photon emission necessitates running a TCSPC measurement until a sufficient number of photons have been amassed for statistically significant results, often requiring counts in the range of 5000 to 10000 in the top channel. A schematic representation of the instrumental setup is depicted in Figure 3.4.

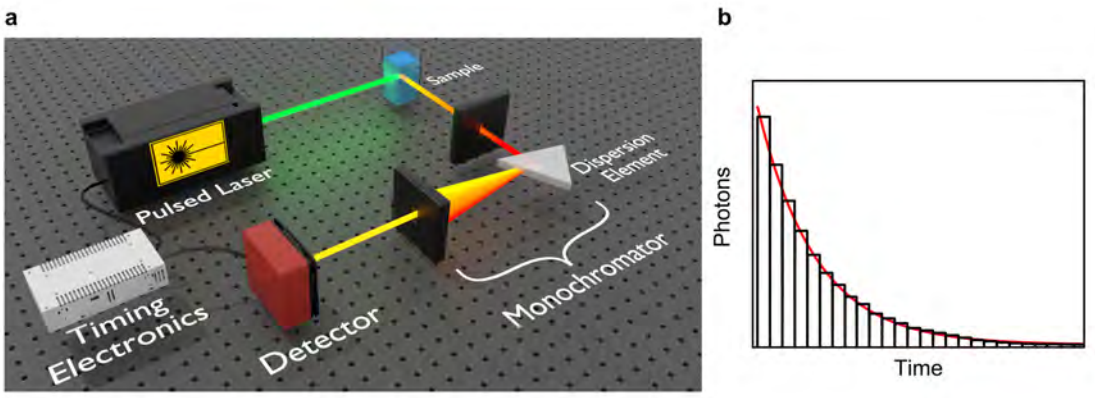

Figure 3.4: a) A 3D schematic model illustrating the experimental setup of a TCSPC instrument b) Example of a histogram from a TCSPC measurement where the red line represents an exponential fit to the data.

One of the most important parameters that can be obtained from a time resolved emission measurement is the lifetime (τ) of the emitting species. The lifetime is defined as the average time the emitting species remains in the excited state subsequent to being excited and it can be extracted from the histogram obtained from a TCSPC measurement. This can be realized by considering the rate expression for how an excited state decays with first order kinetics as shown in Equation 3.6.

$$\frac{dN(t)}{dt} = -\frac{1}{\tau} N(t) \tag{3.6}$$

Here, *N(t)* is the excited state population which decays as a function of time (*t*) and τ is the inverse sum of all first order rate constants that depopulate the excited state including both radiative and non-radiative processes. By integrating the expression and defining the initial population at *t=0* as N_0 one obtains the expression in Equation 3.7.

$$N(t) = N_0\, e^{-(t/\tau)} \tag{3.7}$$

Finally, because the emission intensity *I(t)* is proportional to the excited state population *N(t)* it is possible to fit an exponential function directly to *I(t)* vs. t which is the output from a TCSPC experiment and where τ is the fitting parameter of interest that is extracted. The above description is however limited to a sample with a single emitting species that only decays with a single, so called monoexponential lifetime. For systems containing more than one emissive

specie or a single specie that has several lifetimes, the intensity *vs.* time plot can be fit to a sum of exponential decays according to Equation 3.8.[117]

$$I(t) = \sum_i I_{0,i}\, e^{-(t/\tau_i)} \tag{3.8}$$

It should be noted that the validity of Equation 3.8 is based on the assumption that the lifetime of the emission decay is much longer than the instrument response function (IRF) which in essence is the inherent time resolution of the instrument. If the lifetime of the emission is on the same time scale as the IRF it is necessary to deconvolute the exponential decay with the IRF since a significant fraction of the excited states formed by the early part of the pulse will start to decay at the same time as new excited states are populated from photons from the tail of the pulse. The convolution integral is presented in Equation 3.9

$$I_{measured}(t) = \int_{-\infty}^{t} IRF(t')\, I(t-t')\, dt' \tag{3.9}$$

where $I_{measured}(t)$ is the measured intensity decay and IRF(*t'*) is the intensity decay obtained when only scattered excitation light is allowed to reach the detector. When both $I_{measured}(t)$ and IRF(*t'*) are known it is possible to solve for the true intensity decay *I(t)* which can be a sum of exponentials as in Equation 3.8.[118]

3.4 Transient Absorption Spectroscopy

Whereas steady state absorption generally provides an absorption spectrum of the ground state, transient absorption (TA) spectroscopy can be used to probe the absorption of transient species such as excited states. This technique is particularly useful in cases when dealing with transient species that are non-emissive. TA is often referred to as pump-probe spectroscopy and the basic principle of this technique is that the sample is initially excited by an intense pulse (pump) that populates the excited states. The pump pulse is followed by a weaker pulse (probe) after a certain time delay and the probe beam is subsequently intercepted by a detector as illustrated in Figure 3.5a. The purpose of the probe pulse is to measure the absorption of the excited states that are formed by the first pulse as shown in the diagram in Figure 3.5b.

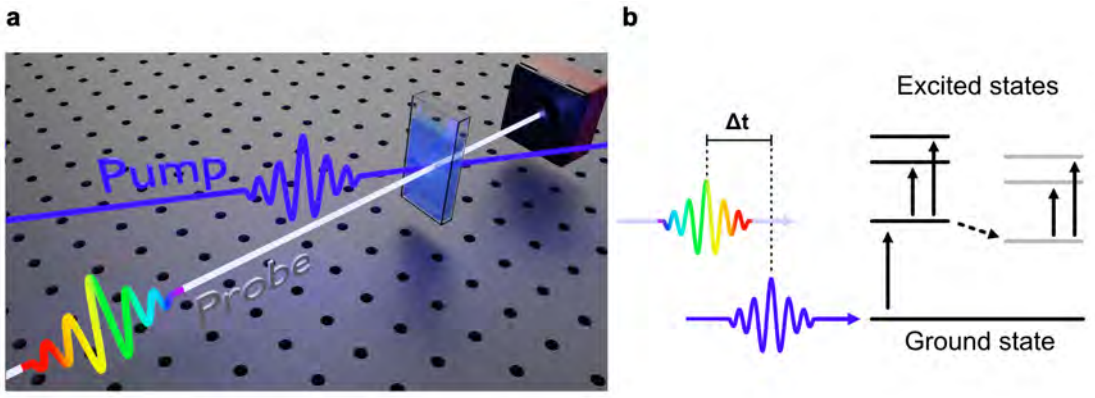

Figure 3.5: a) 3D schematic illustration of TA showing how a sample is photoexcited by a pump pulse and then subsequently interrogated by a probe pulse after some time delay (Δt). b) Schematic of how a TA measurement works. The pump excites a fraction of the ground state molecules to an excited state. The probe arrives at a time delay Δt after the pump, probing the transient species present in the sample at time Δt.

An integral part of pump-probe spectroscopy is that the time delay between the pulses can be varied. By scanning over a certain wavelength region while increasing the time between the arrival of the pump and the probe to the sample an absorption spectra, such as the one presented in Figure 3.6a, can be constructed. An alternative and frequently used method for visualizing TA data is depicted in Figure 3.6b. In this representation, TA data at specific wavelengths are carefully chosen and plotted over time. TA data can also be visualized through 2D heatmaps, and illustrations of all these mentioned representations will be provided in the subsequent chapters. As evident from Figure 3.6a and b the data from a TA experiment is usually presented as a differential absorption spectra where the differential absorption ($\Delta A(\lambda)$) is the absorption measured by the probe beam after exciting the sample with the pump pulse ($A_{I_+}(\lambda)$) subtracted by the absorption without the pump pulse ($A_{I_-}(\lambda)$) as shown in Equation 3.10. Here, ΔA is also expressed as the ratio between the probe light having passed through the sample with (I_+) and without (I_-) a preceding pump pulse, respectively.

$$\Delta A(\lambda) = A_{I_+}(\lambda) - A_{I_-}(\lambda) = \log\frac{I_-(\lambda)}{I_+(\lambda)} \tag{3.10}$$

From this expression it can be seen that some parts of a TA spectra can have a net negative signal and some parts can be positive. There are in principle two main contributions that can give rise to negative signals. The first of these stem from the fact that when the pump beam interacts with the sample, a fraction of the molecules will no longer be in the ground state and instead populate excited states. Consequently, the concentration of ground state molecules will decrease and the ground state absorption will decrease. As such, the absorption without a preceding pump pulse A_{I_-} can be larger than the value of the absorption shortly after the pump pulse A_{I_+}, which will give a net negative ΔA.

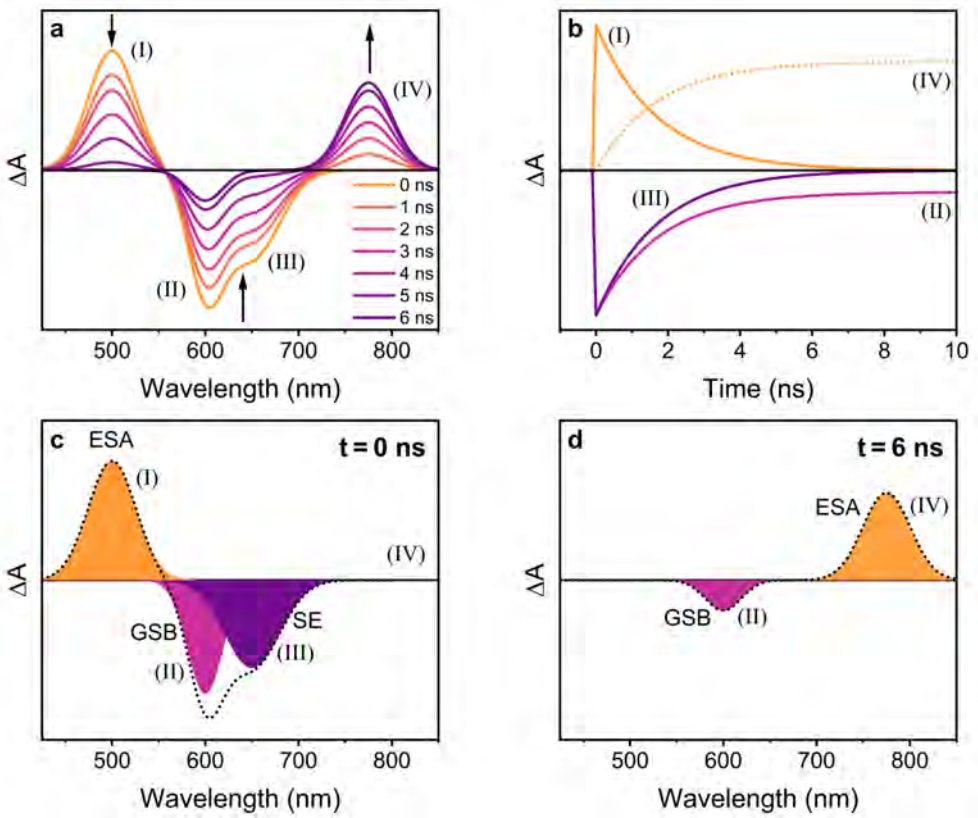

Figure 3.6: a) TA spectra showing the differential absorption as a function of wavelength and with different time delays between the pump and the probe in the legend. b) The corresponding kinetic traces of component (I)-(IV). c) and d) TA spectra where the different contributions to the overall signal has been separated at t = 0 ns and t = 6 ns, respectively. ESA is an abbreviation for excited state absorption, GSB stands for ground state bleaching and SE means stimulated emission.

This is usually referred to as ground state bleaching (*GSB*) and is shown as the pink area in Figure 3.6c and d. The second negative contribution is related to emission from the sample. More specifically it is related to stimulated emission (SE) (purple area in Figure 3.6c) induced by the probe light with some minor contributions from spontaneous emission. This negative contribution can be understood by considering the transmitted intensities (I_+) and (I_-). Assuming a hypothetical scenario where there is no absorption and only SE occurring at a particular wavelength, the number of photons received by the detector in absence of the pump (I_-) will be equal to the number of photons hitting the sample. Conversely, the signal with the pump active (I_+) will, again with the assumption of no absorption, result in the same amount of photons reaching the detector *plus* stimulated emission from the excited states that were populated by the pump. Since this will render $I_+ > I_-$, ΔA will become negative in accordance with Equation 3.10. As a result, negative signals in a TA spectrum will resemble a combination of the steady state absorption and emission spectra. Finally, positive signals correspond to excited state absorption (ESA) which is shown as the orange region in Figure 3.6c and d. This contribution will always be positive to the overall signal since it originates from absorption of excited states following the pump pulse. Note that the ESA can originate from not only singlet excited states, but from

any transient species such as triplet states or charge-separated states that may evolve as a result of energy transfer or electron transfer from the initially excited specie. Careful analysis of the TA spectra can sometimes allow certain features to be assigned to a particular transition and the transitions are commonly denoted as S_1-S_n or T_1-T_n to indicate a transition from the first excited state to a higher excited state of singlet or triplet spin multiplicity.

3.4.1 Femtosecond and Nanosecond Transient Absorption

Both nanosecond (ns) and femtosecond (fs) TA have been used in this work. The time prefix indicates in what time domain the pulse width belongs to for each technique and this parameter also determines the time resolution of the measurement. Even though the two techniques are based on the same principle, the experimental setup and the information that can be acquired is quite different.

In nsTA the pulses typically have a width of a few nanoseconds and with this technique it is possible to monitor photoinduced processes in the order of a few tens of nanoseconds up to milliseconds. The probe lamp can on these timescales be from a continuous light source and the delay between the pump and probe can be controlled electronically.

With fsTA it is possible to monitor ultrafast processes that occur just a few tens to hundreds of femtoseconds after the pump pulse.[119] Contrary to nsTA it is not possible to electronically control the time delay between the pump and the probe pulse on these short timescales. Instead, the probe and pump pulse must originate from the same source and the delay between them is controlled by adjusting the distance each beam travel across the optical table. A schematic of the setup used in this thesis is presented in Figure 3.7. After the regenerative amplifier, which has the purpose of increasing the power of the fs pulses that are generated by a seed-laser, the beam is split into a pump and a probe beam. The pump is directed through an optical parametric amplifier (OPA) which is used to obtain the desired excitation wavelength. The pump beam is subsequently guided towards a bladed chopper wheel operating at half the frequency of the laser which blocks every other pulse thus enabling the acquisition of a differential spectra with (A_{I_+}) and without (A_{I_-}) the pump beam exciting the sample. The pump beam is then directed to the optical delay stage which can be adjusted to adjust the arrival of the pump to the sample relative to the probe beam. The length of the optical delay stage thus determines the maximum time delay that can be probed and is for the setup used in this thesis 10 ns long. After the delay stage the pump is focused and overlapped with the probe beam at the sample. The probe beam has at this point passed through a translating CaF_2 plate which produces a white light continuum[120] and enables probing the transient absorption across a wide wavelength region with the help of a charge coupled device (CCD) camera. The probe and pump beam pass through a number of different optical components along their paths such as polarizers, half-wave plates, Berek compensators and pinholes which are used to tune the intensity, size and polarization of the respective beams.

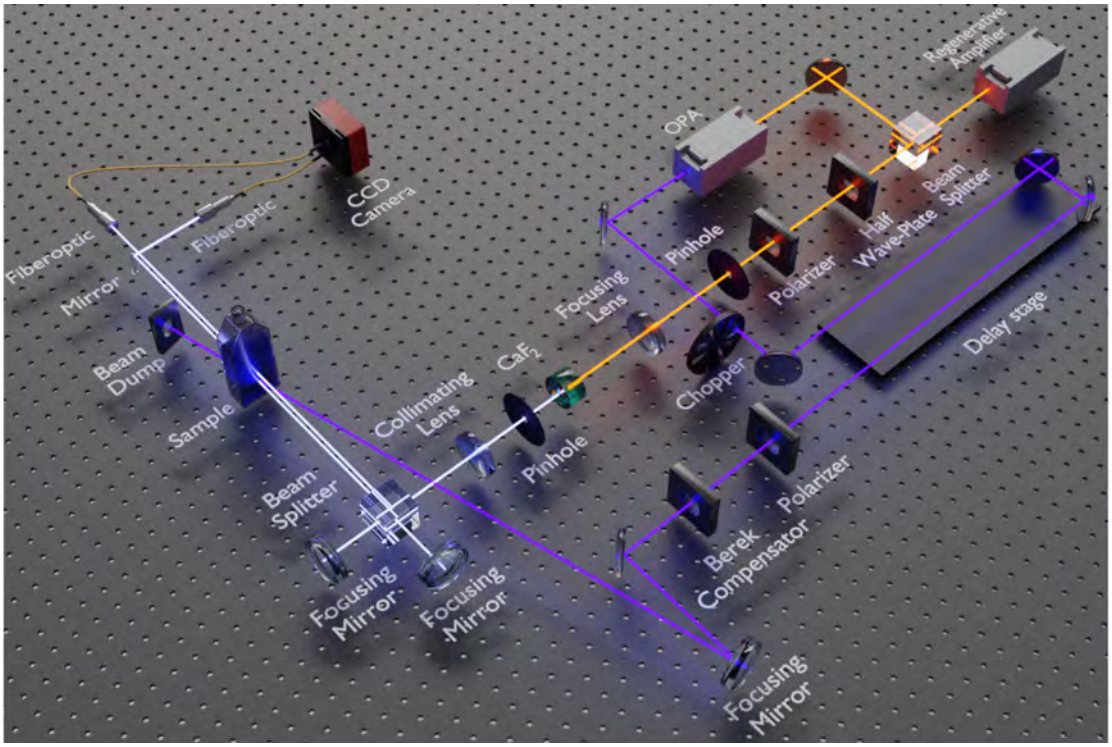

Figure 3.7: A 3D schematic model illustrating the fsTA experimental setup used in this thesis.

3.5 Global Analysis of Spectroscopic Data

A time-resolved spectrum such as the one in Figure 3.6a) obtained from a transient absorption measurement is often not the result of absorption of a single species, but rather a linear combination of several individual absorption spectra from species that form and decay with different rates. For this reason it can be desirable to extract the spectral components that together forms the measured spectra and at the same time solve for the rate constants that governs the systems' dynamics by applying a kinetic model to the data. This can be accomplished using singular value decomposition (SVD) and global analysis. Here, global analysis refers to the simultaneous analysis of multiple decay traces at different wavelengths where the extracted fitting parameters (such as rate constants) can be shared for all the wavelengths or alternatively just be shared for a small part of the entire investigated spectral region.[121,122] SVD is a mathematical tool in linear algebra to factorize matrices. This tool serves two main purposes in the analysis of the raw data. The first is to extract the number of independent components that can describe the data set and thereby also reduce the amount of data that needs to be analyzed. The second purpose is to combine the extracted independent components with a kinetic model and calculate the true spectral components and their corresponding concentration time evolution.[123] The global SVD analysis starts with the experimentally obtained raw data in a matrix, A. The matrix A in the case of a transient absorption experiment consists of columns that correspond to absorption spectra at a certain time and rows that represent the time evolution of the absorbance at a specific wavelength. Thus, if the measurement had 400 wavelengths and 100 time steps, it

would be a 100×400 matrix. The process of SVD separates the matrix A into a product of three matrices U, S and V according to Equation 3.11.

$$A = USV^T \tag{3.11}$$

Here, the matrix U contain the column space of A which corresponds to information about the spectrum at different times. The matrix V contain the row space of A which represents the time evolution of the absorption at individual wavelengths. The third matrix, S, is a diagonal matrix and the values of the diagonal elements in S are weights (or so called singular values) that determines the importance, or equivalently, the relative amount of information in the columns in U and V. Each column of U and V will carry less relevant information in a progressive manner and this is reflected in the diagonal scalar values of S which also decreases until a plateau value of zero. The plateau value indicates that the columns after this point in U and V are superfluous and only carry noise. This is the first part of the SVD analysis which, as previously stated, has the main purpose of finding the number of independent components that can accurately describe the absorption spectra of the raw data in A. The next step is to reduce the matrices U, S and V and only keep the columns that are significant. The matrices are reduced based on analysis of the diagonal values in S and typically the significant columns are the ones before the previously described plateau value. This should also coincide with the columns in U and V, respectively, that do not show clear spectral features. All columns beyond the last significant column are discarded and the result is a reduced matrix A_r as seen in Equation 3.12.

$$A_r = U_r S_r V_r^T \tag{3.12}$$

It is important to note that at this point the independent orthogonal components from the reduced matrices U_r and V_r have no real physical meaning since there are an infinite number of solutions to Equation 3.11. This is where the second part of the SVD analysis enters the picture. The first step of this second part is to define a kinetic model describing how the different absorbing species are related to each other. This step is of paramount importance since there may be several models that can be fit to the experimental data. The model should be chosen while taking into account the number of significant components from the prior SVD analysis as well as any additional knowledge about the system the experimenter might have. An example of such a kinetic model is provided in Figure 3.8 where the concentration matrix (C) is found as the solution to the differential equation system involving the relevant combination of rate constants according to first order kinetics (which most photophysical processes are assumed to follow).

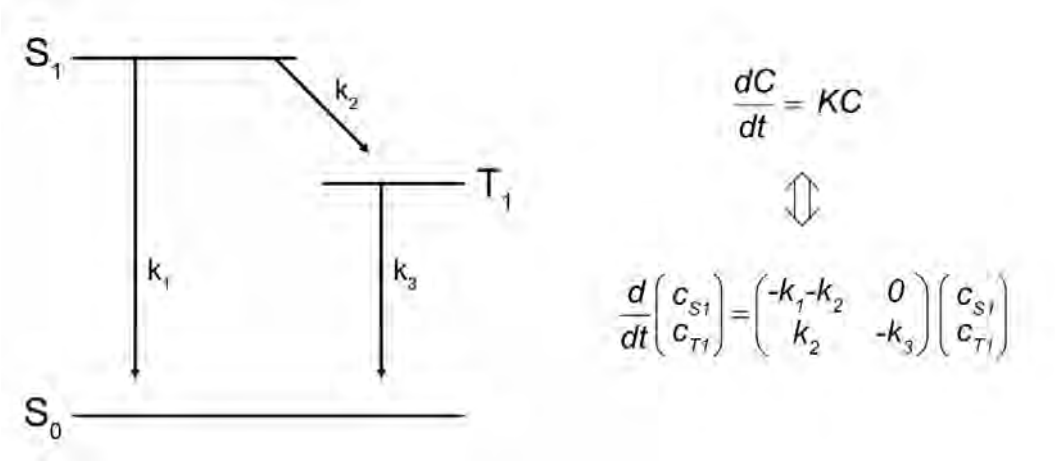

Figure 3.8: Left: Jablonski diagram of a hypothetical kinetic situation involving decay from a singlet excited state (S_1) to the ground state (S_0) or first triplet excited state (T_1). Right: Differential equation system for the kinetic scheme to the left.

The time dependent concentration matrix C is connected to V_r and is ultimately found by matrix rotation of V_r with the rotation matrix (R) according to Equation 3.13.

$$V_r = RC \tag{3.13}$$

Similarly, the true spectral components are found in Equation 3.14 by matrix rotation of U_r with the same rotation matrix resulting in a new matrix, B, which contains the true absorption spectra of each component according to the chosen model.

$$U_r = RB \tag{3.14}$$

The fitting process is repeated many times while minimizing the least square difference between the raw data matrix A and the simulated spectra which corresponds to the product of B and C: ($|A\text{-}BC|$).[123–125] The obtained spectral components are commonly referred to as evolution associated spectra (EAS) in the case of a consecutive model where one specie converts to another specie in a sequential manner (for instance: A→B→C→ground state). The spectral components can also be referred to as species associated spectra (SAS) if a specific model is applied which includes both parallel and sequential decays.[121]

SVD can be very helpful and valuable in the analysis of spectroscopic data. There are, however, several pitfalls that one should be aware of when analysing data using this method. One of the most important factors to consider is the impact of the initial start guesses for the fitted parameters. Start guesses are required to start the fitting process, but great care must be taken to make sure that the initial guesses are good enough. The reason for this is that the fitting algorithm tries to find a minimum in a multidimensional surface of the sum of the residuals vs. every parameter that can influence it (residuals refers to the difference between a measured and a fitted value). This multidimensional surface contains both local and global minima and

if the start guess is chosen poorly there is a risk that the starting point of the iteration is on the inner side of one of the local minima. This will result in that the solution converges to the local minimum and ultimately the wrong answer is obtained from the fitting procedure. One way to circumvent this problem is to try with a multitude of starting guesses and observe the robustness of the fit. Another commonly employed strategy is to initially lock certain parameters (the ones that the experimenter is most sure about) and let the remaining parameters be fit with this constraint. Once a fit has been achieved in this way one can release one parameter at a time and approach a solution that best fit the data. This is particularly useful in fits which involve many parameters. Care must also be taken to avoid overparameterization, which occurs when more parameters than necessary are used to fit the data. This often results in low robustness, *i.e.* that different solutions are obtained for different starting guesses while still having a more or less equal sum of square errors. In addition to checking for robustness, it is also possible to avoid overparameterization by analysing the dependency of each parameter with the others. Furthermore, overparameterization usually results in large standard error values. In conclusion, SVD is a powerful tool for analysis and deconvolution of complicated spectroscopic data, but it comes with certain limitations that must be considered. One of the the most important countermeasures against faulty fitting is the knowledge of the experimenter themselves and their ability to recognize some solutions as unrealistic or improbable.[123,125]

3.6 Cyclic Voltammetry

Cyclic voltammetry (CV) is a versatile electrochemical technique used to investigate the oxidation and reduction processes of chemical species in solution. It involves the application of a controlled potential to an electrode immersed in an electrolyte solution. Typically, the electrolyte solution comprises an organic solvent like dichloromethane or acetonitrile, along with dissolved ions that enhance the solution's conductivity. A schematic depiction of a CV setup can be observed in Figure 3.9. Within this setup, a sample holder contains the electrolyte solution and the dissolved sample, with three submerged electrodes connected to a potentiostat used to regulate the applied potential. The working electrode is where the electrochemical reactions of interest transpire, while the counter electrode plays a vital role in closing the electrical circuit. Lastly, the reference electrode serves as a stable and precisely known reference point for potential measurements within the electrochemical cell. It maintains a consistent potential throughout the measurement, which serves as a reference against which the potential of the working electrode is gauged. During a cyclic voltammetry experiment, the current passing through the electrode is monitored as a function of the applied potential. As the potential varies, electrochemical reactions take place at the electrode surface, leading to fluctuations in the current. These current changes serve as indicators of the oxidation and reduction processes of the analyte species. The outcome of a CV experiment is a voltammogram. An example of a voltammogram displaying a single reversible oxidation and reduction peak is exhibited on the computer monitor in Figure 3.9. Typically, such a voltammogram exhibits a distinctive "duck"-shaped curve, a characteristic arising from the diffusion of reactants towards the electrode surface.

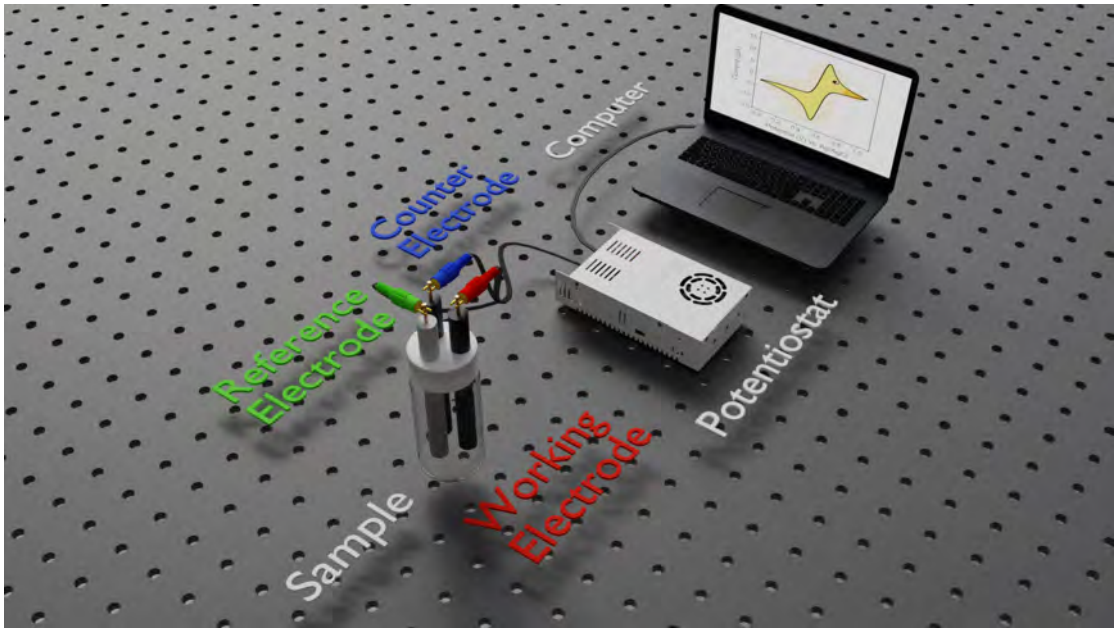

Figure 3.9: A 3D schematic model illustrating a cyclic voltammetry instrumental setup.

3.7 Spectroelectrochemistry

Spectroelectrochemistry encompasses a diverse range of techniques that combine spectroscopy with electrochemistry. In this thesis, the focus is narrowed down to the application of steady-state absorption spectroscopy at various applied potentials. This setup allows for investigation of the spectroscopic signatures of different redox species of a compound by continuously monitoring absorption while applying a potential associated with a specific redox transition. Figure 3.10 illustrates the experimental configuration, which bears foundational resemblance to the CV setup in Figure 3.9. Both setups necessitate a potentiostat, electrolyte solution, along with working, counter, and reference electrodes. However, in the context of spectroelectrochemistry, the working electrode assumes the form of a honeycomb structure, facilitating light transmission in close proximity to the electrode surface. It is worth noting that, for clarity, the perforations in the honeycomb electrode shown in Figure 3.10 are not depicted to scale; they are indeed much smaller in reality. When an experiment is conducted an optical fiber guides the probe light to the electrode interface, and after passing through the honeycomb electrode, another optical fiber collects it and directs it towards a spectrometer connected to a computer. The choice of a short cuvette path length is deliberate, aiming to ensure that the probed sample volume predominantly comprises the redox species under investigation, while minimizing the influence of unoxidized/reduced species in the bulk solution.

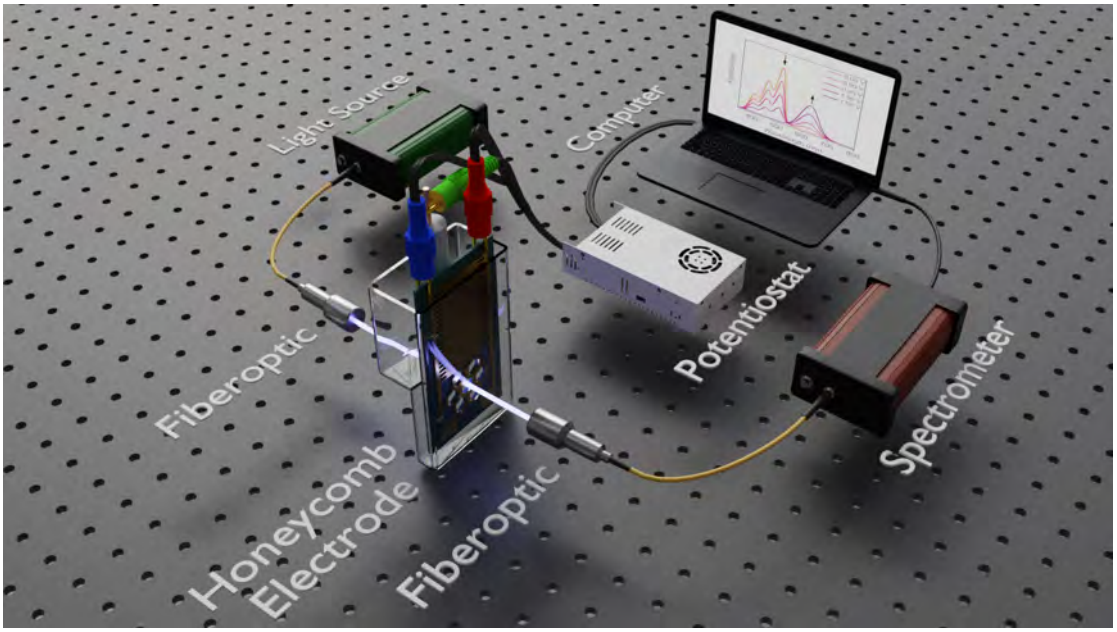

Figure 3.10: A 3D schematic model illustrating a spectroelectrochemistry instrumental setup.

Chapter 4
Heterogenous Intramolecular Singlet Fission

Dimers and other smaller oligomers undergoing intramolecular SF are frequently regarded as static entities, with conclusions typically derived from the optimized structure obtained through methods such as density functional theory (DFT). However, it is crucial to recognize that even small oligomers can exhibit varying degrees of flexibility and that this flexibility can have a substantial impact on their photophysical properties. In pursuit of understanding these dynamics, the investigation undertaken in **Paper I**,[126] summarized in this chapter, aimed to unveil the influence of conformational geometry on the rate of intramolecular SF and the subsequent lifetime of the resulting triplet-pair.

4.1 Molecular Rotational Conformation and Singlet Fission

To achieve this objective, three pentacene dimers were synthesized. Their molecular structures are depicted in Figure 4.1, alongside the structure of the pentacene monomer 6,13-Bis(triisopropylsilylethynyl)pentacene (**PM**), a well-known SF molecule. In all three dimers, the pentacene moieties are linked by a 1,4-diethynylphenylene spacer, designed to permit rotation of the pentacene units relative to each other. Two of the dimers underwent further modifications, incorporating substituents on the central phenylene unit. The substantial size and bulkiness of these substituents introduce steric hindrance, restricting rotational freedom and additionally shifts the equilibrium distribution of the conformational geometries. Figure 4.1b displays the steady-state absorption spectra of **PM** and the three dimers at room temperature. Although there are evident general similarities between the dimer and monomer spectra, notable differences suggest significant electronic interaction between the pentacene moieties. Furthermore, the absorption bands of the dimers are broadened relative to the spectra of the monomer. This can be interpreted as that each dimer can adopt a diverse array of conformations, attributed to the rotational freedom around the ethynyl groups in the spacer.[127,128] Thus, at room temperature there will be a distribution of conformations each with absorption transitions at slightly different energies. To substantiate this observation, DFT calculations were conducted to investigate the rotational freedom of each dimer around the central diethynylphenylene spacer.

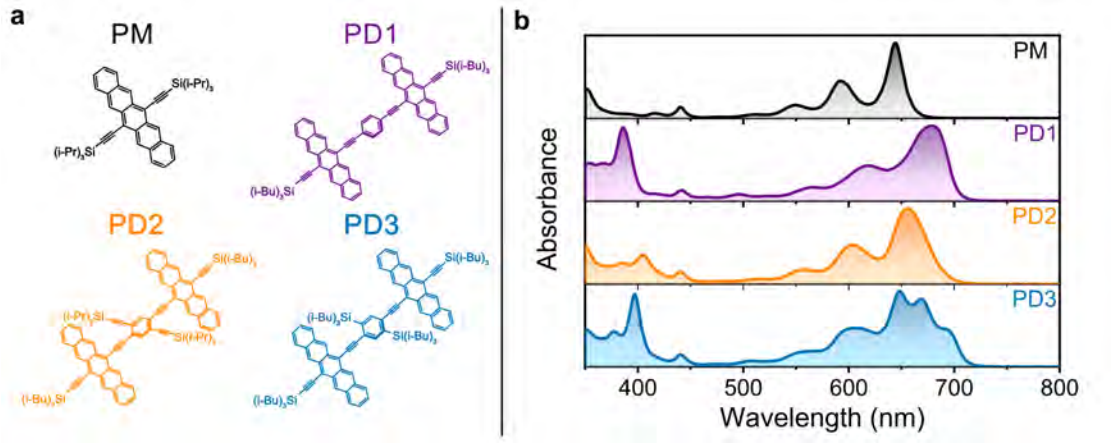

Figure 4.1: a) Molecular structures of 6,13-bis(triisopropylsilylethynyl)pentacene (**PM**) and the dimers **PD1**, **PD2** and **PD3** investigated in this study. b) Steady state absorption spectra of PM and the dimers.

This involved initially calculating the lowest energy conformations that the dimers could adopt. The optimal structure is influenced by the extent of conjugation across the entire molecule, leading to a reduction in potential energy, and by repulsive forces stemming from the steric hindrance caused by the bulky side groups on the central phenylene unit, which elevate the potential energy of the system. The resulting optimum structures are illustrated in Figure 4.2a.

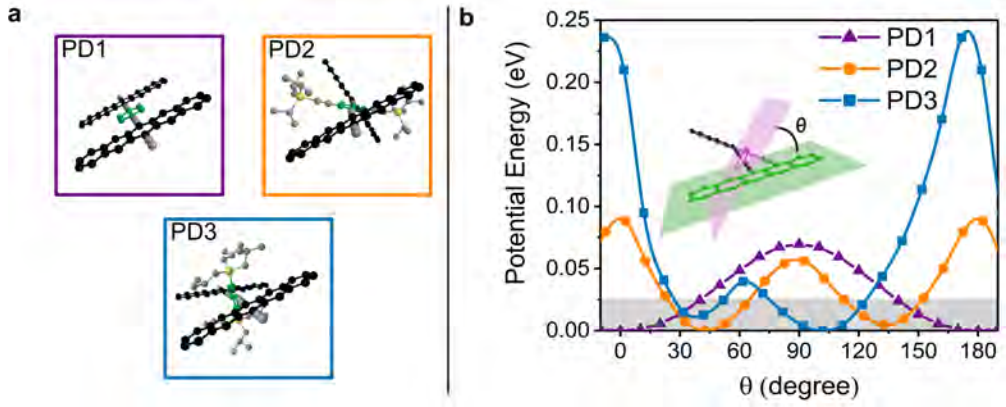

Figure 4.2: a) Lowest energy conformations of **PD1**, **PD2** and **PD3**. b) Potential energy landscape obtained by scanning over a range of dihedral angles θ. Thermal energy at 295 K is highlighted by the shaded area.

The unsubstituted dimer, **PD1**, adopts a perfectly coplanar structure in its lowest energy conformation. In contrast, **PD2** and **PD3** exhibit more twisted conformations due to steric hindrance. These conformations are however merely the conformations that the molecules will adopt at 0 K. At room temperature there will, as previously stated, exist a distribution of conformations. To characterize the potential energy landscape V(θ) for different conformations relative to the lowest energy conformation, a relaxed scan of the dihedral angle θ was conducted. In this context, θ is defined as the angle formed between the plane of one of the pentacene units and the plane created by the central phenylene unit, as illustrated in the inset of Figure 4.2b. The term "relaxed scan" implies setting θ to a specific value and allowing all other coordinates to relax,

determining the lowest energy conformation for that particular θ. The result of the relaxed scan is shown in Figure 4.2b where thermal energy at 295 K is included as the shaded area. The scan reveals a multitude of conformations closely matched in energy to the lowest energy conformations, indicating their coexistence in a room temperature sample. Additionally, the scan highlights that the rotational barrier is most substantial for **PD3**, followed by **PD2**, and is least for **PD1**. This information is crucial for interpreting the fsTA measurements of the dimers, as illustrated in Figure 4.3.

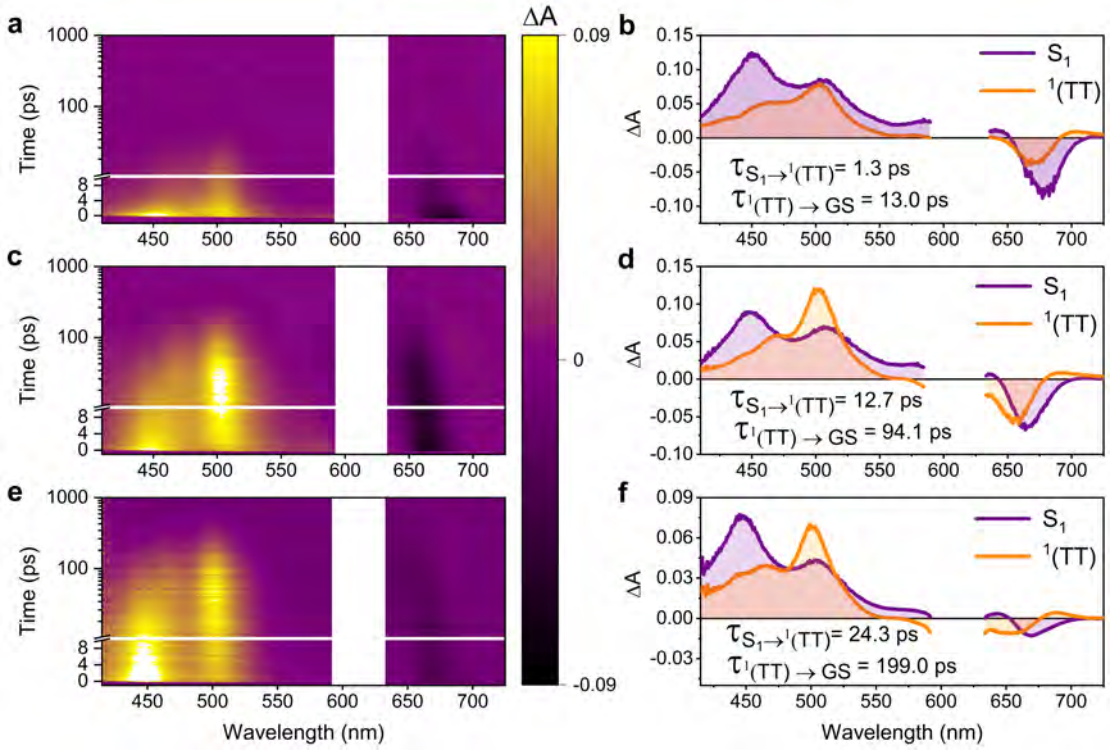

Figure 4.3: Room temperature fsTA spectra and corresponding evolution associated spectra (EAS) of dimers (a and b) **PD1**, (c and d) **PD2**, and (e and f) **PD3**. The kinetics of all three dimers could be accurately described by a two-component sequential model $S_1 \rightarrow {}^1(TT) \rightarrow$ ground state (GS) using global analysis with components and lifetimes indicated in the figure. The measurements were performed in toluene with a pump pulse at 612 nm and the pump scatter near the excitation wavelength has been removed for clarity.

fsTA was used to experimentally determine the influence of the central phenylene unit substitutions on the SF dynamics. The room temperature fsTA spectra and their corresponding evolution associated spectra (EAS) of all the dimers are presented in Figure 4.3. All of the dimers can be accurately modeled with a consecutive model of two components where the first converts to the second. The two components have a unique spectroscopic signature but are more or less identical across the dimer series. The first component is in all cases formed immediately following excitation and display absorption maxima at 460 and 510 nm. This initial component is attributed to the absorption of the singlet excited state S_1, given its instantaneous formation, and aligns with the initial spectra of the monomer **PM** in solution. The singlet excited state has a

very short lifetime and evolves into the second component within 1 to 25 ps for every dimer. The second component is assigned to be the correlated triplet pair ^{1}(TT) based on its similarity with the sensitized triplet spectra as seen in Figure 4.4 where the sensitized triplet spectra of **PD2** is compared to the second component from the fsTA spectra in Figure 4.3. **PD2** is just shown as an example here and the ^{1}(TT) component of **PD1** och **PD3** also match their corresponding sensitized triplet spectra as can be seen in **Paper I**.

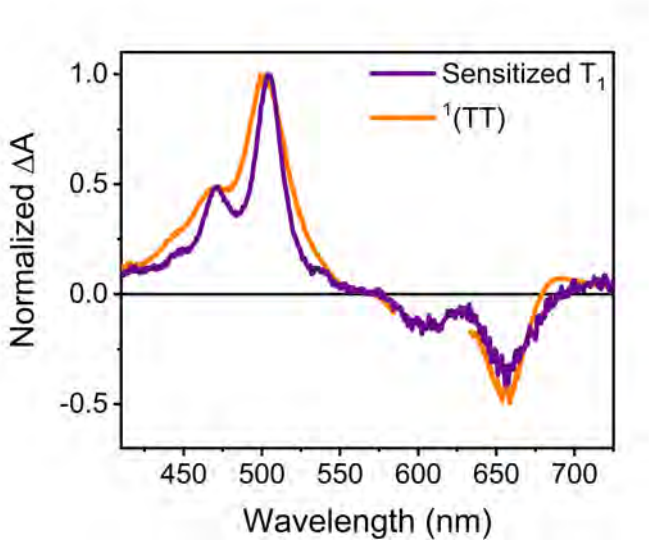

Figure 4.4: Sensitized triplet excited state spectra (purple) of **PD2** obtained via triplet energy transfer from platinum octaethylporphyrin (**PtOEP**) in toluene solution together with the triplet pair EAS of **PD2** (orange) obtained from the SVD analysis as shown in Figure 4.3. A similar comparison of sensitized triplet spectra and triplet pair EAS of **PD1** and **PD3** is presented in **Paper I**.

The ultra-fast formation of the triplet pair is solid evidence that the triplet formation observed is a result of SF and not ISC since ISC typically occurs on much longer time scales for organic molecules. Furthermore, the relatively short lifetime of sub 200 ps in the longest case for **PD3** indicates that no fully independent triplet states are formed and that the correlated triplet-pair is deactivated to the ground state before the triplets can dissociate. Notably, the rate of both triplet pair formation and decay follows the trend of rotational freedom, with **PD1** exhibiting the highest rates, followed by **PD2**, and finally **PD3**—a sequence that aligns with their respective degrees of rotational restriction. From the presented results, it emerges that the fsTA spectra herein represent the average SF kinetics of a distribution of different conformers. Some conformers demonstrate rapid and efficient SF, while others exhibit slightly slower dynamics. On average, the more constrained and twisted dimers, such as **PD2** and, to an even greater extent, **PD3**, display less efficient SF.

To further support the hypothesis that the different conformers present in the sample have absorption transitions at different energies, time dependent DFT (TD-DFT) calculations were employed. The result of these calculations are presented in the top part of Figure 4.5. The calculations were done for the different orientations shown in the inset where the central phenyl unit

is represented as a colored bar relative to the pentacene units which are represented as black bars. The vertical colored bars at various wavelengths represent the lowest energy transitions corresponding to a conformation of a specific orientation of the pentacene units relative to the central phenylene unit as indicated in the inset. The bottom part of Figure 4.5 show the steady state absorption of **PD1** and **PM** showing that the theory in general matches well with the experimental results. It should be noted that the calculation do not take vibrations into account and thus lack the vibronic progression that is observed in the experimental data. The calculations here shows that the more coplanar geometry of the conformer the more red-shifted is the absorption transition. This is reasonable since this conformation is expected to be the most conjugated and have the strongest electronic coupling. These results can also explain the blue shift of the GSB in the fsTA spectra in Figure 4.3 at ∼650 nm for later time delays between the pump and the probe. This blue shift likely corresponds to that the more red-shifted and more strongly coupled conformations undergo SF fast and efficiently while less strongly coupled conformers that have ground state absorption at shorter wavelengths remain in the excited state even at longer time delays.

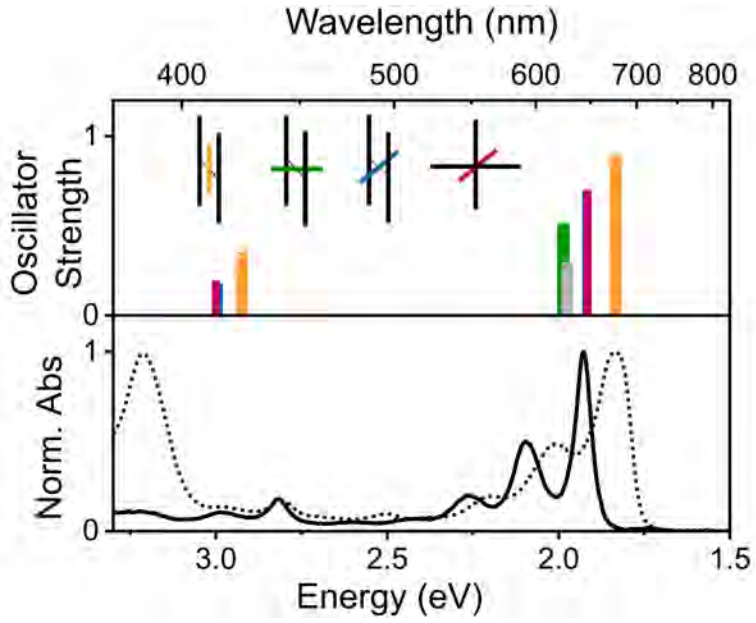

Figure 4.5: Top: Lowest energy transitions in different conformations of an unsubstituted pentacene dimer (**PD1**, orange, red, blue and green bars) and the monomer (**PM**, grey bar), calculated using TD-DFT. The inset illustrates the pentacene-phenylene-pentacene geometry of the respective conformer. The shorter colored bars represent the phenylene-bridge unit at different dihedral angles and the longer black bars represent the pentacene moieties. Note that the blue and red conformations with $\theta = 45°$ have very similar transition energies and oscillator strengths causing their bars to overlap. Bottom: Steady state absorption spectra of **PD1** (dashed) and **PM** (solid) in toluene.

4.2 Selective Excitation of Rotational Conformers

Based on the above results we speculated that it could be possible to selectively photoexcite different conformers and observe different SF rates for the same dimer molecule by simply using different excitation wavelengths. However, as previously mentioned and demonstrated, at room temperature the different conformations have overlapping absorption bands leading to excitation of a range of conformers at any given excitation wavelength. A solution to this could be to lower the temperature since this could provide a more narrow distribution. An estimation of the distribution of conformers at different temperatures can be obtained by using the relative potential energy V(θ) of the various conformers in Figure 4.2 in the Boltzmann distribution function presented in Equation 4.1.

$$P(\theta, T) = \frac{e^{-V(\theta)/k_b T}}{\int e^{-V(\theta)/k_b T} d\theta} \tag{4.1}$$

The resulting probability distribution as a function of the dihedral angle θ and temperature is shown in Figure 4.6.

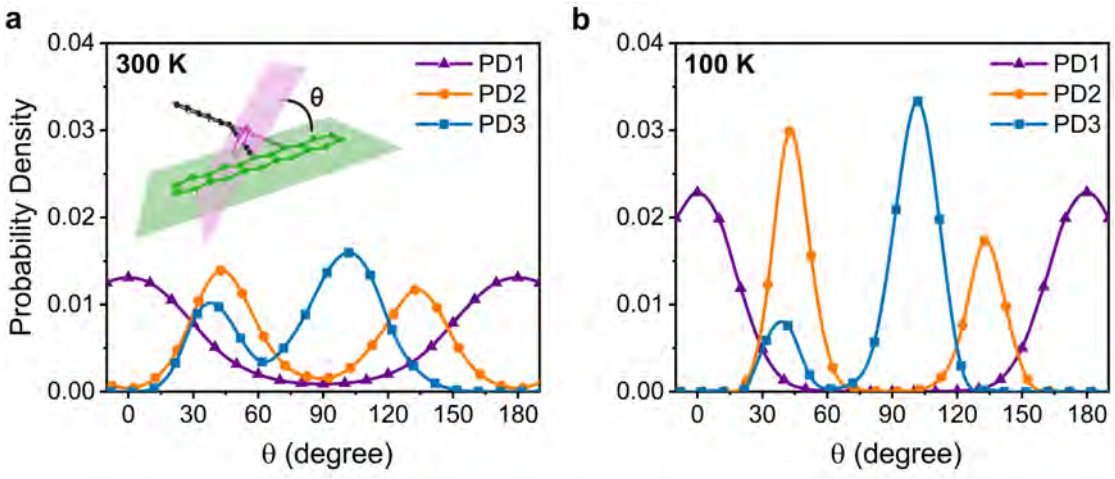

Figure 4.6: Probability distribution function of the dimers' rotational conformers at 300 K and 100 K.

At room temperature, a large range of conformers are available to **PD1**, **PD2**, and **PD3**. However, the probability distribution is significantly narrower at 100 K and at this low temperature a larger fraction of the dimers belong the the conformers of lower energy. Indeed, the steady state absorption of **PD3** in Figure 4.7a) shows that the absorption bands become narrower and more clearly resolved at 100 K compared to room temperature. **PD3** is shown as an example here but similar changes are observed for all dimers upon cooling. Notably, the red-edge of the lowest energy absorption band grows significantly. This is an indication that a large fraction of the dimers in the sample adopt a more strongly coupled conformation with red-shifted absorption at lower temperatures. This conclusion is supported by both the blue shift of the GSB at longer time delays in the fsTA room temperature measurements in Figure 4.3 and the theoretical calculations in Figure 4.5 where it was shown that more co planar conformations have absorption at lower energy. Based on these findings, fsTA measurements at 100 K in 2-methyltetrahydrofuran (MTHF)

were performed on all of the dimers. Figure 4.7b) show the single wavelengths dynamics of the triplet pair of **PD3** when excited with different excitation wavelengths.

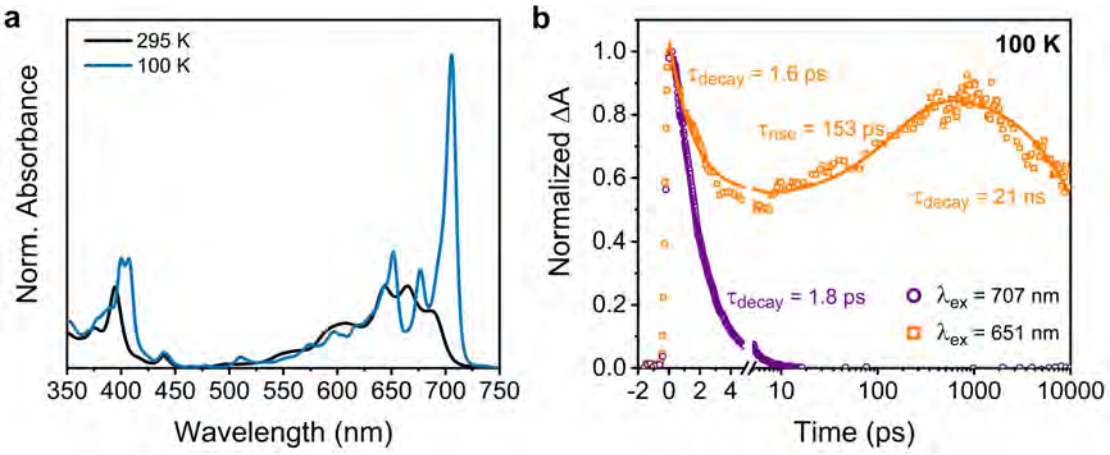

Figure 4.7: a) Steady state absorption spectra of **PD3** at 295 K and 100 K in MTHF. b) fsTA single wavelength kinetics of the triplet-pair peak of **PD3** at 505 nm for with an excitation wavelength (λ_{ex}) of 707 nm and 651 nm at 100 K in MTHF.

Exciting at the red edge of the steady state absorption at 707 nm the formation of the triplet pair occurs within the instrument response time of our fsTA system (∼250 fs). With this excitation wavelength the triplet pair also decays very rapidly with a lifetime of roughly 1.8 ps. In contrast, when shifting the excitation wavelength to 651 nm the kinetics are more complicated and involves species with several different lifetimes. There is a slower rise of the signal at later times where a species form in 153 ps and decay in 21 ns suggesting that excitation at 651 nm results in the population of a more weakly coupled conformer that performs slower SF. Furthermore, it appears as if this excitation wavelength also excites a very strongly coupled conformer that displays kinetics similar to the one that was observed with excitation at 707 nm. The reason for this is likely due to the fact that the conformer with its first absorption transition at 707 nm has a vibronic progression that extends to shorter wavelengths and overlaps partly with conformers of weaker coupling at higher energy.

4.3 The Effect of Viscosity on Excited State Dynamics

The fsTA measurements at 100 K in MTHF reveals that the conformers that are not strongly coupled have much longer triplet pair lifetimes compared to the lifetimes observed at room temperature. At 100 K, MTHF is close to the glass transition temperature and will be highly viscous or even more or less solid.[129] In this environment the movement of the dissolved molecules will be limited and the rotation of the pentacene moieties relative to one another in the dimers will be very slow. It is possible that the limited rotational freedom in this environment is the underlying reason for the longer triplet lifetimes. To gain more insight into the excited state dynamics and its dependence on viscosity, fsTA was performed on the dimers dissolved in highly viscous polystyrene films. The single wavelength fsTA kinetics of the triplet pair at 505 nm for **PD3** is

presented in Figure 4.8 where the rate of formation and decay of the triplet pair in toluene and in polystyrene are compared. Interestingly, the rate of formation of the triplet pair, *i.e.* the SF rate, is similar in the high and low viscosity environment as can be seen by comparing the rise times of the signal which is 28 ps for toluene and 46 ps for polystyrene. However, the lifetime of the triplet pair is almost 45 times longer in polystyrene. Keeping in mind that these measurements were performed at room temperature and thus gives the average kinetics of many conformers, this result indicates that the SF event that initially produces the correlated triplet pair is not strongly dependent on conformational changes in the excited state. In contrast, it seems that the decay of the triplet pair to a larger degree requires a conformational change to a more strongly coupled geometry.

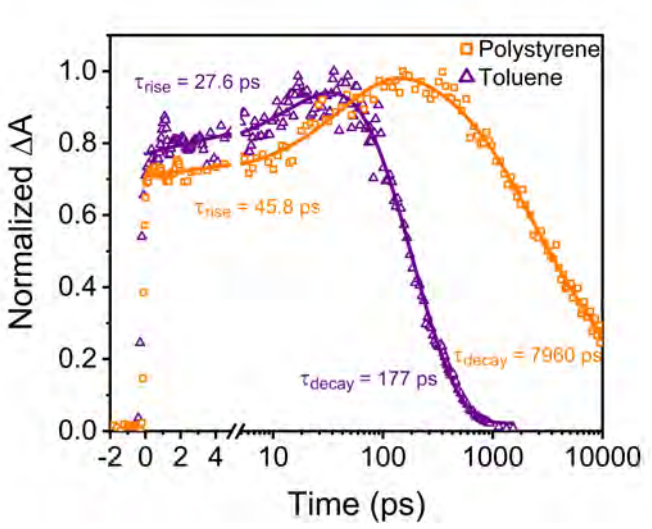

Figure 4.8: Room temperature fsTA single wavelength kinetics of the triplet-pair peak of **PD3** at 505 nm in toluene and in polystyrene obtained with a pump pulse at 612 nm.

Chapter 5

Fission Impossible

The exploration of SF mechanisms, as exemplified by the insights derived from **Paper I** discussed in the preceding chapter, along with various other studies, have enriched our understanding of SF across diverse molecular systems. Despite these advancements, numerous questions persist, and the intricacies of SF continue to be contingent upon the specific characteristics of each individual SF system. In addition to the incomplete mechanistic understanding of SF, a crucial challenge in the field stems from the scarcity of molecules capable of undergoing SF. Moreover, those few molecules that do exhibit SF often suffer from instability under light irradiation, coupled with suboptimal triplet energies that limit their practical utility. For instance, one of the most well-studied SF molecules to date, TIPS-pentacene, possesses a triplet energy of approximately 0.85 eV,[62,130,131] rendering it incompatible with the bandgap of silicon at ca. 1.1 eV.[132,133] This unfavorable matching underscores a significant hurdle in the application of such molecules. Clearly, there is an urgent need for the expansion of the SF library to address these limitations. Motivated by this necessity, **Paper II**,[134] which is summarized in this chapter, focuses on investigating the SF capabilities of a 9,10-bis(phenylethynyl)anthracene (BPEA) monomer, dimer, and trimer in solution. BPEA is a robust and photostable industrial dye with a triplet energy in the range of 1.25-1.35 eV.[135] BPEA has been shown to undergo SF in both thin films and in nanoparticles.[136–139] However, studies using molecular dimers mimicking the slip-stacked nature of solid-state packing have suffered from low yields of SF due to competing excimer formation.[140] Excimer formation has also been detected in alternative SF systems, negatively impacting the overall SF yield.[80,141] However, both excimer formation and SF are heavily dependent on the packing and relative orientation of the two interacting molecules.[53,83,142,143] This observation, coupled with the fact that theoretical calculations suggest that $E(S_1) \geq 2E(T_1)$ for BPEA,[135] it is possible that there are molecular designs that can suppress the excimer decay pathway and promote SF. For this reason, the photophysics of a dimer and trimer with the BPEA moieties connected in the meta position of the central phenylene unit was investigated.

5.1 Absorption and Emission Dynamics

The molecular structures of the monomer (**BPEAmono**), dimer (**BPEAdim**) and trimer (**BPEAtri**) are presented together with their corresponding steady state absorption and emission spectra

in Figure 5.1. The unstructured absorption, which is especially prominent for the monomer, in contrast to the structured emission can be explained by excited state planarization and has previously been studied in detail.[144]

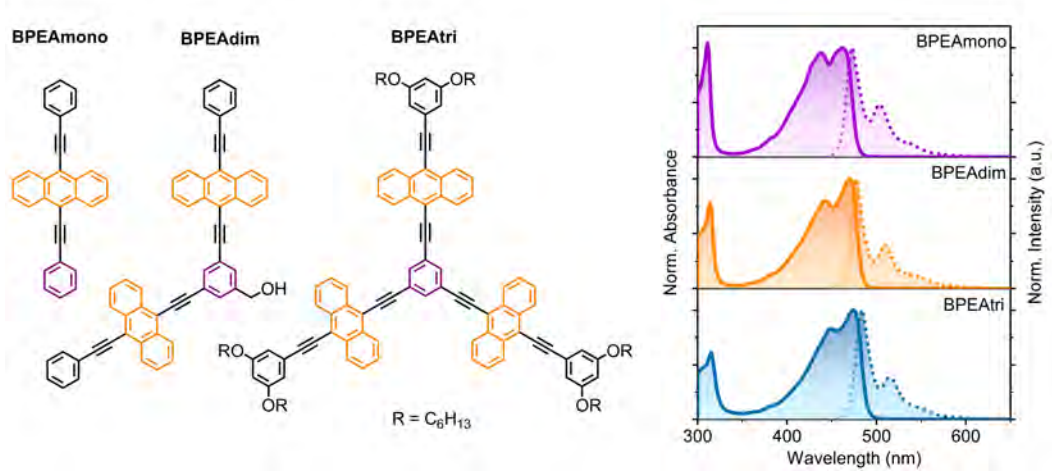

Figure 5.1: Molecular structures of **BPEAmono**, **BPEAdim** and **BPEAtri** together with their normalized steady state absorption and emission spectra.

The emission dynamics further reveal that as the concentration of **BPEAmono** in tetrahydrofuran (THF, $\epsilon = 7.58$) is increased, there is a gradual decrease in fluorescence lifetime as shown in Figure 5.2a. This behaviour is similar to other studies of intermolecular SF in solution where the increased concentration leads to a larger probability of intermolecular collisions.[50,51] However, no triplet formation could be observed using transient absorption suggesting that SF is not the reason for the quenched fluorescence. Emission measurements conducted under TIR conditions to avoid secondary inner-filter effects as shown in Figure 5.2b instead indicate that one of the main decay pathways is excimer formation. This is evidenced by the growth of a new emission band at lower energy. It is possible that the inclination towards excimer formation could explain the poor TTA-UC yields previously reported for **BPEAmono**.[135]

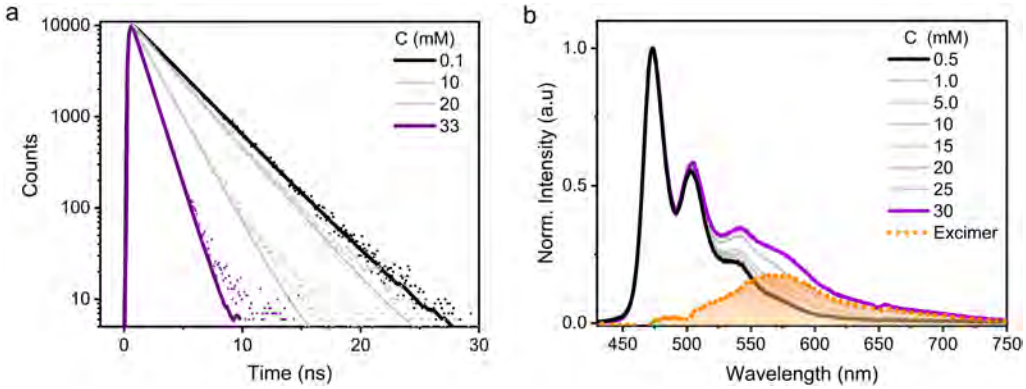

Figure 5.2: Emission characteristics of **BPEAmono** in THF at various concentrations. a) Fluorescence lifetime measured with $\lambda_{ex} = 405$ nm and probed at 473 nm. b) Steady state emission measured under TIR conditions with $\lambda_{ex} = 440$ nm. The excimer emission spectra is the difference spectrum of the 0.5 mM and 30 mM sample.

5.2 Charge Separation and Triplet Formation of BPEAdim

For **BPEAdim**, the absence of excimer formation is evident from the resemblance in the emission spectra of **BPEAdim** and **BPEAmono** in dilute solution, as illustrated in Figure 5.1. This similarity extends to the emission lifetime in non-polar solvents, with **BPEAdim** exhibiting a lifetime of 3.2 ns and **BPEAmono** 3.3 ns, suggesting the absence of substantial new decay pathways due to dimerization (see Figure 5.3a). However, in polar solvents, the emission of **BPEAdim** experiences a significant decay within the response function of the TCSPC instrument, as depicted in Figure 5.3a. To unravel the quenching mechanism, we employed fsTA. Initially, **BPEAdim** was investigated in THF, see Figure 5.3b, as a reference to better understand the more intricate dynamics in polar solvents, which will be presented shortly.

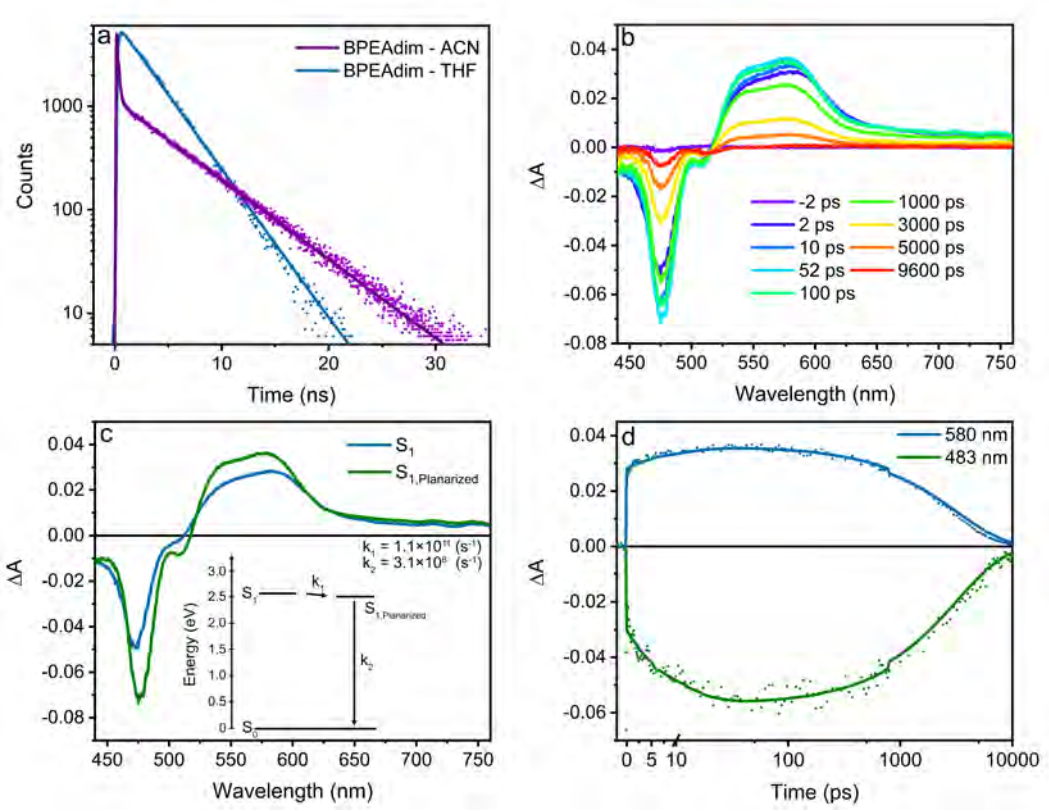

Figure 5.3: a) Time resolved emission of **BPEAdim** in ACN and THF obtained with λ_{ex} = 405 nm and monitored at 473 nm. b) fsTA analyses of **BPEAdim** in a dilute solution of THF (∼10 μM); excitation at 420 nm. c) Species associated spectra of the SVD analysis using the kinetic model shown in the inset. d) Selected kinetics of ground-state bleach and stimulated emission at 483 nm and S_1 excited state absorption at 580 nm with the model data shown as a solid line.

The fsTA spectral evolution in THF closely parallels that of the monomer in dilute solution, a correlation anticipated due to the previously discussed similarity in emission behavior. The fsTA could be satisfactorily fit to a two component sequantial model using SVD and global analysis and the obtained spectral components are shown in Figure 5.3c. Initially, an S_1 excited state absorption emerged at 560 nm, evolving as a result of excited state planarization. The growth

of the GSB and S_1 absorption signals indicates the formation of the planarized conformation, $S_{1,planarized}$, the second component of the kinetic model. After planarization, the spectra decay uniformly, exhibiting a lifetime consistent with that obtained through TCSPC.

In the more polar solvent acetonitrile (ACN, $\epsilon = 37.5$), where the fluorescence is substantially quenched, the spectral evolution initially mirrors that observed in THF, as depicted in Figure 5.4a.

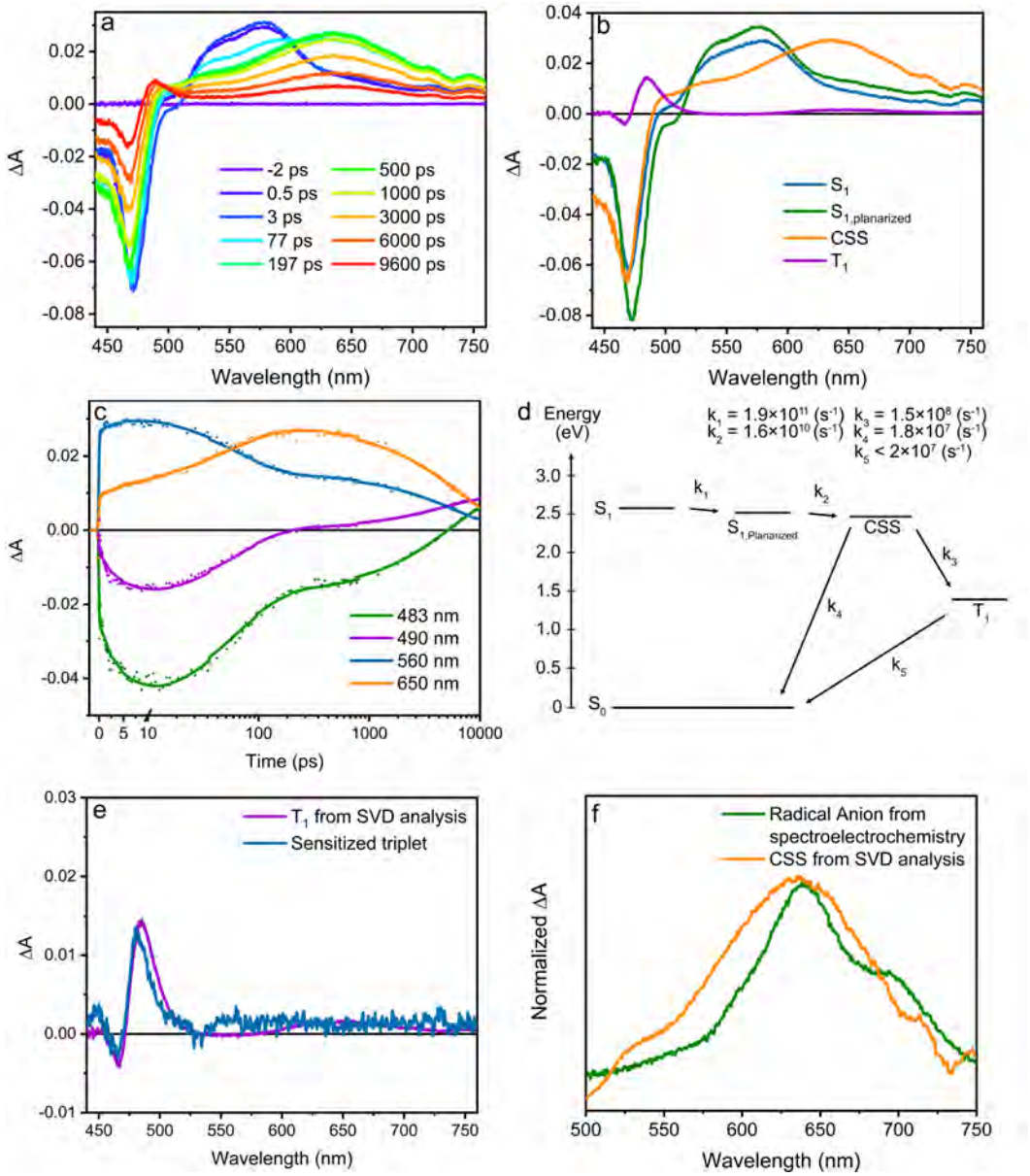

Figure 5.4: a) fsTA analyses of a dilute solution (∼5 μM) of **BPEAdim** in ACN; excitation at 420 nm. b) Species associated spectra of the SVD analysis using the model shown in panel d. c) Selected kinetics of ground state bleach/T_1 at 483 and 490 nm, S_1 at 560 nm and the CS state at 650 nm with the model data shown as a solid line. e) Comparison of the final spectral component from the SVD analysis and kinetic model compared to the sensitized triplet absorption spectrum. f) Comparison of the CS state spectral component with the radical anion obtained via spectroelectrochemical analysis.

Planarization occurs on comparable time-scales as in THF; however, following planarization, a new species emerges concurrently with the decay of the singlet excited state, leading to a broad excited state absorption at 640 nm. This new species, exhibiting a spectroscopic signature akin to the radical anion obtained through spectroelectrochemistry, see Figure 5.4f, is assigned as the CS state. Typically the spectroscopic characteristics of the CS state combine features from both the radical anion and cation. However, for **BPEAdim**, the spectrum of the radical cation has a markedly low molar absorptivity in the visible region compared to the anion and is consequently not used in the comparison to the fsTA data. As the CS state decays a new species with absorption centered at 490 nm becomes apparent, matching the sensitized triplet spectrum of **BPEAdim** which is shown in Figure 5.4e). Consequently, an additional two components, the CS state and the T_1 state, were necessary to model the fsTA data in ACN in addition to the two components observed in THF. The kinetic model is presented in Figure 5.4d, and the extracted spectral components and kinetics at selected wavelengths are illustrated in Figures 5.4b and 5.4c, respectively. The emergence of the triplet excited state signal after the decay of the CS state and complete absence of it in non-polar solvents suggests the formation of one independent triplet excited state per molecule through charge recombination via the CS state, rather than the formation of a correlated triplet pair through SF. Moreover, the lifetime of the triplet excited state was estimated to be in the microsecond time scale using nsTA as shown in **Paper II**. This lifetime significantly exceeds expected triplet-pair lifetimes for dimers with substantial through-bond electronic coupling, as evidenced by the findings in Chapter 4 and other studies, owing to the lack of triplet decorrelation and subsequent separation into free triplets.[53,145–147] The relatively slow rate of triplet formation compared to what is normally seen for the SOCT-ISC mechanism[148] coupled with the relatively large interchromophore center-to-center distance, which exceeds 10 Å, suggests that the mechanism governing triplet formation in this context is RP-ISC, which was described in Chapter 2.

In summary, SF does not appear to occur for the dimer. Despite this, the absence of SF in the dimer did not dissuade further exploration, leading to an investigation involving a trimer, **BPEAtri**, with an additional BPEA moiety attached in the final meta position as shown in Figure 5.1. While previous studies have demonstrated that an increase in the number of connected chromophores for slightly endothermic systems can elevate intramolecular SF rates due to entropy gains from delocalization,[56,149] no such effect was observed in our trimer, which exhibited photophysics very similar to that of the dimer. The details of this investigation can be found in **Paper II**. In addition to this, it was hypothesized that excitation of twisted conformations could lead to SF, given that the twisting of the dihedral angle θ between the two phenyls and anthracene theoretically augments the driving force for SF. This notion is supported by the notably steeper excited state potential of the S_1 state compared to the T_1 state, as depicted in Figure 5.5. Based on similar arguments as those presented in chapter 4 and other reports on BPEA[144] excitation at the red edge of the absorption spectra should primarily excite planar conformations. Conversely, higher energy excitation should primarily excite twisted conformations. However, the fsTA results obtained with an excitation wavelength of 420 nm in Figure 5.3 and 5.4, target-

ing twisted conformations, clearly demonstrate that planarization precedes SF in this particular case.

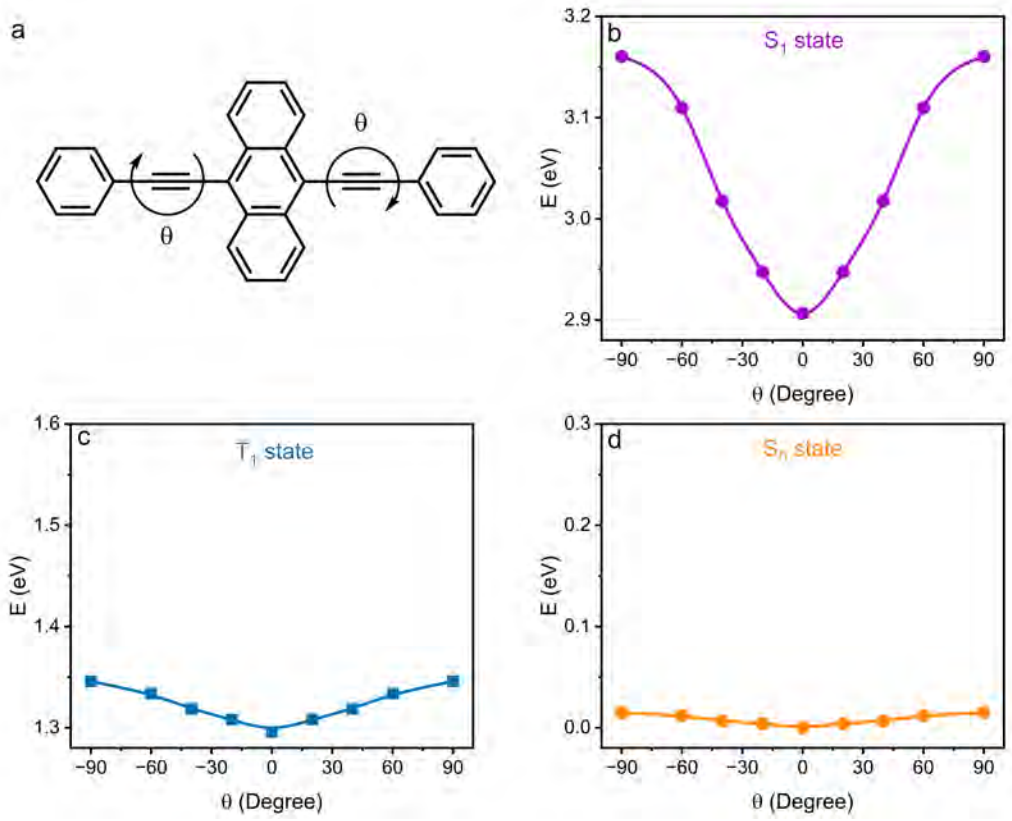

Figure 5.5: a) Molecular structure of **BPEAmono** indicating the dihedral angle θ between the two phenyls and anthracene. Calculated energy of the b) S_1 c) T_1 and d) S_0 states as a function of θ. Adapted from reference [135] with permission from the Royal Society of Chemistry.[135]

Despite the absence of SF, this study remains valuable as it unveils alternative pathways for triplet formation, often overlooked in the SF field. For instance, in BPEA thin films, the spectroscopic signature of the CS state has been observed previously, but have been attributed to a shifted and broadened S_1 absorption.[136] Our findings suggest that some of their triplet excited state formation might originate from a CR process. Indeed, CR as a mechanism for forming the triplet excited state has been proposed in other thin film systems, such as the indigo derivative cibalackrot, where transient intermediates with charge-transfer character are observed prior to triplet formation.[150] Moreover, anthracene has previously been demonstrated to form CS states in crystals.[151,152] This being said, it is worth noting that the interpretation of the spectral feature as a shifted and broadened S_1 absorption in BPEA thin films could be accurate. This consideration stems from the recognition that excited state absorption of various compounds, including polyacenes, can exhibit significant differences between solution and film states.[153–155]

Towards Singlet Fission Applications

Chapter 6

The shared objective of the two studies presented in this chapter is to identify methods for harnessing the energy of the two triplet excited states formed after the SF event. It should be emphasized that the investigation does not extend to the development of fully operational devices; rather, it serves as a step towards eventual implementation by exploring model systems. Two distinct projects with diverse objectives have been undertaken. The initial project, detailed in **Paper III**,[156] is centered around the integration of a known SF molecule, 1,3-diphenylisobenzofuran (DPIBF),[66,157,158] with semiconductor thin films. The primary goal is to investigate ET and SF dynamics when attached to thin films, examining the processes' dependencies on driving force and solvent environment. In the second project, still in a conceptual stage, we initiate the foundational steps towards a SF system based on supramolecular coordination cages. This system is envisioned to be able to incorporate a molecular electron acceptor, thereby opening up new opportunities for two-electron photocatalysis.

6.1 Singlet Fission on Semiconductor Thin Films

Conventional dye sensitized solar cells (DSSC) consist of a mesoporous semiconductor (often TiO_2) with an adsorbed dye to allow for a larger part of the solar spectrum to be utilized.[159] The focus of this project was to replace conventional dyes, which generate at best one electron-hole pair per absorbed photon, with a SF molecule capable of ideally transferring two electrons for each absorbed photon.[160] While previous studies have explored this concept, a lack of systematic investigations across various solvents and substrates motivated us to explore this further.[161] In our investigation, we paired a DPIBF-derivative named **DPIBF-C6** with three different mesoporous semiconductors; ZrO_2, TiO_2, and SnO_2. A schematic illustration of the attachment of **DPIBF-C6** to the semiconductor surfaces is illustrated in Figure 6.1. The semiconductors possess varying reduction potentials resulting in different CS state energies, **DPIBF-C6**$^+$/$MO_2{}^-$, as illustrated in the schematic energy diagram in Figure 6.1b. The energy diagram also presents the energy of the S_1 and T_1 states from which the ET driving force from each state to the respective semiconductors can be assessed. The S_1 energy was determined from the intersection of the absorption and emission spectrum which are presented in Figure 6.1c and the T_1 energy is based on a previously reported value.[162] It is essential to note that the energy diagram only provides a

rough approximation of the expected driving forces since it is known that mesoporous semiconductor conduction band energies can be influenced by factors such as morphology, solvent, pH, and adsorbed molecules.

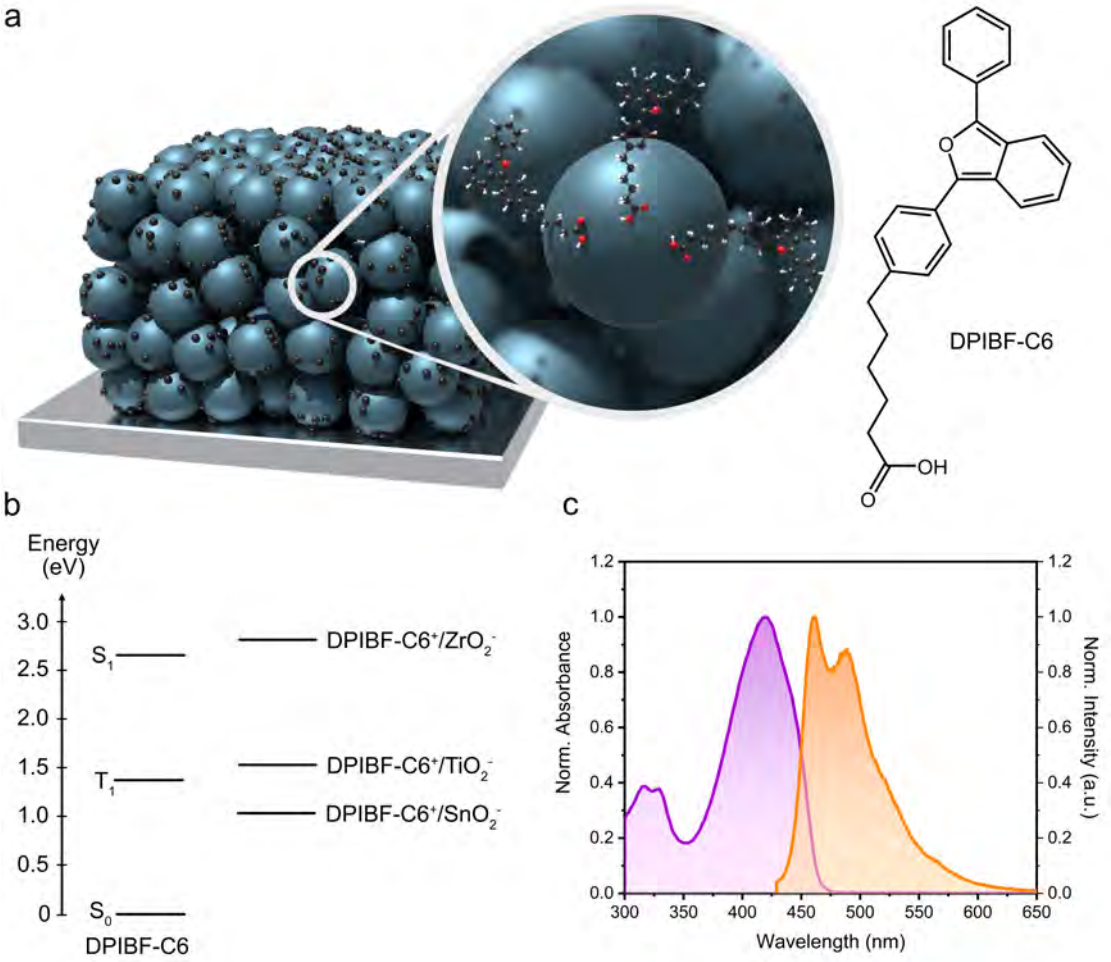

Figure 6.1: a) Schematic illustration of a thin film consisting of a mesoporous network of either SnO_2, TiO_2 or ZrO_2 on a glass substrate with **DPIBF-C6** chemisorbed to the surface of the semiconductor nanoparticles. b) Schematic energy diagram showing the **DPIBF-C6** S_1 and T_1 energies relative to the CS states of the respective mesoporous semiconductors used in this study which were estimated from the oxidation potential of DPIBF in ACN[67] and the conduction band energy levels of the semiconductors.[163,164] c) Steady state absorption and emission spectra of **DPIBF-C6** in toluene.

Initial measurements on the integrated thin film and **DPIBF-C6** systems utilized emission as a proxy to assess potential intermolecular or interfacial interactions. Figure 6.2a illustrates some of these measurements with **DPIBF-C6** attached to ZrO_2 at both low and high surface coverage. In contrast to the monoexponential lifetime observed in solution, the quenched emission of **DPIBF-C6** on ZrO_2 necessitates a multi-exponential model to accurately fit the data. Notably, the average lifetime becomes progressively more quenched with increasing surface concentration, suggesting the involvement of processes such as SF or other interactions requiring close molecular proximity. To get more information regarding the photophysical processes that occur on the

surface we turn to fs- and nsTA. We begin by examining **DPIBF-C6** in dilute solution before moving on to the more complicated dynamics of the thin film systems. Given DPIBF-C6s nearly unity fluorescence quantum yield in dilute solution, the fsTA spectra of **DPIBF-C6** in toluene (Figure 6.2b) primarily comprise ESA bands arising from S_1-S_n transitions, accompanied by negative contributions from SE and GSB. In addition to knowledge about the S_1 ESA, another essential element for understanding the transient absorption of the thin film systems is the T_1 absorption obtained via sensitization, depicted in Figure 6.2c.

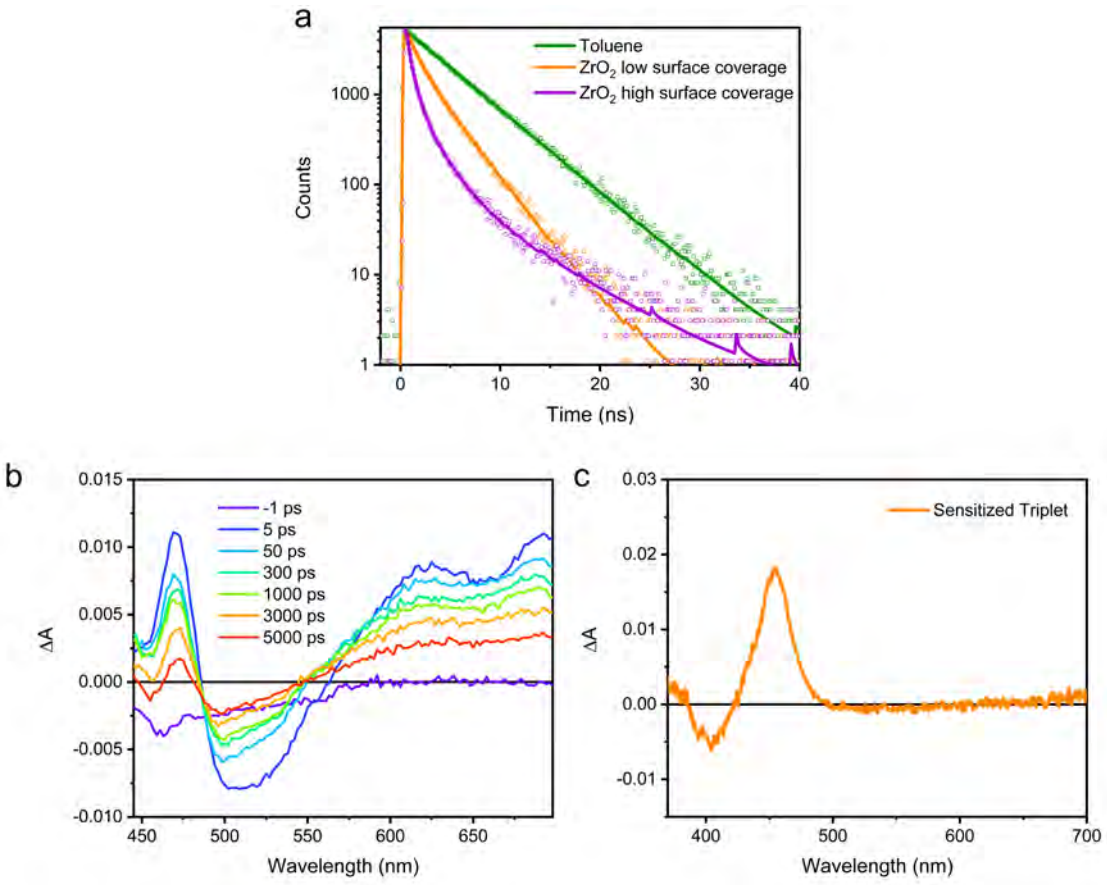

Figure 6.2: a) Time resolved emission of **DPIBF-C6** in toluene and when attached to ZrO_2 immersed in toluene with high (∼100 nmol/cm^2) and low (∼1 nmol/cm^2) surface coverage. The emission was monitored at 500 nm and the sample was excited at 405 nm. b) fsTA spectra of **DPIBF-C6** in solution. The fs measurements were performed in toluene with a pump pulse at 405 nm. c) Sensitized triplet excited state spectra of **DPIBF-C6** obtained via triplet energy transfer from **PtOEP** in toluene solution.

6.1.1 DPIBF-C6 attached to ZrO_2

As shown in the energy diagram in Figure 6.1b, when **DPIBF-C6** is affixed to ZrO_2, there is next to no driving force for ET from either the S_1 or the T_1 state. This prediction is corroborated by the fsTA measurements of **DPIBF-C6**/ZrO_2 in toluene shown in Figure 6.3a. Here, the initial spectra closely resembles the S_1 absorption that was observed when investigating **DPIBF-C6** free in solution. However, the singlet excited state decays much more rapidly compared to solution, which is in line with the substantially quenched fluorescence in Figure 6.2a. Furthermore, new

absorption bands that are not observed in solution become discernible as the S_1 ESA decays. Firstly, a feature centered around 550 nm evolves at early time delays. This ESA feature have in previous studies been demonstrated to originate from the DPIBF radical cation. The formation of the radical cation could be a result of either ET from **DPIBF-C6** forming **DPIBF-C6**$^+$/ZrO_2^- or alternatively the molecular CS state **DPIBF-C6**$^+$/**DPIBF-C6**$^-$ which lies close in energy to to the S_1 state. Additional measurements, shown in **Paper III**, reveals that the radical anion signal appears together with the radical cation when the more polar solvent ACN is used as surrounding solvent instead of toluene. This indicates that a molecular CS state is formed in the more polar solvent and that the presence of the radical cation alone in toluene could be a result of a small amount of ET from the S_1 state to ZrO_2 despite the small driving force. Importantly, at later time delays a signal centered at 460 nm which matches with the sensitized T_1 spectrum becomes discernible and the signal is also seen in the μs time scale using nsTA as seen in Figure 6.3b. The triplet formation could be a result of SF, but the rather weak signal indicate that the SF is not very efficient on the films even if considering that fact that the T_1 state has a slightly higher molar absorptivity than the S_1 state.[158]

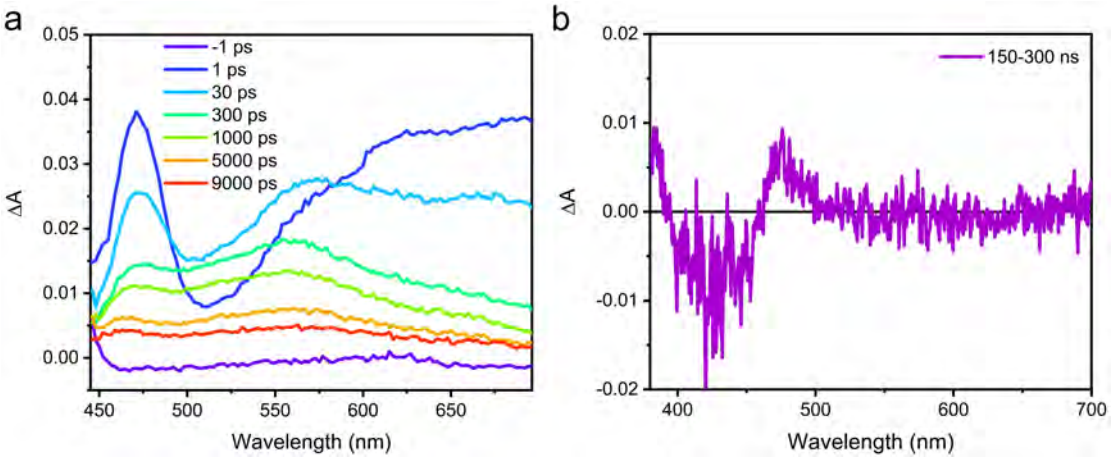

Figure 6.3: a) fsTA and b) nsTA spectra of **DPIBF-C6** attached to ZrO_2 in toluene using an excitation wavelength of 405 nm.

6.1.2 DPIBF-C6 attached to TiO_2

As depicted in the energy diagram of Figure 6.1b, the **DPIBF-C6**/TiO_2 system exhibits a large driving force for the formation of **DPIBF-C6**$^+$/TiO_2^- through electron transfer (ET) from the S_1 state. This increased driving force relative to **DPIBF-C6**/ZrO_2 is evident in the considerably stronger radical cation signal at 550 nm, which becomes more pronounced at early times, coinciding with the decay of the S_1 signal, as shown in Figure 6.4a. Surprisingly, despite the pronounced loss of S_1 states by direct ET from the S_1 state, the T_1 signal at 460 nm emerges as notably stronger in comparison to the **DPIBF-C6**/ZrO_2 assembly, where ET from the S_1 state occurs to a lesser extent. Since the decay of the radical cation at 550 nm is accompanied by a rise of the T_1 signal it is possible that the triplet formation is a result of charge recombination from the CB of TiO_2 to the T_1 state of **DPIBF-C6** rather than the ground state. Alternatively, it

is conceivable that SF of **DPIBF-C6** is more efficient on TiO_2 and occurs efficiently in paralell to the S_1 charge injection. The variation in SF rates on the different substrates may be attributed to differences in the morphology and size of nanoparticles comprising the mesoporous network. These disparities can result in distinct surface packings, consequently favoring for instance SF interactions over other decay pathways. Nevertheless, the persistence of the T_1 signal as the **DPIBF-C6**$^+$/TiO_2^- state decays suggests that ET from the T_1 state is relatively inefficient. This observation is further supported by the nanosecond transient absorption (nsTA) results, depicted in Figure 6.4b, where the T_1 signal is the sole species remaining on the microsecond time-scale.

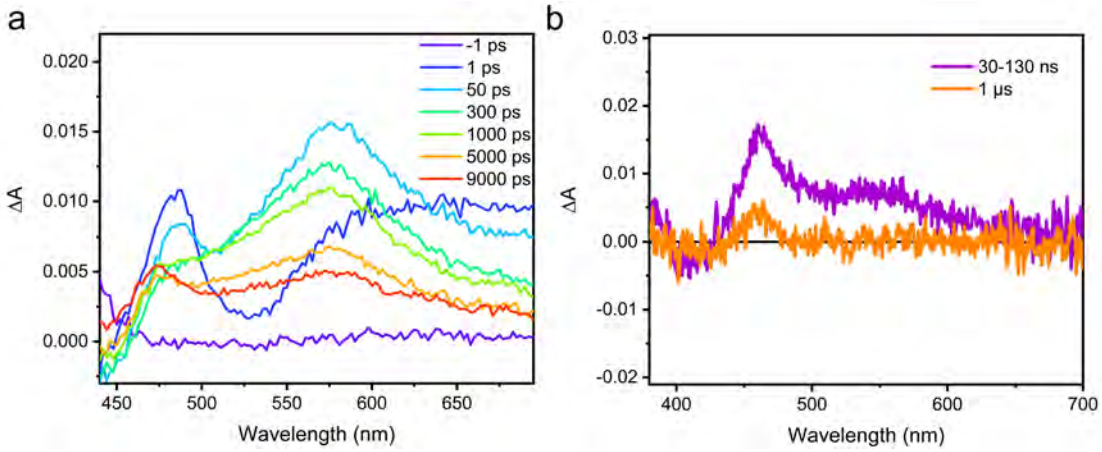

Figure 6.4: a) fsTA and b) nsTA spectra of **DPIBF-C6** attached to TiO_2 in toluene using an excitation wavelength of 405 nm.

6.1.3 DPIBF-C6 attached to SnO_2

The last semiconductor assembly under investigation, **DPIBF-C6**/SnO_2, exhibits the lowest lying CS state, as illustrated in the energy diagram of Figure 6.1b. In the fsTA measurements presented in Figure 6.5a the spectral evolution is similar to that observed in **DPIBF-C6**/TiO_2 implying once again a significant ET from the S_1 state and parallel formation of the T_1 state, likely through SF.

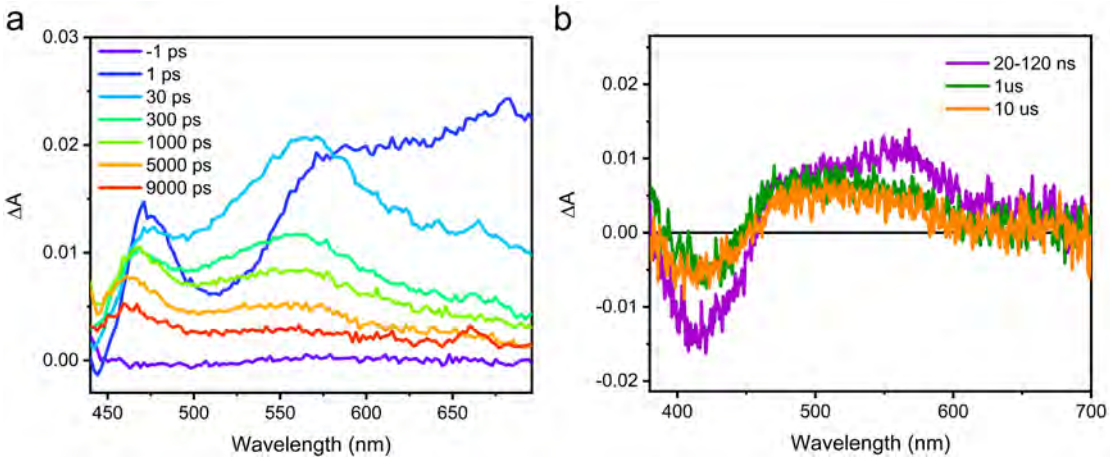

Figure 6.5: a) fsTA and b) nsTA spectra of **DPIBF-C6** attached to SnO_2 in toluene using an excitation wavelength of 405 nm.

However, **DPIBF-C6**/SnO_2 diverges notably in the nsTA measurements in Figure 6.5b, where there is an absence of discernible T_1 absorption. Instead, the nsTA spectra are dominated by the spectroscopic signature of the radical cation, indicating that the T_1 state has decayed due to ET. This observation aligns with the predictions based on the driving forces depicted in Figure 6.1b.

As a closing remark, it should be acknowledged that the conclusions drawn in this chapter may appear qualitative to the reader. This stems from the inherent nature of the study, where the significant instability of DPIBF due to its susceptibility to photooxidation, coupled with sample heterogeneity, poses challenges in accurately quantifying the kinetics and yields of the various processes. Despite these challenges, the study remains crucial as it underscores several obstacles associated with integrating SF into DSSCs. A paramount challenge to address is how to design systems that prevent ET from the S_1 state before SF can occur. In this project, the introduction of a saturated carbon chain aimed to increase the distance between the semiconductor surface and the DPIBF moiety, intending to, on average, slow down the ET rate. However, the efficient S_1 ET to both TiO_2 and SnO_2 suggests that this design strategy was not successful. Exploring alternatives such as using dimers and relying on intra- rather than intermolecular SF, or incorporating passivating layers, as explored in other studies,[165] could offer promising avenues to overcome these challenges.

6.2 Singlet Fission in Supramolecular Coordination Cages

Accumulative charge separation is a central concept in the conversion and storage of solar energy into fuels. The term originates from the fact that the fuel generating photocatalysis reactions often involve transfer of multiple electrons to form a particular product.[166] Consequently, since absorption of a single photon typically only gives rise to the formation of a single electron-hole pair, the reactions require sequential absorption of photons and accumulation of the formed CS states. Achieving this is not a trivial feat and considerable attention has been devoted to mitigating CR following the initial ET event.[167,168] However, there are still challenges associated with the known strategies such as formation of highly reactive intermediates resulting in low yields due to competing side reactions and the general issue of CR before a second photon can be absorbed. The ability of SF to produce two electron-hole pairs simultaneously from one photon consequently has potential to remedy some of the issues found in the field of accumulative charge transfer. Combining SF and photocatalysis presents a fascinating opportunity, but it also brings forth a unique set of challenges. One of the primary challenges stems from the requirement of strong electronic communication between at least two molecules for efficient SF to occur while simultaneously maintaining proximity to the electron acceptor. Ideally, this should be achieved without covalently linking the acceptor moiety to the SF unit since this would be impractical for any future applications if the reduced acceptor is the final desired product. Additionally, relying on diffusional encounters of the acceptor moiety and SF unit would likely not result in utilization of both triplet excited states. This is due to the short lifetime of diffusional encounter complexes, coupled with their essentially singular geometric arrangement which is not conducive

to facilitating efficient electron transfer from both sites of the singlet fission molecule where the triplets are localized. One possible solution, which is explored in this chapter, is to construct supramolecular coordination complexes based on SF capable ligands that can self-assemble to form cage structures such as the one shown schematically in Figure 6.6a.

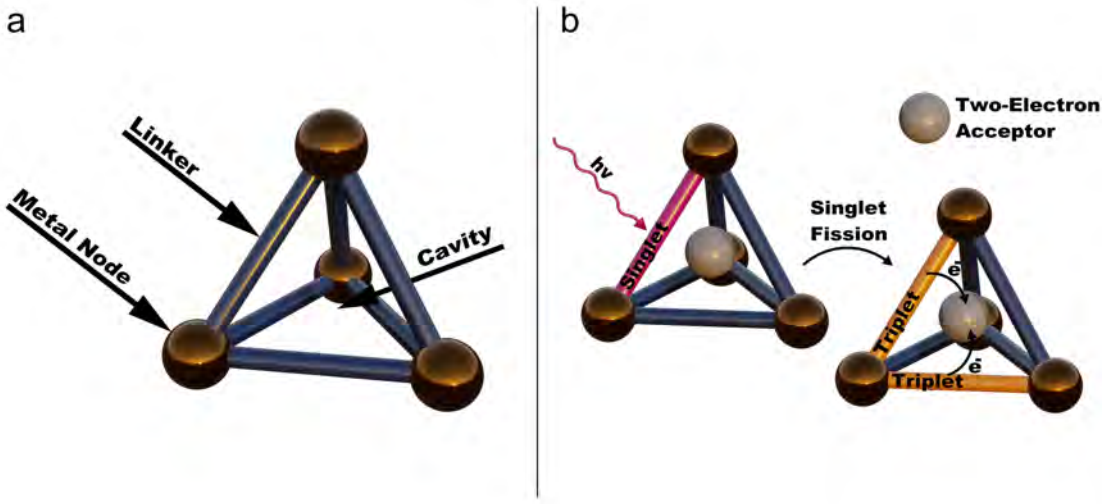

Figure 6.6: a) Schematic of the supramolecular coordination complex. b) Schematic illustration of SF occurring and subsequent ET from the formed triplet excited states to the two-electron acceptor.

For this project we are interested in a tetrahedral coordination cage that provides a single, defined cavity, which is easily accessible by substrates from bulk solution through dynamic exchange. The cavity is intended to host a single two-electron acceptor molecule, thereby ensuring proximity between acceptor and ligands without requiring covalent binding. The ligands that form the cage will be the actual SF molecules and the aim is, in short, to excite a ligand, let SF occur with a neighboring ligand and subsequently have electron transfer to the acceptor in the cavity from each of the formed triplet excited states as illustrated in Figure 6.6b. Previous studies on tetrahedral cages suggest that the small angles and distance between the ligands imposed by this geometry are favorable for inter-ligand electronic interactions which is why this particular geometry was chosen.[169] The non-covalent interaction between the acceptor and the ligands is expected to effectively decrease the ET rate compared to a covalently linked system, especially a system with a conjugated bridge. This reduction should hopefully reduce the likelyhood of ET from the singlet excited state before SF can occur becomes a less significant concern. Likewise, the system design will similarly impact the rate of electron transfer from the triplet excited states. However, due to the significantly prolonged lifetime of the triplet excited states, the likelihood of successful electron transfer remains promising in this case.

As of writing this thesis, the synthesis of the supramolecular cage depicted in Figure 6.7 is underway, and photophysical characterization remains pending. While it may initially appear counterintuitive to once again employ pentacene as the SF molecule, despite prior acknowledgment of its comparatively low triplet energy, its unparalleled SF efficiency in solution renders it

an enticing choice for initial feasibility investigations. Computational modeling suggests that the resulting cage will feature an inter-pentacene center-to-center distance of approximately 11 Å, with the shortest distance being merely 4 Å. Past studies on through-space SF interactions indicate that this proximity should suffice for efficient SF.[84,170,171]

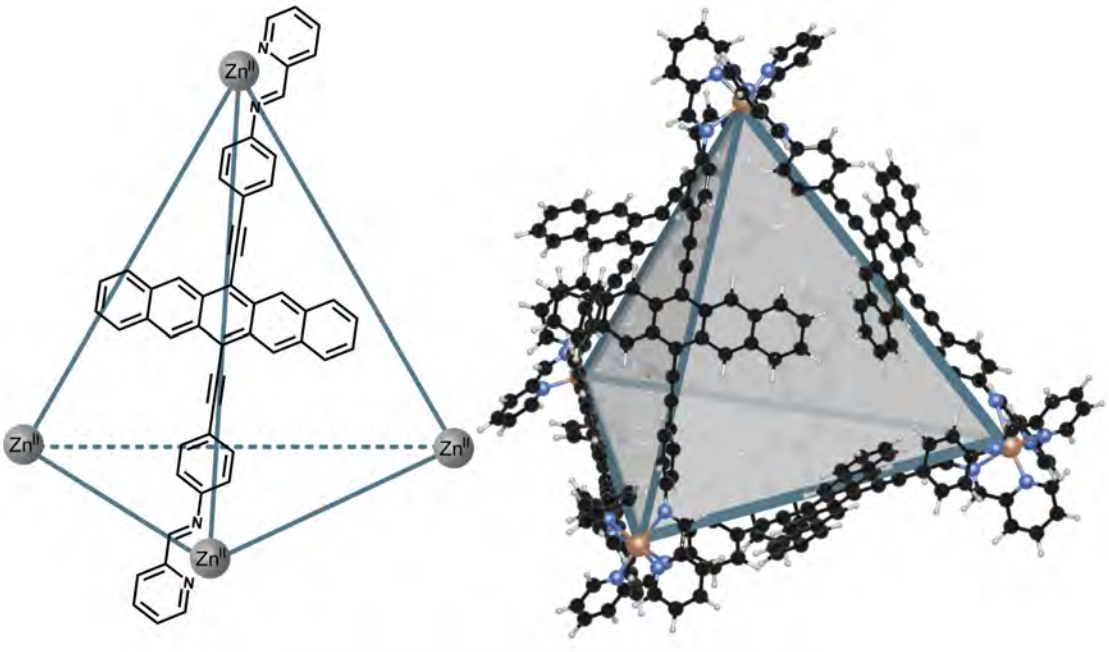

Figure 6.7: Left: Structure of the supramolecular tetrahedral cage where only one ligand is shown for clarity. Right: Structure of the cage as derived from geometry optimization.

Chapter 7
Minimizing Energy Losses Using Exciton Coupling

The upcoming chapter takes a slight departure from the SF theme while still maintaining alignment with the overarching thesis theme - efficient utilization of the energy of light. This chapter focuses on the discoveries outlined in **Paper IV**, where exciton coupling was employed to lower the energy of the singlet excited state while leaving the triplet excited state unaffected. In this study, our primary emphasis was on mitigating energy losses associated with a triplet photosensitizer. However, we posit that the proposed methodology holds potential applicability to diverse scenarios, such as optimizing thermally activated delayed fluorescence (TADF) molecules. These molecules play a pivotal role in various applications, including but not limited to organic light-emitting diodes (OLEDs), where a minimal singlet-triplet energy gap is crucial for enhanced performance.

7.1 Choosing a Suitable System

Triplet photosensitizers are molecules that readily form triplet excited states through ISC. This class of molecules finds applications in various fields, such as photocatalysis,[172–176] triplet-triplet annihilation upconversion,[14,177,178] and photodynamic therapy.[110,179–181] In the conversion from a state of singlet character to one of triplet character the energy loss can be dissected into quantum yield losses (reduction in the number of formed triplet excited states per initial singlet excited state) and energetic losses (loss of energy during the conversion event). This study focuses on the energetic loss, i.e., the energy difference between the singlet and triplet states. Reducing the singlet and triplet energy gap by molecular design have received significant attention in the field of photophysics in the past, particularly following the discovery that organic dyes with small singlet-triplet energy gaps enhance the efficiency of OLEDs.[182] The groundbreaking insight from this seminal work proposed that the singlet-triplet energy gap could be reduced by spatially separating the HOMO and LUMO.[183] This remains to this day one of the few available methods to reduce the singlet-triplet energy gap.[184] However, in **Paper IV**, we introduce a new design strategy aimed at selectively lowering the singlet excited state energy while leaving the triplet excited state unaffected. The design strategy involves the use of exciton coupling which was described in section 2.3. As indicated by Equation 2.7 the strength of the exciton coupling is directly related to the magnitude of the TDM of the states that are coupled, which in turn is pro-

portional to the oscillator strength of a given transition. Consequently, due to the considerably larger oscillator strength associated with singlet excited states of organic molecules compared to their triplet counterparts,[185,186] there exists a potential to selectively lower the singlet excited state energy by aligning molecules into a J-aggregate configuration. This arrangement holds the promise of mitigating energy losses by red-shifting the minimum required excitation wavelength while leaving the triplet energy unperturbed. In pursuit of this aim, boron dipyrromethene (BODIPY)-anthracene dyads were selected for investigation and different sizes of oligomers were synthesized by connecting the BODIPY moieties at the β-position as illustrated in Figure 7.1.

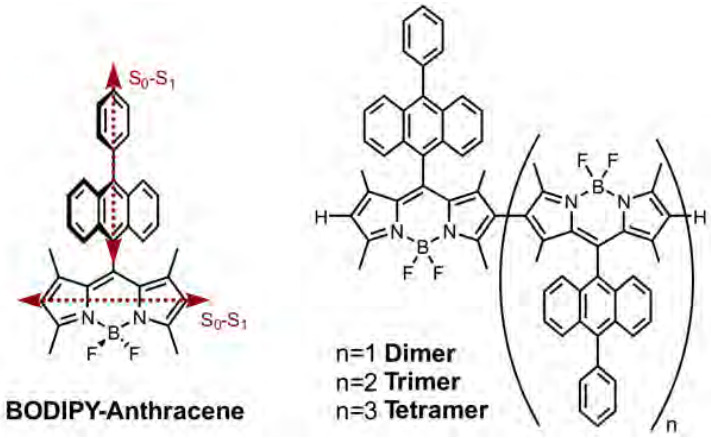

Figure 7.1: The BODIPY-Anthracene dyad and its oligomers. The S_0-S_1 transition dipole moments for the anthracene and BODIPY units are depicted as red, dashed arrows.

Several factors influenced the selection of the molecular system and the specific configuration in which the BODPIY moieties were interconnected. To elucidate, we will begin by examining the rationale behind the choice of the molecular system. As previously mentioned, for the design strategy to work it is imperative that the magnitude of the S_0-T_1 transition dipole moment is negligibly small. Achieving this necessitates avoiding compounds with heavy elements like Pt, Pd, Ru, and Ir, which are commonly found in conventional triplet photosensitizers such as coordination complexes. These complexes often employ heavy atoms to enhance SO coupling, thereby increasing the rate of ISC.[187] It is worth noting that even heavy metal containing coordination complexes typically have very small oscillator strengths for the S_0-T_1 transition compared to the S_0-S_1. There are, however, examples with 5d metal containing complexes such as $Os(bpy)_3$[188,189] with substantial S_0-T_1 oscillator strength and the same is true for many 4d metals, but to a smaller degree.[190,191] Nevertheless, the application of the proposed design strategy to coordination complexes poses challenges beyond the potential non-zero S_0-T_1 oscillator strength. In most metal complexes, especially highly symmetric ones like $Ru(bpy)_3$ or PtOEP, assigning a specific direction for the TDM is non-trivial. A potential workaround could involve using molecules like $Ru(py)(NH_3)_5$, designed such that only one ligand participates in the metal-ligand charge transfer transition.[192] However, to mitigate concerns related to coordination compounds altogether, a purely organic system was chosen in which the orientation of the TDM is much more well-defined. An added benefit of opting for an organic system is the

elimination of dependence on costly precious metals. Moreover, the heightened SO coupling induced by the heavy-atom effect carries the drawback of concurrently diminishing the triplet excited state lifetime. Ideally, a photosensitizer benefits from a prolonged triplet excited state lifetime, making this reduction undesirable for optimal performance.

That being said, organic molecules generally exhibit a limited yield of ISC, making them less practical as viable triplet photosensitizers. Nevertheless, as demonstrated in the preceding chapter for BPEA, alternative methods exist to achieve triplet formation in organic molecules and ISC yields can approach unity even for organic systems if designed carefully. A noteworthy example of such a system gaining recent attention involves dyads consisting of BODIPY covalently linked to an electron donor.[193–195] Among these recently published BODIPY derivatives, BODIPY-anthracene dyads stands out with a high yield of ISC, which is why this particular scaffold was chosen for evaluation of the proposed exciton coupling methodology.[196,197] The specific configuration in which the BODIPY and anthracene moieties are connected facilitates efficient ISC through the SOCT-ISC mechanism which was described in Chapter 2. As evident from the molecular structure of the BODIPY-anthracene dyad used in this work in Figure 7.1 the α positions of the BODIPY are decorated with methyl groups. This deliberate choice aims to align the S_0-T_1 TDMs without extending the aromatic network by conjugation - a critical requirement for the design to succeed since this would lower both the singlet and triplet excited state energies. The presence of methyl substituents is intended to ensure a nearly orthogonal alignment of the connected BODIPY units due to the induced steric hindrance.

7.2 Selective Lowering of the Singlet Excited State

The primary step in gauging the design's efficacy in selectively reducing the energy of the first singlet excited state is to experimentally assess the extent of the energy shift as a result of oligomerization and subsequently compare it with the predictions derived from the exciton coupling theory. In Figure 7.2, the absorption spectra of the monomer, dimer, trimer, and tetramer are depicted.

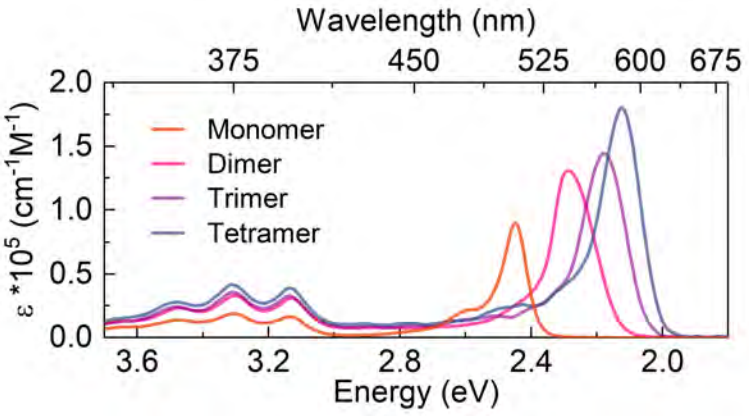

Figure 7.2: Molar absorptivity spectra of the monomer, dimer, trimer and tetramer in DCM.

The absorption spectra shows the lowest energy absorption maxima at 506, 542, 569, and 583 nm, respectively - corresponding to absorption from the BODIPY moieties. Notably, there is no observable shift in the anthracene absorption within the 350-400 nm region, indicating that the anthracene moieties are either too distant or in unfavorable orientations for significant Coulombic interactions to occur. To estimate the energy shift of the BODIPY absorption solely attributable to exciton coupling, we employ the exciton coupling theory outlined in section 2.3. Given the head-to-tail connection of the BODIPY moieties, all angles involved in calculating the orientation factor (Equation 2.8) are zero, simplifying the orientation factor to 2. The TDM of the BODIPY monomer S_0-S_1 transition can be estimated from the molar absorptivity spectrum (Equation 2.9) to 6.7 Debye in DCM (n=1.4244). Consequently, the matrix V can be defined (see below with values in eV), and matrices E and C can subsequently be obtained through matrix diagonalization. While the matrices for the most complicated case of the tetramer are presented below, it should be noted that an analog analysis was conducted for both the dimer and the trimer.

$$V\ (\text{eV}) = \begin{bmatrix} v_{11} & v_{12} & v_{13} & v_{14} \\ v_{21} & v_{22} & v_{23} & v_{24} \\ v_{31} & v_{32} & v_{33} & v_{34} \\ v_{41} & v_{42} & v_{43} & v_{44} \end{bmatrix} = \begin{bmatrix} 0 & -0.1533 & -0.0192 & -0.0057 \\ -0.1533 & 0 & -0.1533 & -0.0192 \\ -0.0192 & -0.1533 & 0 & -0.1533 \\ -0.0057 & -0.0192 & -0.1533 & 0 \end{bmatrix}$$

$$E\ (\text{eV}) = \begin{bmatrix} -0.2671 & 0 & 0 & 0 \\ 0 & -0.0736 & 0 & 0 \\ 0 & 0 & 0.1081 & 0 \\ 0 & 0 & 0 & 0.2325 \end{bmatrix} \quad C = \begin{bmatrix} 0.3894 & 0.6087 & -0.5902 & 0.3598 \\ 0.5902 & 0.3598 & 0.3894 & -0.6087 \\ 0.5902 & -0.3598 & 0.3894 & 0.6087 \\ 0.3894 & -0.6087 & -0.5902 & -0.3598 \end{bmatrix}$$

Examining the eigenvalues in matrix E reveals that the most notable energy shift, registering at -0.2671 eV, aligns with the strongest transition, as indicated by the shared sign of the eigenvector values in the first column of matrix C. In contrast, shifts corresponding to energies of -0.0736 and 0.2325 eV result in a zero summation of eigenvectors, rendering them forbidden transitions. Although the final shift of 0.1081 eV appears permissible, its oscillator strength is significantly lower compared to the -0.2671 eV transition, where all contributions align positively. Performing a similar analysis for the dimer and trimer results in a calculated energy shift of -0.153 and -0.226 eV, respectively. The energy shifts derived from the exciton coupling model are presented together with the shift based on the absorption spectra in Figure 7.3a. Evidently, the experimentally observed shift aligns remarkably well with the predictions of the exciton coupling model. This alignment strongly suggests that exciton coupling, rather than extended conjugation, primarily underlies the observed energy shift. Furthermore, Figure 7.3a incorporates TD-DFT excitation energy calculations for the singlet and triplet excited states based on geometry optimized singlet and triplet ground states. Notably, these calculations slightly overestimate the reduction of the S_1 energy, yet overall, they aptly capture the underlying trend. Particularly encouraging is the constancy of the T_1 energy across the series, a crucial aspect for the success of the design. This consistency aligns with expectations if exciton coupling indeed governs the observed energy shift in S_1. Moreover, as illustrated in Figure 7.3b, the experimentally derived

TDM of the oligomers, calculated from the molar absorptivity and Equation 2.9, closely aligns with the TDM predicted by the exciton coupling theory. In this theoretical framework, the TDM scales proportionally to $\sqrt{N}$, where N represents the number of BODIPY units in the oligomer. It is noteworthy that, once again, the DFT calculations exhibit a consistent trend, albeit with a tendency to overestimate the absolute values.

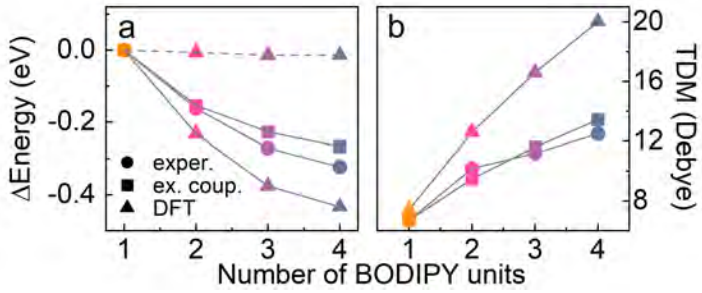

Figure 7.3: a) The energy shift of the oligomers in comparison to the monomer's energy is depicted, with circles representing experimental values obtained from absorption, squares indicating values derived from the exciton coupling model, and triangles representing the calculated shifts of the singlet (solid line) and triplet (dashed line) states using TD-DFT. b) Magnitude of the TDM in Debye.

7.3 Evaluating the ISC Efficiency

After establishing that exciton coupling predominantly contributes to the reduction of the S_1 energy, the system's efficacy as a triplet photosensitizer was assessed. As previously mentioned, the triplet formation mechanism for this specific system involves SOCT-ISC. Consequently, the initial stage in the spin conversion process is the creation of a CS state. Recalling insights from Chapters 5, 6 and Equation 2.10, the energy of the CS state, and consequently the driving force for its formation, can be manipulated by adjusting the solvent polarity. The energy of the CS state in toluene ($\epsilon = 2.38$), DCM ($\epsilon = 8.93$), and ACN ($\epsilon = 37.5$), determined from CV measurements presented in **Paper IV**, is depicted in Figure 7.4, alongside the energies of the S_1 and T_1 states.

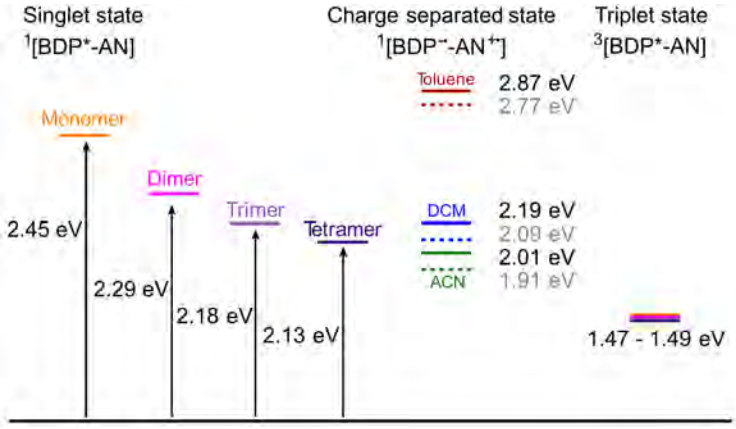

Figure 7.4: Schematic energy diagram illustrating the lowered S_1 energy levels of the oligomers. The CS state energies were estimated from the redox potentials and are shown for the monomer in solid lines and dimer in dotted lines. The energies of the T_1 states were taken from quantum mechanical calculations.

For the monomer, the CS state is energetically accessible in both DCM and ACN, but not in toluene. This observation is consistent with the emission dynamics as illustrated in Figure 7.5. The emission spectra in these three solvents, along with corresponding emission quantum yields provided in Table 7.1, underscore the solvent-dependent behavior. In the more polar solvents, namely DCM and ACN, the low quantum yield of emission suggests that the S_1 state undergoes near-complete conversion to the CS state. The emergence of new low-energy emission bands in these solvents can be attributed to CS state emission. A similar trend is generally observed for the oligomers; however, the reduced driving force for CS, stemming from the diminished S_1 energy, results in substantial quenching only in the highly polar solvent ACN. Despite a modest reduction in the CS state energy due to oligomerization (indicated by the dotted lines in Figure 7.4), the shifted S_1 energy causes the CS state emission to overlap with prompt S_1 for the oligomers. Consequently, clear resolution of the CS state emission becomes challenging, particularly in comparison to the monomer. It is noteworthy that despite the greatly reduced emission quantum yield for the monomer in DCM and ACN, the emission lifetime is not reduced to the same extent, see Table 7.1. This can be rationalized by considering that the prompt fluorescence, which is underresolved using our instrumentation and only present when probing in the higher energy part of the emission, is not included here. The long-lived component that is shown in the table is a result of endothermic charge recombination (CR) from the CS state back to the S_1 and is thus representative of the CS lifetime. A more detailed analysis of this is provided in **Paper IV**.

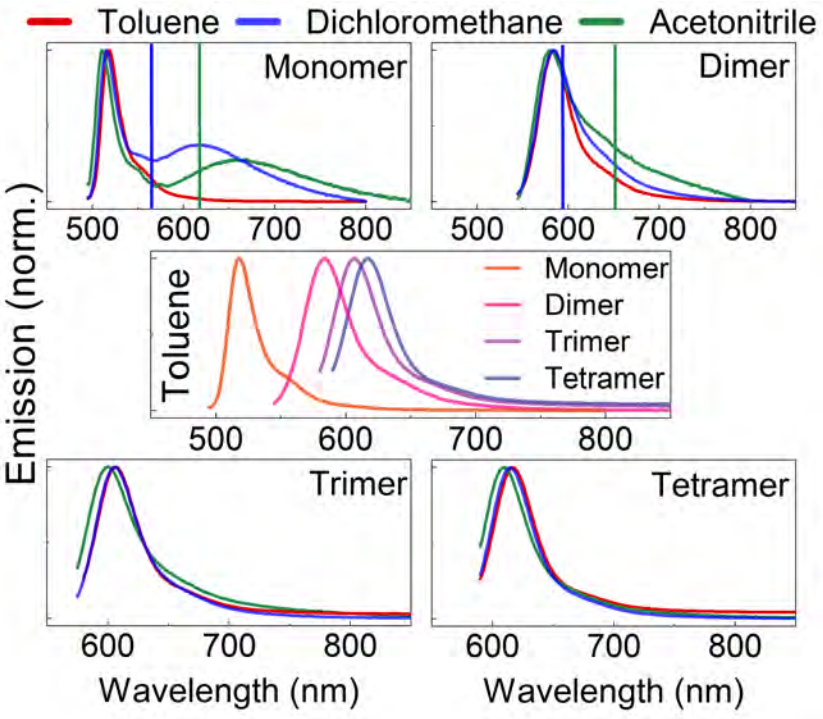

Figure 7.5: The graphs in the top and bottom panels depict the emission profiles of the oligomers separately in the solvents toluene, DCM, and ACN. The middle graph shows the emission spectra of all oligomers in toluene. The energy of the CS state in DCM and ACN based on electrochemical data is represented with vertical lines.

Table 7.1: Spectroscopic data of the BODIPY oligomers collected in different solvents.

Compound	Solvent	Φ_{Em}	τ_{Em} (ns)
Monomer	Toluene	0.8[a]	5.29[d]
	DCM	0.05[a,b]	5.17[d,e]/4.99[d,f]
	ACN	0.02[a,b]	5.90[d,e]/3.11[d,e]
Dimer	Toluene	0.7[c]	3.05[g]
	DCM	0.54[c]	3.68[g]
	ACN	0.01[c]	0.51[g]
Trimer	Toluene	0.72[c]	2.29[g]
	DCM	0.62[c]	2.65[g]
	ACN	0.05[c]	0.57[g]
Tetramer	Toluene	0.55[c]	1.9[g]
	DCM	0.45[c]	2.09[g]
	ACN	0.07[c]	0.66[g]

[a]Fluorescein in 0.1 M NaOH (Φ_f = 0.91)[198] was used as reference compound (excitation at 491 nm, refractive index: 1.33). [b]The CS state emission was fitted to a Gaussian function (on the energy scale) and subtracted from the total emission to extract the BODIPY fluorescence quantum yield contribution to 0.02 and 0.01 in DCM and ACN, respectively. [c]The monomer was used as reference compound (excitation at 375 nm). [d]Fluorescence lifetime was measured upon excitation at 510 nm. [e]A second decay was observed which was underresolved by our instrumentation. [f]Lifetime of the CS state emission probed at 650 nm in DCM and 680 nm in ACN. [g]Emission lifetime was measured upon excitation at 375 nm.

Having established that the capacity to generate the CS state persists upon oligomerization, our focus shifts to the subsequent step: CR leading to the formation of the triplet excited state. The triplet quantum yield (Φ_T) for the oligomers was determined through relative actinometry combined with nsTA, utilizing the known quantum yield of the monomer as a reference.[196] Separate solutions of the monomer and oligomers were prepared with identical absorption at the excitation wavelengths corresponding to their respective absorption maxima. The excitation pulse power was adjusted to yield an equivalent photon count per pulse across the different excitation wavelengths. The transient absorption spectra of all investigated compounds in both DCM and ACN are presented in Figure 7.6 together with the triplet quantum yields. Notably, the triplet excited state lifetime of the oligomers is comparable to or even longer than that of the monomer at 40 μs. This observation is another indication that the triplet excited state energy remains relatively constant across the series. If there was a reduction in the triplet excited state energy, it would presumably lead to a shorter triplet excited state lifetime, in accordance with the energy gap law.[34,199]

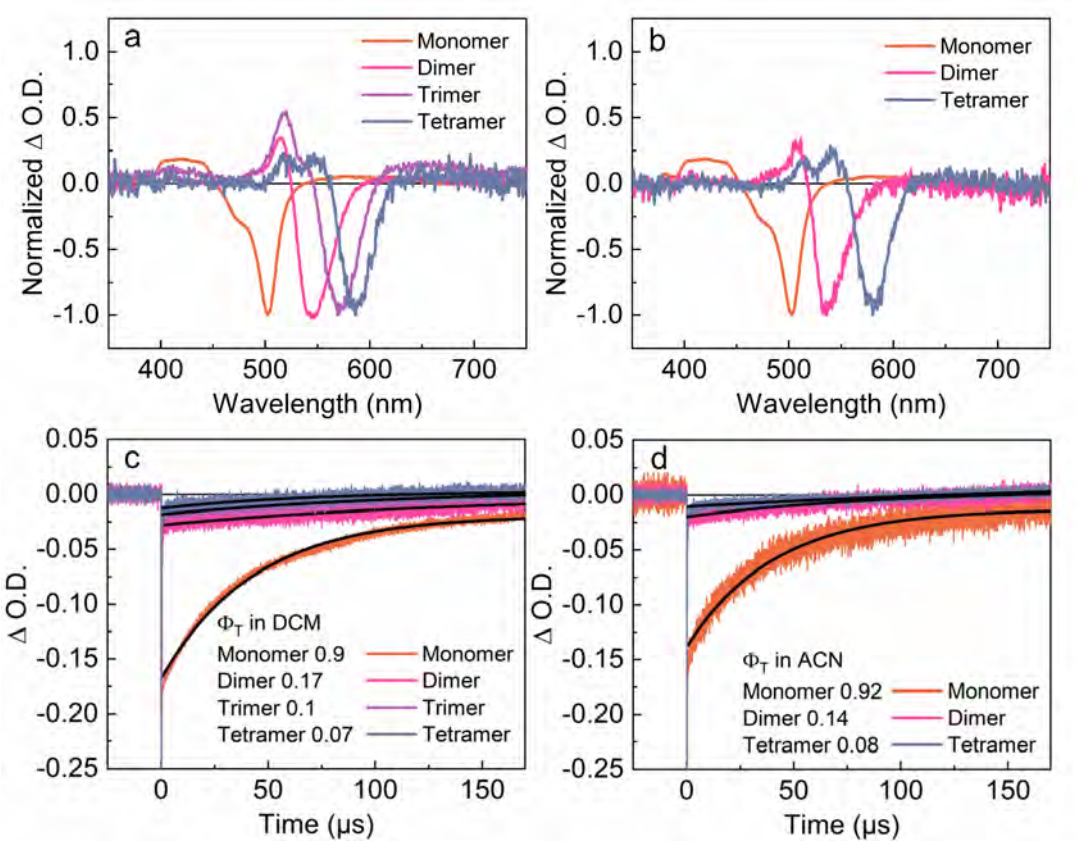

Figure 7.6: Nanosecond transient absorption. Normalized transient absorption spectra of the investigated compounds in a) DCM and b) ACN at a time delay of 1 μs obtained with an excitation wavelength corresponding to the absorption maximum of each of the compounds. c) and d) Show the ground state bleach kinetics of the monomer, dimer, trimer and tetramer probed at the respective ground state bleach maxima in DCM and ACN, respectively. Limited solubility of the trimer prevented quantification of Φ_T in ACN.

Notably, the triplet quantum yield experiences a substantial decrease in the oligomers compared to the monomer. A minor overall reduction in the triplet quantum yield is anticipated for both DCM and ACN, owing to the accelerated radiative and non-radiative decay rates of the S_1 state due to oligomerization. This phenomenon is attributed to superradiance[200,201] as a consequence of the increased TDM and the energy gap law, respectively. The consequences of these processes are evident in the diminished emission quantum yields and shorter emission lifetimes, as outlined in Table 7.1. Examining the same table reveals that the CS state is not significantly populated in DCM, elucidating the low yield in that specific case. However, rationalizing the low yield of triplet formation in ACN for all oligomers is more challenging. The primary reason for this reduced yield likely stems from the short lifetime of the CS state in ACN, which is reduced to a few hundred picoseconds for the oligomers, as indicated by the emission lifetime in Table 7.1. To gain more insight into the shortened CS state lifetime resulting from oligomerization, we turn our attention to fsTA. Here, our focus is narrowed down to a comparative analysis between the monomer and dimer in ACN, as the behavior of the dimer appears to parallel that of the trimer and tetramer, particularly concerning the short CS state lifetime. Figure 7.7a illustrates the kinetic model applied to the fsTA data for both the monomer and dimer. In Figure 7.7b

the kinetic traces for the monomer are depicted, showcasing both raw data points (dots) and modeled data (lines) at specific wavelengths, such as the GSB maxima at 503 nm. Additionally, the extracted spectral components of the S_1, CS, and T_1 states are presented in Figure 7.7c. Similarly, the graphs in Figure 7.7d,e illustrate the same for the dimer, with the extracted rate constants provided separately in Table 7.2. Notably, the applied kinetic model fits the data of both monomer and dimer satisfactorily and the extracted CS state lifetime calculated from the rate constants $\tau_{CSS,monomer} = 1/(k_{CS\rightarrow T1} + k_{CS\rightarrow S0}) = 2.97$ ns and $\tau_{CS,dimer} = 1/(k_{CS\rightarrow T1} + k_{CS\rightarrow S0}) = 0.52$ ns corroborates well with the CS state lifetime obtained through TCSPC in Table 7.1.

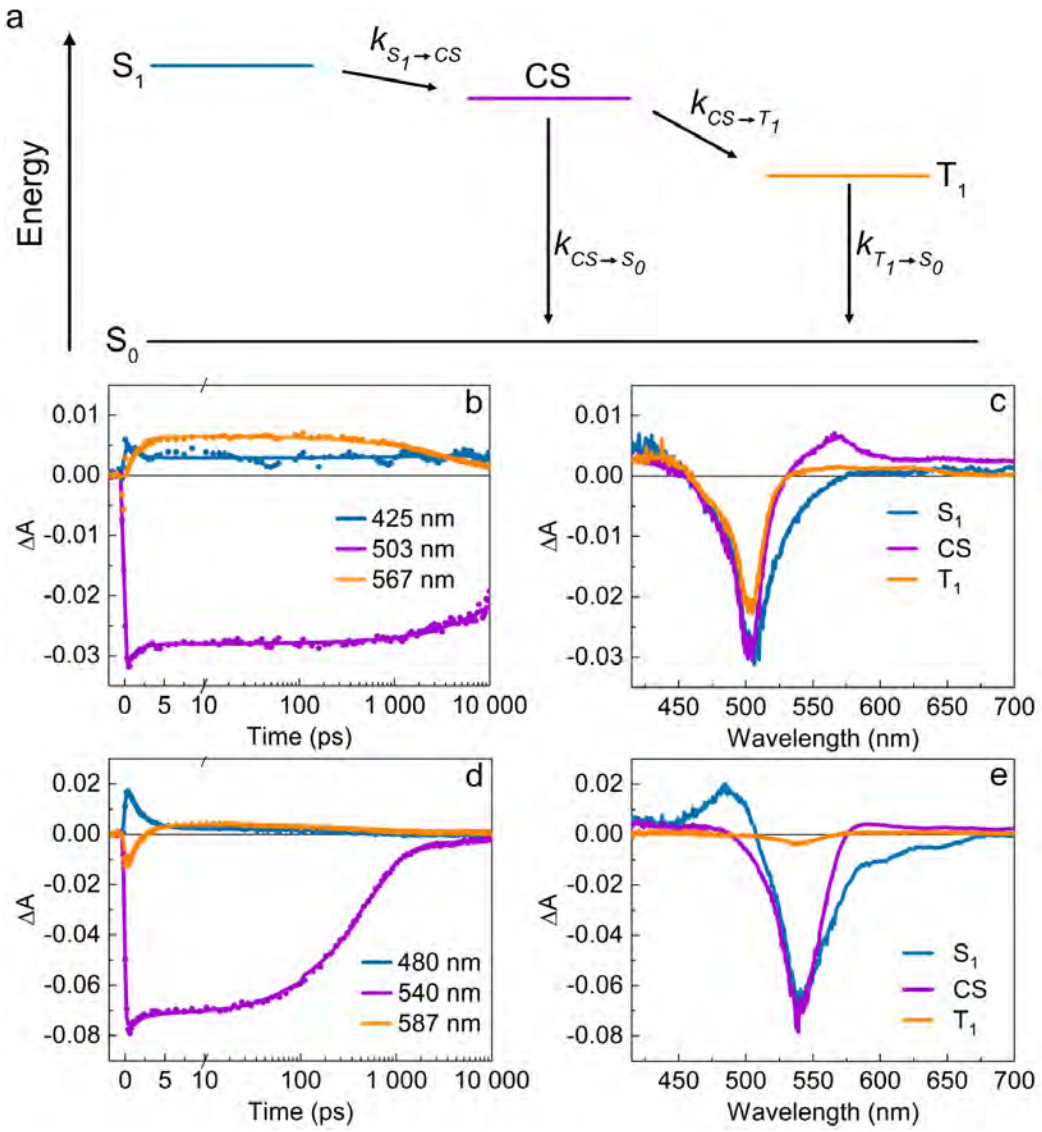

Figure 7.7: Femtosecond transient absorption of the monomer and dimer in ACN. a) Kinetic model applied to the transient absorption data in the global analysis. b) Presentation of the temporal evolution of the differential absorption at select wavelengths for the monomer, with solid lines representing modeled data and dots indicating raw data points. c) Illustration of the spectral components of the monomer obtained through Singular Value Decomposition (SVD) and global analysis utilizing the model from (a). d) and e) shows the same but for the dimer. $\lambda_{ex} = 390$ nm.

Table 7.2: Rate constants from the global analysis of the fsTA of the monomer and dimer in Figure 7.7.

Compound	$k_{S1\rightarrow CS}$ (s^{-1})	$k_{CS\rightarrow T1}$ (s^{-1})	$k_{CS\rightarrow S0}$ (s^{-1})	$k_{T1\rightarrow S0}$ (s^{-1})
Monomer	7.8×10^{11}	2.7×10^{8}	6.7×10^{7}	$<2\times10^{7}$
Dimer	6.8×10^{11}	1.1×10^{8}	1.8×10^{9}	$<2\times10^{7}$

As discernible from the time-dependent progression of the dimer's GSB at 540 nm in Figure 7.7d, it undergoes a rapid initial recovery, ultimately reaching a plateau during later time delays, indicative of the attainment of the final population corresponding to the formed triplet excited state. Consequently, the brief lifetime of the CS state in the oligomers in ACN can not be attributed to an ultrafast intramolecular relaxation to another transient state. Thus, an alternative explanation must be sought. A potential explanation lies in the minor stabilization of the CS state energy in the oligomers compared to the monomer, as depicted in the energy diagram of Figure 7.4. Specifically, it is possible that the slightly lower CS state energy of the dimer could result in a larger rate constant for CR to the ground state if the CR to the ground state is in the Marcus inverted region. Conversely, if CR to the triplet state falls within the Marcus normal region, a marginally lower CS state energy would lead to a diminished driving force (given the approximate equality of T_1 energies for both the monomer and dimer). This, in turn, would yield a smaller rate constant for triplet formation. To validate this hypothesis, the relationship of the rate constants obtained from the fsTA measurements and corresponding driving forces from electrochemistry were compared to predictions derived from Marcus theory.

Recalling from section 2.4 the rate constant of electron transfer as a function of driving force, ΔG_0, can be calculated using Equation 2.12. This entails estimating the total reorganization energy, λ, and the electronic coupling, H_{DA}, between the anthracene and BODIPY moieties' wavefunctions. For the purpose of these calculations we are merely interested in an estimation of where the inverted region and normal regions are located energy wise. Consequently, we will make a few assumptions, beginning with the approximation of the total reorganization energy. Specifically, we will consider only the outer sphere contribution, which is determined through the application of Equation 2.13 to 1.16 eV (refer to Supplementary Information in **Paper IV** for comprehensive details). For simplicity, H_{DA} is assumed to be identical for both CR to the ground and triplet states. It is determined by solving Equation 2.12 with the previously computed reorganization energy, along with the known $k_{CSS\rightarrow S0}$ = 6.7×10^{7} s^{-1} for the monomer from Table 7.2, and the corresponding driving force ΔG_0 = -2.01 eV for CR to S_0, derived from the CS state energy in ACN (Figure 7.4). H_{DA} can thus be calculated to 0.0013 eV. With all parameters defined in Equation 2.12, plotting k_{CR} against ΔG_0 reveals the anticipated parabolic curve in Figure 7.8, depicting the Marcus normal and inverted regions, respectively. The graph also incorporates the experimentally measured CR rate constants from Table 7.2. Notably, it illustrates that CR to the triplet excited state falls within the normal regime, while CR to the ground state aligns with the inverted regime. The slight deviation from the quadratic curve for certain data points is understandable given the simplifications made in our assumptions. However, it should

be stressed that we are mainly interested in the general trend here, which clearly shows that even if the estimated value of λ is off by $\pm$ 0.4 eV it would still place the CR to ground and triplet excited states in the inverted and normal Marcus regimes, respectively. These findings suggest that the short CS state lifetime, and by extension the low yield of triplet formation, for the oligomers can be explained by a minor reduction in the CS state energy. The reduced CS state energy, in turn, can be attributed to a slight degree of conjugation and electron delocalization within the oligomers. This might occur despite the presence of the methyl groups in the α-positions of the BODIPY units, which were incorporated to enforce a perpendicular orientation of the BODIPY moieties and disrupt the conjugation between them.

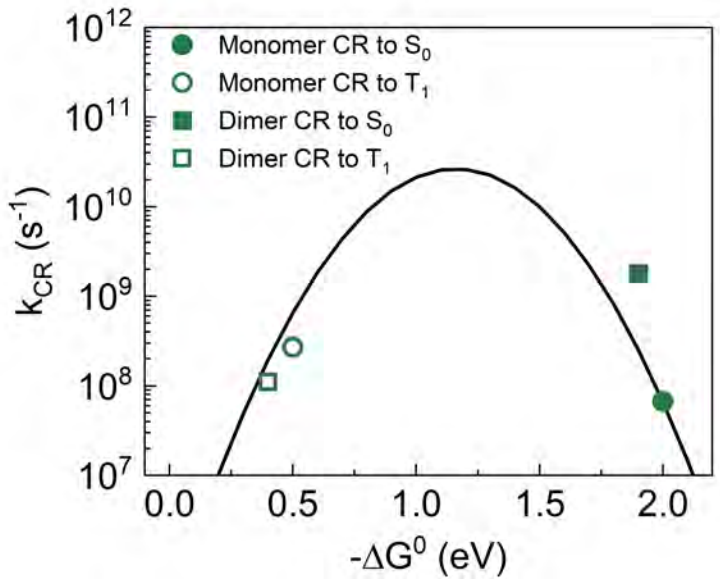

Figure 7.8: CR rate constants (k_{CR}) from the CS state to the ground and triplet states, showing the dependence on the corresponding free energy change, ΔG^0 calculated using Equation 2.12. Experimentally obtained rate constants represented as circles and squares were taken from Table 7.2.

Chapter 8

Summary of Papers

Paper I

Molecular Rotational Conformation Controls the Rate of Singlet Fission and Triplet Decay in Pentacene Dimers

In **Paper I** the conformational dependence of SF in pentacene dimers has been experimentally investigated and theoretical calculations have been used to support the conclusions. Selective photoexcitation of different conformers have revealed that a dimer can have rates for SF and triplet pair recombination several orders of magnitude different depending the conformation that is initially photoexcited. Furthermore, studies in environments of varying viscosity have shown that triplet pair recombination is heavily dependent on conformational relaxation in the excited state, whereas the rate of triplet formation is largely unaffected by increasing the viscosity. Since it is rare to have efficient SF together with slow triplet recombination in a single system this design parameter could be important for future applications which will likely require both quantitative SF and triplet states that are long lived.

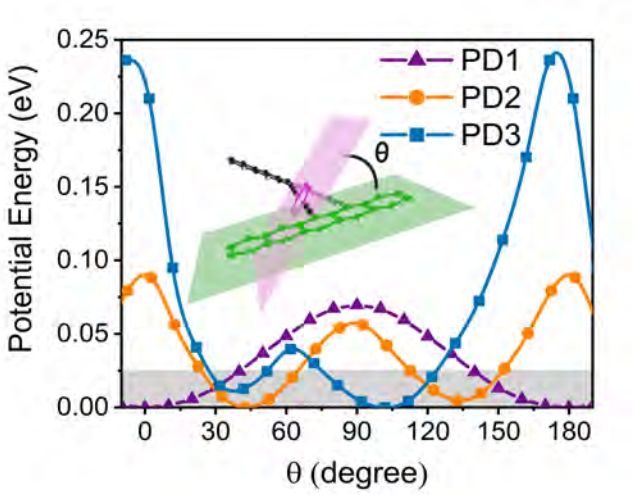

Figure 8.1: Potential energy landscape obtained by scanning over a range of dihedral angles θ demonstrating the distribution of conformations available to the investigated dimers.

Paper II

Triplet Formation in a 9,10-Bis(phenylethynyl)anthracene Dimer and Trimer Occurs by Charge Recombination Rather than Singlet Fission

In **Paper II** the photophysical properties of a BPEA monomer, dimer, and trimer were investigated. Our findings show that in highly concentrated solutions, BPEAmono exhibits excimer formation, and SF could not be observed. The photophysics of BPEAdim and BPEAtri in polar solvents are primarily governed by CS, which outcompetes SF. However, triplet excited states are generated by CR, where the CS state acts as an intermediate. In non-polar solvents at low concentration the dimer and trimer exhibit similar photophyical properties as the monomer with fluorescence being the main decay pathway.

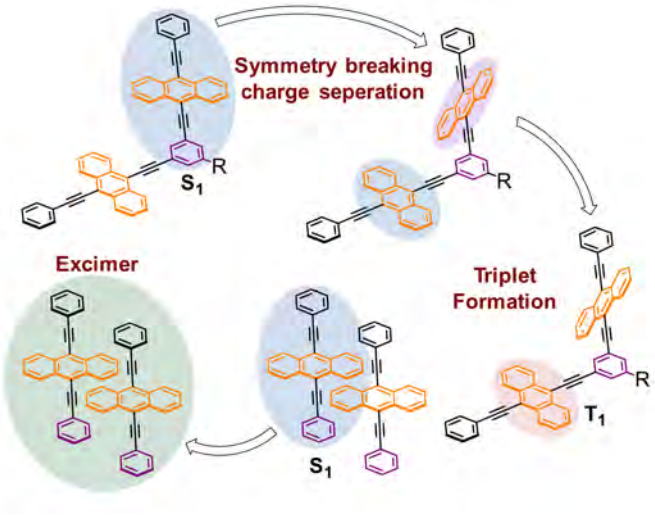

Figure 8.2: Illustration of the photophysical decay pathways for the BPEA monomer and dimer.

Paper III

Singlet Fission and Electron Injection from the Triplet Excited State in Diphenylisobenzofuran-Semiconductor Assemblies: Effects of Solvent Polarity and Driving Force

In **Paper III** the characterization of the SF and ET capabilities of **DPIBF-C6** attached to several different mesoporous semiconductors in solvents of varying polarity was investigated. The study demonstrates how different processes can be favoured by altering the solvent polarity and by changing the driving force for electron injection. On ZrO_2 SF is most efficient in non-polar solvents which is at least partially a consequence of formation of a molecular CS state DPIBF-C6$^+$/DPIBF-C6$^-$ in more polar solvents. On TiO_2 electron injection from the singlet excited state is the dominating process in both solvents. However, in non-polar solvents there is still substantial triplet formation, likely as a consequence of charge recombination from the CB of TiO_2 rather than SF. Finally, on SnO_2 SF appears to occur in parallel with electron injection from S_1 and the formed triplet excited states are capable of ET.

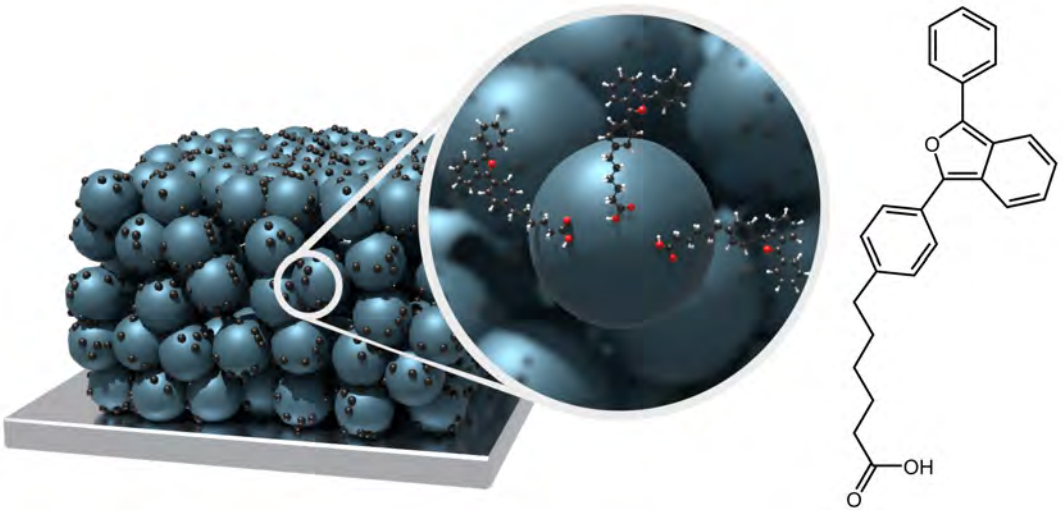

Figure 8.3: Schematic illustration of a thin film consisting of a mesoporous network of either SnO_2, TiO_2 or ZrO_2 on a glass substrate with **DPIBF-C6** chemisorbed to the surface of the semiconductor nanoparticles.

Paper IV

Selective Lowering of the Singlet Excited State Energy to Decrease the Singlet-Triplet Gap *via* Intramolecular Exciton-Exciton Coupling

In **Paper IV**, the objective was to minimize the energy gap between the singlet and triplet excited states. The approach employed focused on strategic design involving exciton coupling, where oligomers of the triplet photosensitizer dyad BODIPY-anthracene were arranged in a J-aggregate configuration. The findings demonstrate the feasibility of selectively reducing the energy of the singlet excited state while keeping the energy of the triplet excited state unchanged. This accomplishment is made possible by leveraging the principle that the strength of exciton coupling correlates directly with the magnitude of the transition dipole moments (TDMs) of the coupled states. Essentially, since singlet excited states exhibit significantly larger TDM magnitudes compared to triplet excited states, it becomes feasible to selectively influence the singlet state while leaving the triplet state unaltered. However, a notable decrease in triplet quantum yield is observed as a consequence of oligomerization. The decreased yield can be traced back to a subtle stabilization of the CS state within the oligomers when compared to the monomer. This CS state serves as an intermediate in the process of triplet formation, following the SOCT-ISC mechanism. As a result, the altered energy of the CS state markedly influences the overall triplet yield given that the charge recombination CR to the triplet excited state transpires within the Marcus normal region, while CR to the ground state occurs in the inverted region.

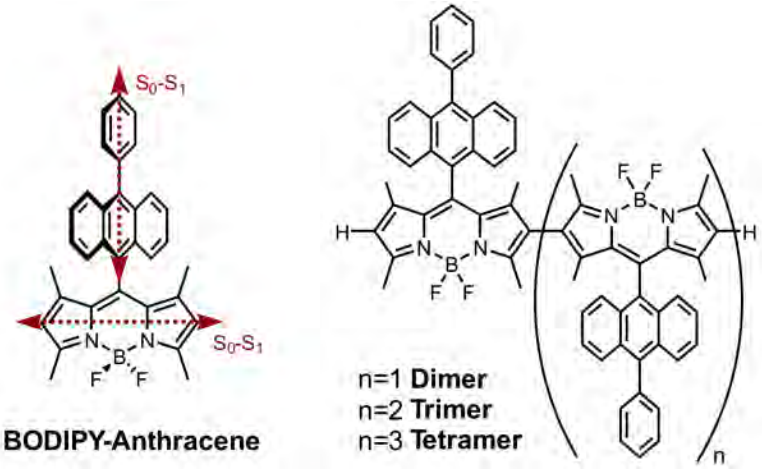

Figure 8.4: Molecular structure of the investigated BODIPY-anthracene dyad and its oligomers demonstrating how the BODIPY moieties are connected in a J-aggregate geometry.

Concluding Remarks and Outlook

Chapter 9

The central focus of this thesis is the strategic design of molecular systems with the common goal of utilizing the energy of photons more efficiently. The primary emphasis has been on exploring two key photophysical processes: SF and exciton coupling. While SF shows promise as a directly applicable technology, particularly in enhancing the efficiency of solar cells, there remain numerous unanswered questions within this research field. This thesis has sought to shed light on some of these questions. Conversely, exciton coupling, in isolation, cannot be directly associated with a specific application, as it merely describes the Coulombic interaction between molecules. However, within the scope of this thesis, it is regarded as a fundamental design principle for customizing the photophysical properties of various molecular systems, thereby enhancing their suitability for specific applications. Both SF and exciton coupling are heavily reliant on the relative orientation of the interacting molecules. Thus, at the core of the investigations presented in this thesis lies the intricate relationship between molecular structure and photophysical properties. The thesis highlights how different arrangements of the same type of molecule can yield vastly different photophysical outcomes. Moreover, the importance of considering both the manner in which molecules are interconnected from a Lewis structure and optimal energy configuration perspective, as well as their ability to adopt various conformations is demonstrated.

The Chapters 4,5 and 6 that revolves around SF highlights the nuanced dynamics in two separate intramolecular SF systems in solution and one intermolecular system integrated with semiconductor thin films. The investigation of dimers based on 6,13-bis(triisopropylsilylethynyl)pentacene have revealed that even small intramolecular systems such as dimers are not fully static systems and that a heterogeneous distribution of dimers with varying electronic couplings may exist simultaneously in solution. This study demonstrate that the relative orientation of involved molecules governs both the formation and decay rates of resultant triplet states in the SF process. Additionally, leveraging conformational changes in the excited state has shown promise in extending the lifetime of triplet pairs, which could be of importance in future device implementation. In a separate study, it was found that triplet formation in a potential SF system based on 9,10-bis(phenylethynyl)anthracene proceeds via charge recombination rather than SF. This

insight is important since alternative triplet formation pathways are not always considered in existing literature on various SF systems. The final SF study took some initial strides toward applying SF materials in DSSCs using 1,3-diphenylisobenzofuran, shedding light on a primary challenge: striking a balance between interchromophore coupling and donor/acceptor interface coupling. Notably, the energetics of the substrate and solvent polarity emerge as pivotal factors dictating the favored photophysical process on the surface, with highly polar solvents impeding SF due to charge-separated state stabilization.

The last investigation, outlined in Chapter 7, introduces a novel application of exciton coupling. It reveals that through the strategic alignment of a molecular system comprising boron dipyrromethene and anthracene in a covalent J-aggregate-like configuration, it becomes feasible to selectively decrease the energy of the singlet excited state while leaving the triplet excited state energy unaffected. Despite the successful mitigation of energetic losses during the singlet-to-triplet excited state conversion, an unintended reduction in the yield of triplet formation ensued. This phenomenon appears to be intricately linked to the SOCT-ISC mechanism within the examined system, wherein a series of ET events occurs, the rates of which are notably influenced by the relative orientation of the boron dipyrromethene moieties.

It is essential to underscore that while both SF and the proposed exciton coupling design principle ultimately aim for application in solar energy technologies, the studies presented in this thesis should be viewed as proof-of-principle. Specifically concerning SF, future applications demand more robust systems characterized by photostability and high triplet energies. While attempts were made in this direction, as exemplified by the utilization of 9,10-bis(phenylethynyl)anthracene, it regrettably did not yield success in this case. However, delving into the study of known SF systems, even those currently of lesser utility, remains crucial. Mechanistic comprehension gleaned from such studies will play a pivotal role in future applications, particularly when compounds more amenable to real-world scenarios become available. Moreover, as hinted at and discussed earlier in the thesis, the future applications of SF extend beyond enhancing solar cell efficiency. One promising avenue involves employing SF for photocatalysis, where the conceptual idea proposed in Chapter 6 involving supramolecular coordination cages presents itself as a promising system. In the case of the exciton coupling system, the results unfortunately revealed that for the specific system evaluated, the connection of the boron dipyrromethene had a deleterious effect on overall performance, indicating its unsuitability for the proposed design principle involving exciton coupling. Nonetheless, the primary goal of selectively reducing the singlet excited state energy while leaving the triplet excited state energy unaffected was achieved successfully. This design strategy can now be applied and evaluated across various other systems and for applications beyond triplet photosensitizers explored herein. One such application area ripe for exploration is the realm of thermally activated delayed fluorescence (TADF) molecules, crucial in for instance the OLED industry. Given their sensitivity to the singlet and triplet energy gap, they exemplify a class of molecules where the proposed design could prove instrumental.

Bibliography

[1] S. Dahl and I. Chorkendorff. Towards practical implementation. *Nature Materials*, 11(2):100–101, February 2012.

[2] IEA (2021), W. E. B. O., IEA, Paris https://www.iea.org/reports/world-energy-balances-overview, License: CC BY 4.0.

[3] D. Feldman, V. Ramasamy, R. Fu, A. Ramdas, J. Desai, and R. Margolis. U.S. Solar Photovoltaic System and Energy Storage Cost Benchmark: Q1 2020, 2021. NREL/TP-6A20-77324.

[4] W. Bludau, A. Onton, and W. Heinke. Temperature dependence of the band gap of silicon. *Journal of Applied Physics*, 45(4):1846–1848, April 1974.

[5] M. Woodhouse, R. Jones-Albertus, D. Feldman, R. Fu, K. Horowitz, D. Chung, D. Jordan, and S. Kurtz. On the Path to SunShot: The Role of Advancements in Solar Photovoltaic Efficiency, Reliability, and Costs, 2016. NREL/TP-6A20-65872.

[6] National Renewable Energy Laboratory, Reference air mass 1.5 spectra. https://www.nrel.gov/grid/solar-resource/spectra-am1.5.html. Accessed: 2022-06-29.

[7] A. Rao and R. H. Friend. Harnessing singlet exciton fission to break the Shockley–Queisser limit. *Nature Reviews Materials*, 2(11):17063, 2017. Publisher: Springer Science and Business Media LLC.

[8] W. Shockley and H. J. Queisser. Detailed Balance Limit of Efficiency of *p-n* Junction Solar Cells. *Journal of Applied Physics*, 32(3):510–519, March 1961.

[9] M. B. Smith and J. Michl. Singlet Fission. *Chemical Reviews*, 110(11):6891–6936, November 2010.

[10] J. Lee, P. Jadhav, P. D. Reusswig, S. R. Yost, N. J. Thompson, D. N. Congreve, E. Hontz, T. Van Voorhis, and M. A. Baldo. Singlet Exciton Fission Photovoltaics. *Accounts of Chemical Research*, 46(6):1300–1311, June 2013.

[11] M. C. Hanna and A. J. Nozik. Solar conversion efficiency of photovoltaic and photoelectrolysis cells with carrier multiplication absorbers. *Journal of Applied Physics*, 100(7):074510, October 2006.

[12] M. J. Y. Tayebjee, A. A. Gray-Weale, and T. W. Schmidt. Thermodynamic Limit of Exciton Fission Solar Cell Efficiency. *The Journal of Physical Chemistry Letters*, 3(19):2749–2754, October 2012.

[13] G. Kopp and J. L. Lean. A new, lower value of total solar irradiance: Evidence and climate significance: FRONTIER. *Geophysical Research Letters*, 38(1):n/a–n/a, January 2011.

[14] T. N. Singh-Rachford and F. N. Castellano. Photon upconversion based on sensitized triplet–triplet annihilation. *Coordination Chemistry Reviews*, 254(21-22):2560–2573, November 2010.

[15] J. Feng, J. Alves, D. M. De Clercq, and T. W. Schmidt. Photochemical Upconversion. *Annual Review of Physical Chemistry*, 74(1):145–168, April 2023.

[16] M. Pawlicki, H. Collins, R. Denning, and H. Anderson. Two-Photon Absorption and the Design of Two-Photon Dyes. *Angewandte Chemie International Edition*, 48(18):3244–3266, April 2009.

[17] P. A. Franken, A. E. Hill, C. W. Peters, and G. Weinreich. Generation of Optical Harmonics. *Physical Review Letters*, 7(4):118–119, August 1961.

[18] M. P. Rauch and R. R. Knowles. Applications and Prospects for Triplet–Triplet Annihilation Photon Upconversion. *CHIMIA*, 72(7-8):501, August 2018.

[19] T. J. B. Zähringer, J. A. Moghtader, M. Bertrams, B. Roy, M. Uji, N. Yanai, and C. Kerzig. Blue-to-UVB Upconversion, Solvent Sensitization and Challenging Bond Activation Enabled by a Benzene-Based Annihilator. *Angewandte Chemie International Edition*, 62(8):e202215340, February 2023.

[20] A. J. Bard and M. A. Fox. Artificial Photosynthesis: Solar Splitting of Water to Hydrogen and Oxygen. *Accounts of Chemical Research*, 28(3):141–145, March 1995.

[21] A. Fujishima and K. Honda. Electrochemical Photolysis of Water at a Semiconductor Electrode. *Nature*, 238(5358):37–38, July 1972.

[22] C.-H. Liao, C.-W. Huang, and J. C. S. Wu. Hydrogen Production from Semiconductor-based Photocatalysis via Water Splitting. *Catalysts*, 2(4):490–516, October 2012.

[23] A. Yamauchi, K. Tanaka, M. Fuki, S. Fujiwara, N. Kimizuka, T. Ryu, M. Saigo, K. Onda, Y. Kobori, K. Miyata, and N. Yanai. Room-temperature quantum coherence of entangled multiexcitons in a metal-organic framework. preprint, Chemistry, April 2023.

[24] L.-C. Lin, T. Smith, Q. Ai, B. K. Rugg, C. Risko, J. E. Anthony, N. H. Damrauer, and J. C. Johnson. Multiexciton quintet state populations in a rigid pyrene-bridged parallel tetracene dimer. *Chemical Science*, 14(41):11554–11565, 2023.

[25] T. Wang, H. Liu, X. Wang, L. Tang, J. Zhou, X. Song, L. Lv, W. Chen, Y. Chen, and X. Li. Employing Singlet Fission into Boosting the Generation of Singlet Oxygen and Superoxide Radicals for Photooxidation Reactions. *ACS Catalysis*, 13(21):13902–13911, November 2023.

[26] J. M. Hollas. *Modern spectroscopy*. J. Wiley, Chichester ; Hoboken, NJ, 4th ed edition, 2004.

[27] P. W. Atkins, J. De Paula, and R. Friedman. *Physical chemistry: quanta, matter, and change*. Oxford University Press, Oxford, United Kingdom, second edition edition, 2014. OCLC: ocn870161002.

[28] P. W. Atkins and R. Friedman. *Molecular quantum mechanics*. Oxford University Press, Oxford ; New York, 5th ed edition, 2011.

[29] M. Montalti, A. Credi, L. Prodi, and M. T. Gandolfi. *Handbook of Photochemistry*. CRC Press, 0 edition, February 2006.

[30] W. Kutzelnigg and J. D. Morgan. Hund's rules. *Zeitschrift fr Physik D Atoms, Molecules and Clusters*, 36(3-4):197–214, September 1996.

[31] C. Schweitzer and R. Schmidt. Physical Mechanisms of Generation and Deactivation of Singlet Oxygen. *Chemical Reviews*, 103(5):1685–1758, May 2003.

[32] W. T. Silfvast. *Laser Fundamentals*. Cambridge University Press, 2 edition, January 2004.

[33] W. Siebrand. Radiationless Transitions in Polyatomic Molecules. II. Triplet-Ground-State Transitions in Aromatic Hydrocarbons. *The Journal of Chemical Physics*, 47(7):2411–2422, October 1967.

[34] R. Englman and J. Jortner. The energy gap law for non-radiative decay in large molecules. *Journal of Luminescence*, 1-2:134–142, January 1970.

[35] M. Kasha. Characterization of electronic transitions in complex molecules. *Discussions of the Faraday Society*, 9:14, 1950.

[36] N. J. Turro, V. Ramamurthy, and J. C. Scaiano. *Modern molecular photochemistry of organic molecules*. University Science Books, Sausalito, Calif, 2010. OCLC: ocn396185412.

[37] A. Köhler and H. Bässler. Triplet states in organic semiconductors. *Materials Science and Engineering: R: Reports*, 66(4-6):71–109, November 2009.

[38] M. B. Smith and J. Michl. Recent Advances in Singlet Fission. *Annual Review of Physical Chemistry*, 64(1):361–386, April 2013.

[39] S. Singh, W. J. Jones, W. Siebrand, B. P. Stoicheff, and W. G. Schneider. Laser Generation of Excitons and Fluorescence in Anthracene Crystals. *The Journal of Chemical Physics*, 42(1):330–342, January 1965.

[40] R. Merrifield, P. Avakian, and R. Groff. Fission of singlet excitons into pairs of triplet excitons in tetracene crystals. *Chemical Physics Letters*, 3(3):155–157, March 1969.

[41] N. Geacintov, M. Pope, and F. Vogel. Effect of Magnetic Field on the Fluorescence of Tetracene Crystals: Exciton Fission. *Physical Review Letters*, 22(12):593–596, March 1969.

[42] N. E. Geacintov, M. Binder, C. E. Swenberg, and M. Pope. Exciton dynamics in \alpha - particle tracks in organic crystals: Magnetic field study of the scintillation in tetracene crystals. *Physical Review B*, 12(10):4113–4134, November 1975.

[43] W. G. Albrecht, H. Coufal, R. Haberkorn, and M. E. Michel-Beyerle. Excitation Spectra of Exciton Fission in Organic Crystals. *physica status solidi (b)*, 89(1):261–265, September 1978.

[44] R. E. Merrifield. Magnetic effects on triplet exciton interactions. *Pure and Applied Chemistry*, 27(3):481–498, January 1971.

[45] J. J. Burdett, G. B. Piland, and C. J. Bardeen. Magnetic field effects and the role of spin states in singlet fission. *Chemical Physics Letters*, 585:1–10, October 2013.

[46] G. B. Piland, J. J. Burdett, R. J. Dillon, and C. J. Bardeen. Singlet Fission: From Coherences to Kinetics. *The Journal of Physical Chemistry Letters*, 5(13):2312–2319, July 2014.

[47] A. J. Musser and J. Clark. Triplet-Pair States in Organic Semiconductors. *Annual Review of Physical Chemistry*, 70(1):323–351, June 2019.

[48] D. Dexter. Two ideas on energy transfer phenomena: Ion-pair effects involving the OH stretching mode, and sensitization of photovoltaic cells. *Journal of Luminescence*, 18-19:779–784, January 1979.

[49] T. Ullrich, D. Munz, and D. M. Guldi. Unconventional singlet fission materials. *Chemical Society Reviews*, 50(5):3485–3518, 2021.

[50] B. J. Walker, A. J. Musser, D. Beljonne, and R. H. Friend. Singlet exciton fission in solution. *Nature Chemistry*, 5(12):1019–1024, December 2013.

[51] M. Dvořák, S. K. K. Prasad, C. B. Dover, C. R. Forest, A. Kaleem, R. W. MacQueen, A. J. Petty, R. Forecast, J. E. Beves, J. E. Anthony, M. J. Y. Tayebjee, A. Widmer-Cooper, P. Thordarson, and T. W. Schmidt. Singlet Fission in Concentrated TIPS-Pentacene Solutions: The Role of Excimers and Aggregates. *Journal of the American Chemical Society*, 143(34):13749–13758, September 2021.

[52] J. R. Allardice, A. Thampi, S. Dowland, J. Xiao, V. Gray, Z. Zhang, P. Budden, A. J. Petty, N. J. L. K. Davis, N. C. Greenham, J. E. Anthony, and A. Rao. Engineering Molecular Ligand Shells on Quantum Dots for Quantitative Harvesting of Triplet Excitons Generated by Singlet Fission. *Journal of the American Chemical Society*, 141(32):12907–12915, August 2019.

[53] N. V. Korovina, N. F. Pompetti, and J. C. Johnson. Lessons from intramolecular singlet fission with covalently bound chromophores. *The Journal of Chemical Physics*, 152(4):040904, January 2020.

[54] A. B. Pun, A. Asadpoordarvish, E. Kumarasamy, M. J. Y. Tayebjee, D. Niesner, D. R. McCamey, S. N. Sanders, L. M. Campos, and M. Y. Sfeir. Ultra-fast intramolecular singlet fission to persistent multiexcitons by molecular design. *Nature Chemistry*, 11(9):821–828, September 2019.

[55] T. Mukhopadhyay, A. J. Musser, B. Puttaraju, J. Dhar, R. H. Friend, and S. Patil. Is the Chemical Strategy for Imbuing "Polyene" Character in Diketopyrrolopyrrole-Based Chromophores Sufficient for Singlet Fission? *The Journal of Physical Chemistry Letters*, 8(5):984–991, March 2017.

[56] H. Liu, Z. Wang, X. Wang, L. Shen, C. Zhang, M. Xiao, and X. Li. Singlet exciton fission in a linear tetracene tetramer. *Journal of Materials Chemistry C*, 6(13):3245–3253, 2018.

[57] A. M. Müller, Y. S. Avlasevich, W. W. Schoeller, K. Müllen, and C. J. Bardeen. Exciton Fission and Fusion in Bis(tetracene) Molecules with Different Covalent Linker Structures. *Journal of the American Chemical Society*, 129(46):14240–14250, November 2007.

[58] N. V. Korovina, J. Joy, X. Feng, C. Feltenberger, A. I. Krylov, S. E. Bradforth, and M. E. Thompson. Linker-Dependent Singlet Fission in Tetracene Dimers. *Journal of the American Chemical Society*, 140(32):10179–10190, August 2018.

[59] I. Papadopoulos, J. Zirzlmeier, C. Hetzer, Y. J. Bae, M. D. Krzyaniak, M. R. Wasielewski, T. Clark, R. R. Tykwinski, and D. M. Guldi. Varying the Interpentacene Electronic Coupling

to Tune Singlet Fission. *Journal of the American Chemical Society*, 141(15):6191–6203, April 2019.

[60] S. Lukman, K. Chen, J. M. Hodgkiss, D. H. P. Turban, N. D. M. Hine, S. Dong, J. Wu, N. C. Greenham, and A. J. Musser. Tuning the role of charge-transfer states in intramolecular singlet exciton fission through side-group engineering. *Nature Communications*, 7(1):13622, December 2016.

[61] M. W. B. Wilson, A. Rao, J. Clark, R. S. S. Kumar, D. Brida, G. Cerullo, and R. H. Friend. Ultrafast Dynamics of Exciton Fission in Polycrystalline Pentacene. *Journal of the American Chemical Society*, 133(31):11830–11833, August 2011.

[62] J. Zirzlmeier, D. Lehnherr, P. B. Coto, E. T. Chernick, R. Casillas, B. S. Basel, M. Thoss, R. R. Tykwinski, and D. M. Guldi. Singlet fission in pentacene dimers. *Proceedings of the National Academy of Sciences*, 112(17):5325–5330, April 2015.

[63] S. N. Sanders, E. Kumarasamy, A. B. Pun, M. T. Trinh, B. Choi, J. Xia, E. J. Taffet, J. Z. Low, J. R. Miller, X. Roy, X.-Y. Zhu, M. L. Steigerwald, M. Y. Sfeir, and L. M. Campos. Quantitative Intramolecular Singlet Fission in Bipentacenes. *Journal of the American Chemical Society*, 137(28):8965–8972, July 2015.

[64] J. J. Burdett, D. Gosztola, and C. J. Bardeen. The dependence of singlet exciton relaxation on excitation density and temperature in polycrystalline tetracene thin films: Kinetic evidence for a dark intermediate state and implications for singlet fission. *The Journal of Chemical Physics*, 135(21):214508, December 2011.

[65] J. C. Johnson and J. Michl. 1,3-Diphenylisobenzofuran: a Model Chromophore for Singlet Fission. *Topics in Current Chemistry*, 375(5):80, October 2017.

[66] J. C. Johnson, A. J. Nozik, and J. Michl. High Triplet Yield from Singlet Fission in a Thin Film of 1,3-Diphenylisobenzofuran. *Journal of the American Chemical Society*, 132(46):16302–16303, November 2010.

[67] A. Akdag, A. Wahab, P. Beran, L. Rulíšek, P. I. Dron, J. Ludvík, and J. Michl. Covalent Dimers of 1,3-Diphenylisobenzofuran for Singlet Fission: Synthesis and Electrochemistry. *The Journal of Organic Chemistry*, 80(1):80–89, January 2015.

[68] R. J. Dillon, G. B. Piland, and C. J. Bardeen. Different Rates of Singlet Fission in Monoclinic versus Orthorhombic Crystal Forms of Diphenylhexatriene. *Journal of the American Chemical Society*, 135(46):17278–17281, November 2013.

[69] O. Millington, S. Montanaro, A. Leventis, A. Sharma, S. A. Dowland, N. Sawhney, K. J. Fallon, W. Zeng, D. G. Congrave, A. J. Musser, A. Rao, and H. Bronstein. Soluble Diphenylhexatriene Dimers for Intramolecular Singlet Fission with High Triplet Energy. *Journal of the American Chemical Society*, 145(4):2499–2510, February 2023.

[70] S. W. Eaton, L. E. Shoer, S. D. Karlen, S. M. Dyar, E. A. Margulies, B. S. Veldkamp, C. Ramanan, D. A. Hartzler, S. Savikhin, T. J. Marks, and M. R. Wasielewski. Singlet Exciton Fission in Polycrystalline Thin Films of a Slip-Stacked Perylenediimide. *Journal of the American Chemical Society*, 135(39):14701–14712, October 2013.

[71] M. Chen, N. E. Powers-Riggs, A. F. Coleman, R. M. Young, and M. R. Wasielewski. Singlet Fission in Quaterrylenediimide Thin Films. *The Journal of Physical Chemistry C*, 124(5):2791–2798, February 2020.

[72] A. K. Le, J. A. Bender, and S. T. Roberts. Slow Singlet Fission Observed in a Polycrystalline Perylenediimide Thin Film. *The Journal of Physical Chemistry Letters*, 7(23):4922–4928, December 2016.

[73] A. K. Le, J. A. Bender, D. H. Arias, D. E. Cotton, J. C. Johnson, and S. T. Roberts. Singlet Fission Involves an Interplay between Energetic Driving Force and Electronic Coupling in Perylenediimide Films. *Journal of the American Chemical Society*, 140(2):814–826, January 2018.

[74] Y. J. Bae, X. Zhao, M. D. Kryzaniak, H. Nagashima, J. Strzalka, Q. Zhang, and M. R. Wasielewski. Spin Dynamics of Quintet and Triplet States Resulting from Singlet Fission in Oriented Terrylenediimide and Quaterrylenediimide Films. *The Journal of Physical Chemistry C*, 124(18):9822–9833, May 2020.

[75] S. R. Yost, J. Lee, M. W. B. Wilson, T. Wu, D. P. McMahon, R. R. Parkhurst, N. J. Thompson, D. N. Congreve, A. Rao, K. Johnson, M. Y. Sfeir, M. G. Bawendi, T. M. Swager, R. H. Friend, M. A. Baldo, and T. Van Voorhis. A transferable model for singlet-fission kinetics. *Nature Chemistry*, 6(6):492–497, June 2014.

[76] P. M. Zimmerman, F. Bell, D. Casanova, and M. Head-Gordon. Mechanism for Singlet Fission in Pentacene and Tetracene: From Single Exciton to Two Triplets. *Journal of the American Chemical Society*, 133(49):19944–19952, December 2011.

[77] N. Monahan and X.-Y. Zhu. Charge Transfer–Mediated Singlet Fission. *Annual Review of Physical Chemistry*, 66(1):601–618, April 2015.

[78] B. S. Basel, J. Zirzlmeier, C. Hetzer, S. R. Reddy, B. T. Phelan, M. D. Krzyaniak, M. K. Volland, P. B. Coto, R. M. Young, T. Clark, M. Thoss, R. R. Tykwinski, M. R. Wasielewski, and D. M. Guldi. Evidence for Charge-Transfer Mediation in the Primary Events of Singlet Fission in a Weakly Coupled Pentacene Dimer. *Chem*, 4(5):1092–1111, May 2018.

[79] M. Chen, Y. J. Bae, C. M. Mauck, A. Mandal, R. M. Young, and M. R. Wasielewski. Singlet Fission in Covalent Terrylenediimide Dimers: Probing the Nature of the Multiexciton State Using Femtosecond Mid-Infrared Spectroscopy. *Journal of the American Chemical Society*, 140(29):9184–9192, July 2018.

[80] C. B. Dover, J. K. Gallaher, L. Frazer, P. C. Tapping, A. J. Petty, M. J. Crossley, J. E. Anthony, T. W. Kee, and T. W. Schmidt. Endothermic singlet fission is hindered by excimer formation. *Nature Chemistry*, 10(3):305–310, March 2018.

[81] H. L. Stern, A. Cheminal, S. R. Yost, K. Broch, S. L. Bayliss, K. Chen, M. Tabachnyk, K. Thorley, N. Greenham, J. M. Hodgkiss, J. Anthony, M. Head-Gordon, A. J. Musser, A. Rao, and R. H. Friend. Vibronically coherent ultrafast triplet-pair formation and subsequent thermally activated dissociation control efficient endothermic singlet fission. *Nature Chemistry*, 9(12):1205–1212, December 2017.

[82] H. L. Stern, A. J. Musser, S. Gelinas, P. Parkinson, L. M. Herz, M. J. Bruzek, J. Anthony, R. H. Friend, and B. J. Walker. Identification of a triplet pair intermediate in singlet exciton

fission in solution. *Proceedings of the National Academy of Sciences*, 112(25):7656–7661, June 2015.

[83] C. M. Mauck, P. E. Hartnett, E. A. Margulies, L. Ma, C. E. Miller, G. C. Schatz, T. J. Marks, and M. R. Wasielewski. Singlet Fission via an Excimer-Like Intermediate in 3,6-Bis(thiophen-2-yl)diketopyrrolopyrrole Derivatives. *Journal of the American Chemical Society*, 138(36):11749–11761, September 2016.

[84] B. S. Basel, J. Zirzlmeier, C. Hetzer, B. T. Phelan, M. D. Krzyaniak, S. R. Reddy, P. B. Coto, N. E. Horwitz, R. M. Young, F. J. White, F. Hampel, T. Clark, M. Thoss, R. R. Tykwinski, M. R. Wasielewski, and D. M. Guldi. Unified model for singlet fission within a non-conjugated covalent pentacene dimer. *Nature Communications*, 8(1):15171, May 2017.

[85] L. R. Weiss, S. L. Bayliss, F. Kraffert, K. J. Thorley, J. E. Anthony, R. Bittl, R. H. Friend, A. Rao, N. C. Greenham, and J. Behrends. Strongly exchange-coupled triplet pairs in an organic semiconductor. *Nature Physics*, 13(2):176–181, February 2017.

[86] W. Kim, N. A. Panjwani, K. C. Krishnapriya, K. Majumder, J. Dasgupta, R. Bittl, S. Patil, and A. J. Musser. Heterogeneous Singlet Fission in a Covalently Linked Pentacene Dimer. 2023. Publisher: arXiv Version Number: 1.

[87] M. Einzinger, T. Wu, J. F. Kompalla, H. L. Smith, C. F. Perkinson, L. Nienhaus, S. Wieghold, D. N. Congreve, A. Kahn, M. G. Bawendi, and M. A. Baldo. Sensitization of silicon by singlet exciton fission in tetracene. *Nature*, 571(7763):90–94, July 2019.

[88] N. J. L. K. Davis, J. R. Allardice, J. Xiao, A. J. Petty, N. C. Greenham, J. E. Anthony, and A. Rao. Singlet Fission and Triplet Transfer to PbS Quantum Dots in TIPS-Tetracene Carboxylic Acid Ligands. *The Journal of Physical Chemistry Letters*, 9(6):1454–1460, March 2018.

[89] A. Rao, M. W. B. Wilson, J. M. Hodgkiss, S. Albert-Seifried, H. Bässler, and R. H. Friend. Exciton Fission and Charge Generation via Triplet Excitons in Pentacene/C $_{60}$ Bilayers. *Journal of the American Chemical Society*, 132(36):12698–12703, September 2010.

[90] M. Kasha. Energy Transfer Mechanisms and the Molecular Exciton Model for Molecular Aggregates. *Radiation Research*, 20(1):55, September 1963.

[91] N. J. Hestand and F. C. Spano. Expanded Theory of H- and J-Molecular Aggregates: The Effects of Vibronic Coupling and Intermolecular Charge Transfer. *Chemical Reviews*, 118(15):7069–7163, August 2018.

[92] M. Kasha, H. R. Rawls, and M. Ashraf El-Bayoumi. The exciton model in molecular spectroscopy. *Pure and Applied Chemistry*, 11(3-4):371–392, January 1965.

[93] Z. S. Yoon, M.-C. Yoon, and D. Kim. Excitonic coupling in covalently linked multiporphyrin systems by matrix diagonalization. *Journal of Photochemistry and Photobiology C: Photochemistry Reviews*, 6(4):249–263, December 2005.

[94] H. Van Amerongen, R. Van Grondelle, and L. Valkunas. *Photosynthetic Excitons*. WORLD SCIENTIFIC, June 2000.

[95] J. Lewis and M. Maroncelli. On the (uninteresting) dependence of the absorption and emission transition moments of coumarin 153 on solvent. *Chemical Physics Letters*, 282(2):197–203, January 1998.

[96] A. Weller. Photoinduced Electron Transfer in Solution: Exciplex and Radical Ion Pair Formation Free Enthalpies and their Solvent Dependence. *Zeitschrift für Physikalische Chemie*, 133(1):93–98, January 1982.

[97] E. Vauthey. Photoinduced Symmetry-Breaking Charge Separation. *ChemPhysChem*, 13(8):2001–2011, June 2012.

[98] K. Kilså, A. N. Macpherson, T. Gillbro, J. Mårtensson, and B. Albinsson. Control of electron transfer in supramolecular systems. *Spectrochimica Acta Part A: Molecular and Biomolecular Spectroscopy*, 57(11):2213–2227, September 2001.

[99] B. S. Brunschwig and N. Sutin. Energy surfaces, reorganization energies, and coupling elements in electron transfer. *Coordination Chemistry Reviews*, 187(1):233–254, June 1999.

[100] R. A. Marcus. Local Approximation of Potential-Energy Surfaces by Surfaces Permitting Separation of Variables. *The Journal of Chemical Physics*, 41(3):610–616, August 1964.

[101] E. J. Piechota and G. J. Meyer. Introduction to Electron Transfer: Theoretical Foundations and Pedagogical Examples. *Journal of Chemical Education*, 96(11):2450–2466, November 2019.

[102] R. A. Marcus. On the Theory of Oxidation-Reduction Reactions Involving Electron Transfer. I. *The Journal of Chemical Physics*, 24(5):966–978, May 1956.

[103] R. A. Marcus. Electrostatic Free Energy and Other Properties of States Having Nonequilibrium Polarization. I. *The Journal of Chemical Physics*, 24(5):979–989, May 1956.

[104] P. F. Barbara, T. J. Meyer, and M. A. Ratner. Contemporary Issues in Electron Transfer Research. *The Journal of Physical Chemistry*, 100(31):13148–13168, January 1996.

[105] G. L. Closs and J. R. Miller. Intramolecular Long-Distance Electron Transfer in Organic Molecules. *Science*, 240(4851):440–447, April 1988.

[106] J. Jortner. Temperature dependent activation energy for electron transfer between biological molecules. *The Journal of Chemical Physics*, 64(12):4860–4867, June 1976.

[107] L. S. Fox, M. Kozik, J. R. Winkler, and H. B. Gray. Gaussian Free-Energy Dependence of Electron-Transfer Rates in Iridium Complexes. *Science*, 247(4946):1069–1071, March 1990.

[108] Y. Hou, X. Zhang, K. Chen, D. Liu, Z. Wang, Q. Liu, J. Zhao, and A. Barbon. Charge separation, charge recombination, long-lived charge transfer state formation and intersystem crossing in organic electron donor/acceptor dyads. *Journal of Materials Chemistry C*, 7(39):12048–12074, 2019.

[109] D. J. Gibbons, A. Farawar, P. Mazzella, S. Leroy-Lhez, and R. M. Williams. Making triplets from photo-generated charges: observations, mechanisms and theory. *Photochemical & Photobiological Sciences*, 19(2):136–158, February 2020.

[110] V.-N. Nguyen, Y. Yan, J. Zhao, and J. Yoon. Heavy-Atom-Free Photosensitizers: From Molecular Design to Applications in the Photodynamic Therapy of Cancer. *Accounts of Chemical Research*, 54(1):207–220, January 2021.

[111] Y. Dong, A. A. Sukhanov, J. Zhao, A. Elmali, X. Li, B. Dick, A. Karatay, and V. K. Voronkova. Spin–Orbit Charge-Transfer Intersystem Crossing (SOCT-ISC) in Bodipy-Phenoxazine Dyads: Effect of Chromophore Orientation and Conformation Restriction on the Photophysical Properties. *The Journal of Physical Chemistry C*, 123(37):22793–22811, September 2019.

[112] Z. E. X. Dance, Q. Mi, D. W. McCamant, M. J. Ahrens, M. A. Ratner, and M. R. Wasielewski. Time-Resolved EPR Studies of Photogenerated Radical Ion Pairs Separated by *p* -Phenylene Oligomers and of Triplet States Resulting from Charge Recombination. *The Journal of Physical Chemistry B*, 110(50):25163–25173, December 2006.

[113] Z. E. X. Dance, S. M. Mickley, T. M. Wilson, A. B. Ricks, A. M. Scott, M. A. Ratner, and M. R. Wasielewski. Intersystem Crossing Mediated by Photoinduced Intramolecular Charge Transfer: Julolidine-Anthracene Molecules with Perpendicular \pi Systems. *The Journal of Physical Chemistry A*, 112(18):4194–4201, May 2008.

[114] S. K. Lower and M. A. El-Sayed. The Triplet State and Molecular Electronic Processes in Organic Molecules. *Chemical Reviews*, 66(2):199–241, April 1966.

[115] M. T. Colvin, A. B. Ricks, A. M. Scott, A. L. Smeigh, R. Carmieli, T. Miura, and M. R. Wasielewski. Magnetic Field-Induced Switching of the Radical-Pair Intersystem Crossing Mechanism in a Donor-Bridge-Acceptor Molecule for Artificial Photosynthesis. *Journal of the American Chemical Society*, 133(5):1240–1243, February 2011.

[116] M. T. Colvin, A. B. Ricks, A. M. Scott, D. T. Co, and M. R. Wasielewski. Intersystem Crossing Involving Strongly Spin Exchange-Coupled Radical Ion Pairs in Donor–bridge-Acceptor Molecules. *The Journal of Physical Chemistry A*, 116(8):1923–1930, March 2012.

[117] J. R. Lakowicz. *Principles of fluorescence spectroscopy*. Springer, New York, 3rd ed edition, 2006.

[118] D. V. O'Connor and D. Phillips. *Time-correlated single photon counting*. Academic Press, London ; Orlando, 1984.

[119] A. H. Zewail. Femtochemistry: Atomic-Scale Dynamics of the Chemical Bond. *The Journal of Physical Chemistry A*, 104(24):5660–5694, June 2000.

[120] A. Brodeur and S. L. Chin. Ultrafast white-light continuum generation and self-focusing in transparent condensed media. *Journal of the Optical Society of America B*, 16(4):637, April 1999.

[121] I. H. van Stokkum, D. S. Larsen, and R. van Grondelle. Global and target analysis of time-resolved spectra. *Biochimica et Biophysica Acta (BBA) - Bioenergetics*, 1657(2-3):82–104, July 2004.

[122] C. Ruckebusch, M. Sliwa, P. Pernot, A. de Juan, and R. Tauler. Comprehensive data analysis of femtosecond transient absorption spectra: A review. *Journal of Photochemistry and Photobiology C: Photochemistry Reviews*, 13(1):1–27, March 2012.

[123] R. W. Hendler and R. I. Shrager. Deconvolutions based on singular value decomposition and the pseudoinverse: a guide for beginners. *Journal of Biochemical and Biophysical Methods*, 28(1):1–33, January 1994.

[124] J. M. Beechem. [2] Global analysis of biochemical and biophysical data. In *Methods in Enzymology*, volume 210, pages 37–54. Elsevier, 1992.

[125] H. Satzger and W. Zinth. Visualization of transient absorption dynamics – towards a qualitative view of complex reaction kinetics. *Chemical Physics*, 295(3):287–295, December 2003.

[126] R. Ringström, F. Edhborg, Z. W. Schroeder, L. Chen, M. J. Ferguson, R. R. Tykwinski, and B. Albinsson. Molecular rotational conformation controls the rate of singlet fission and triplet decay in pentacene dimers. *Chemical Science*, 13(17):4944–4954, 2022.

[127] M. U. Winters, J. Kärnbratt, M. Eng, C. J. Wilson, H. L. Anderson, and B. Albinsson. Photophysics of a Butadiyne-Linked Porphyrin Dimer: Influence of Conformational Flexibility in the Ground and First Singlet Excited State. *The Journal of Physical Chemistry C*, 111(19):7192–7199, May 2007.

[128] K. Schmieder, M. Levitus, H. Dang, and M. A. Garcia-Garibay. Photophysical Properties of Coplanar and Twisted 1,4-Bis(9-ethynylanthracenyl)benzene. Rotational Equilibration in the Excited States of Diaryalkynes. *The Journal of Physical Chemistry A*, 106(8):1551–1556, February 2002.

[129] M. Mizukami, H. Fujimori, and M. Oguni. Glass Transitions and the Responsible Molecular Motions in 2-Methyltetrahydrofuran. *Progress of Theoretical Physics Supplement*, 126(0):79–82, May 2013.

[130] N. Geacintov, J. Burgos, M. Pope, and C. Strom. Heterofission of pentacene excited singlets in pentacene-doped tetracene crystals. *Chemical Physics Letters*, 11(4):504–508, November 1971.

[131] V. K. Thorsmølle, R. D. Averitt, J. Demsar, D. L. Smith, S. Tretiak, R. L. Martin, X. Chi, B. K. Crone, A. P. Ramirez, and A. J. Taylor. Morphology Effectively Controls Singlet-Triplet Exciton Relaxation and Charge Transport in Organic Semiconductors. *Physical Review Letters*, 102(1):017401, January 2009.

[132] D. M. Chapin, C. S. Fuller, and G. L. Pearson. A New Silicon *p-n* Junction Photocell for Converting Solar Radiation into Electrical Power. *Journal of Applied Physics*, 25(5):676–677, May 1954.

[133] M. Wolf. Limitations and Possibilities for Improvement of Photovoltaic Solar Energy Converters: Part I: Considerations for Earth's Surface Operation. *Proceedings of the IRE*, 48(7):1246–1263, July 1960.

[134] R. Ringström, Z. W. Schroeder, L. Mencaroni, P. Chabera, R. R. Tykwinski, and B. Albinsson. Triplet Formation in a 9,10-Bis(phenylethynyl)anthracene Dimer and Trimer Occurs by Charge Recombination Rather than Singlet Fission. *The Journal of Physical Chemistry Letters*, 14(35):7897–7902, September 2023.

[135] V. Gray, A. Dreos, P. Erhart, B. Albinsson, K. Moth-Poulsen, and M. Abrahamsson. Loss channels in triplet–triplet annihilation photon upconversion: importance of annihilator

singlet and triplet surface shapes. *Physical Chemistry Chemical Physics*, 19(17):10931–10939, 2017.

[136] Y. J. Bae, G. Kang, C. D. Malliakas, J. N. Nelson, J. Zhou, R. M. Young, Y.-L. Wu, R. P. Van Duyne, G. C. Schatz, and M. R. Wasielewski. Singlet Fission in 9,10-Bis(phenylethynyl)anthracene Thin Films. *Journal of the American Chemical Society*, 140(45):15140–15144, November 2018.

[137] B. Manna, A. Nandi, and R. Ghosh. Ultrafast Singlet Exciton Fission Dynamics in 9,10-Bis(phenylethynyl)anthracene Nanoaggregates and Thin Films. *The Journal of Physical Chemistry C*, 122(36):21047–21055, September 2018.

[138] S. Fan, W. Li, T. Li, F. Gao, W. Hu, S. Liu, X. Wang, H. Liu, Z. Liu, Z. Li, Y. Chen, and X. Li. Singlet fission in colloid nanoparticles of amphipathic 9,10-bis(phenylethynyl)anthracene derivatives. *Journal of Photochemistry and Photobiology A: Chemistry*, 427:113826, May 2022.

[139] Y. J. Bae, J. A. Christensen, G. Kang, J. Zhou, R. M. Young, Y.-L. Wu, R. P. Van Duyne, G. C. Schatz, and M. R. Wasielewski. Substituent effects on energetics and crystal morphology modulate singlet fission in 9,10-bis(phenylethynyl)anthracenes. *The Journal of Chemical Physics*, 151(4):044501, July 2019.

[140] Y. J. Bae, D. Shimizu, J. D. Schultz, G. Kang, J. Zhou, G. C. Schatz, A. Osuka, and M. R. Wasielewski. Balancing Charge Transfer and Frenkel Exciton Coupling Leads to Excimer Formation in Molecular Dimers: Implications for Singlet Fission. *The Journal of Physical Chemistry A*, 124(41):8478–8487, October 2020.

[141] R. M. Young and M. R. Wasielewski. Mixed Electronic States in Molecular Dimers: Connecting Singlet Fission, Excimer Formation, and Symmetry-Breaking Charge Transfer. *Accounts of Chemical Research*, 53(9):1957–1968, September 2020.

[142] R. D. Pensack, A. J. Tilley, S. R. Parkin, T. S. Lee, M. M. Payne, D. Gao, A. A. Jahnke, D. G. Oblinsky, P.-F. Li, J. E. Anthony, D. S. Seferos, and G. D. Scholes. Exciton Delocalization Drives Rapid Singlet Fission in Nanoparticles of Acene Derivatives. *Journal of the American Chemical Society*, 137(21):6790–6803, June 2015.

[143] A. Olesund, V. Gray, J. Mårtensson, and B. Albinsson. Diphenylanthracene Dimers for Triplet–Triplet Annihilation Photon Upconversion: Mechanistic Insights for Intramolecular Pathways and the Importance of Molecular Geometry. *Journal of the American Chemical Society*, 143(15):5745–5754, April 2021.

[144] I. Fureraj, D. S. Budkina, and E. Vauthey. Torsional disorder and planarization dynamics: 9,10-bis(phenylethynyl)anthracene as a case study. *Physical Chemistry Chemical Physics*, 24(42):25979–25989, 2022.

[145] K. C. Krishnapriya, P. Roy, B. Puttaraju, U. Salzner, A. J. Musser, M. Jain, J. Dasgupta, and S. Patil. Spin density encodes intramolecular singlet exciton fission in pentacene dimers. *Nature Communications*, 10(1):33, January 2019.

[146] S. N. Sanders, A. B. Pun, K. R. Parenti, E. Kumarasamy, L. M. Yablon, M. Y. Sfeir, and L. M. Campos. Understanding the Bound Triplet-Pair State in Singlet Fission. *Chem*, 5(8):1988–2005, August 2019.

[147] S. Lukman, A. J. Musser, K. Chen, S. Athanasopoulos, C. K. Yong, Z. Zeng, Q. Ye, C. Chi, J. M. Hodgkiss, J. Wu, R. H. Friend, and N. C. Greenham. Tuneable Singlet Exciton Fission and Triplet–Triplet Annihilation in an Orthogonal Pentacene Dimer. *Advanced Functional Materials*, 25(34):5452–5461, September 2015.

[148] M. A. Filatov. Heavy-atom-free BODIPY photosensitizers with intersystem crossing mediated by intramolecular photoinduced electron transfer. *Organic & Biomolecular Chemistry*, 18(1):10–27, 2020.

[149] N. V. Korovina, C. H. Chang, and J. C. Johnson. Spatial separation of triplet excitons drives endothermic singlet fission. *Nature Chemistry*, 12(4):391–398, April 2020.

[150] J. L. Ryerson, A. Zaykov, L. E. Aguilar Suarez, R. W. A. Havenith, B. R. Stepp, P. I. Dron, J. Kaleta, A. Akdag, S. J. Teat, T. F. Magnera, J. R. Miller, Z. Havlas, R. Broer, S. Faraji, J. Michl, and J. C. Johnson. Structure and photophysics of indigoids for singlet fission: Cibalackrot. *The Journal of Chemical Physics*, 151(18):184903, November 2019.

[151] M. Silver, D. Olness, M. Swicord, and R. C. Jarnagin. Photogeneration of Free Carriers in Organic Crystals Via Exciton-Exciton Interactions. *Physical Review Letters*, 10(1):12–14, January 1963.

[152] J. Jortner. Collisions of Singlet Excitons in Molecular Crystals. *Physical Review Letters*, 20(6):244–247, February 1968.

[153] R. D. Pensack, E. E. Ostroumov, A. J. Tilley, S. Mazza, C. Grieco, K. J. Thorley, J. B. Asbury, D. S. Seferos, J. E. Anthony, and G. D. Scholes. Observation of Two Triplet-Pair Intermediates in Singlet Exciton Fission. *The Journal of Physical Chemistry Letters*, 7(13):2370–2375, July 2016.

[154] M. J. Y. Tayebjee, K. N. Schwarz, R. W. MacQueen, M. Dvořák, A. W. C. Lam, K. P. Ghiggino, D. R. McCamey, T. W. Schmidt, and G. J. Conibeer. Morphological Evolution and Singlet Fission in Aqueous Suspensions of TIPS-Pentacene Nanoparticles. *The Journal of Physical Chemistry C*, 120(1):157–165, January 2016.

[155] R. D. Pensack, C. Grieco, G. E. Purdum, S. M. Mazza, A. J. Tilley, E. E. Ostroumov, D. S. Seferos, Y.-L. Loo, J. B. Asbury, J. E. Anthony, and G. D. Scholes. Solution-processable, crystalline material for quantitative singlet fission. *Materials Horizons*, 4(5):915–923, 2017.

[156] E. Sundin, R. Ringström, F. Johansson, B. Küçüköz, A. Ekebergh, V. Gray, B. Albinsson, J. Mårtensson, and M. Abrahamsson. Singlet Fission and Electron Injection from the Triplet Excited State in Diphenylisobenzofuran–Semiconductor Assemblies: Effects of Solvent Polarity and Driving Force. *The Journal of Physical Chemistry C*, 124(38):20794–20805, September 2020.

[157] J. L. Ryerson, J. N. Schrauben, A. J. Ferguson, S. C. Sahoo, P. Naumov, Z. Havlas, J. Michl, A. J. Nozik, and J. C. Johnson. Two Thin Film Polymorphs of the Singlet Fission Compound 1,3-Diphenylisobenzofuran. *The Journal of Physical Chemistry C*, 118(23):12121–12132, June 2014.

[158] J. N. Schrauben, J. L. Ryerson, J. Michl, and J. C. Johnson. Mechanism of Singlet Fission in Thin Films of 1,3-Diphenylisobenzofuran. *Journal of the American Chemical Society*,

136(20):7363–7373, May 2014.

[159] B. O'Regan and M. Grätzel. A low-cost, high-efficiency solar cell based on dye-sensitized colloidal TiO2 films. *Nature*, 353(6346):737–740, October 1991.

[160] J. C. Wang, S. P. Hill, T. Dilbeck, O. O. Ogunsolu, T. Banerjee, and K. Hanson. Multimolecular assemblies on high surface area metal oxides and their role in interfacial energy and electron transfer. *Chemical Society Reviews*, 47(1):104–148, 2018.

[161] J. N. Schrauben, Y. Zhao, C. Mercado, P. I. Dron, J. L. Ryerson, J. Michl, K. Zhu, and J. C. Johnson. Photocurrent Enhanced by Singlet Fission in a Dye-Sensitized Solar Cell. *ACS Applied Materials & Interfaces*, 7(4):2286–2293, February 2015.

[162] A. F. Schwerin, J. C. Johnson, M. B. Smith, P. Sreearunothai, D. Popović, J. Černý, Z. Havlas, I. Paci, A. Akdag, M. K. MacLeod, X. Chen, D. E. David, M. A. Ratner, J. R. Miller, A. J. Nozik, and J. Michl. Toward Designed Singlet Fission: Electronic States and Photophysics of 1,3-Diphenylisobenzofuran. *The Journal of Physical Chemistry A*, 114(3):1457–1473, January 2010.

[163] P. Tiwana, P. Docampo, M. B. Johnston, H. J. Snaith, and L. M. Herz. Electron Mobility and Injection Dynamics in Mesoporous ZnO, SnO $_2$, and TiO $_2$ Films Used in Dye-Sensitized Solar Cells. *ACS Nano*, 5(6):5158–5166, June 2011.

[164] M. A. Butler and D. S. Ginley. Prediction of Flatband Potentials at Semiconductor-Electrolyte Interfaces from Atomic Electronegativities. *Journal of The Electrochemical Society*, 125(2):228–232, February 1978.

[165] T. Banerjee, S. P. Hill, M. A. Hermosilla-Palacios, B. D. Piercy, J. Haney, B. Casale, A. E. DePrince, M. D. Losego, V. D. Kleiman, and K. Hanson. Diphenylisobenzofuran Bound to Nanocrystalline Metal Oxides: Excimer Formation, Singlet Fission, Electron Injection, and Low Energy Sensitization. *The Journal of Physical Chemistry C*, 122(50):28478–28490, December 2018.

[166] L. Hammarström. Accumulative Charge Separation for Solar Fuels Production: Coupling Light-Induced Single Electron Transfer to Multielectron Catalysis. *Accounts of Chemical Research*, 48(3):840–850, March 2015.

[167] M. R. Wasielewski. Photoinduced electron transfer in supramolecular systems for artificial photosynthesis. *Chemical Reviews*, 92(3):435–461, May 1992.

[168] A. Pannwitz and O. S. Wenger. Proton-coupled multi-electron transfer and its relevance for artificial photosynthesis and photoredox catalysis. *Chemical Communications*, 55(28):4004–4014, 2019.

[169] R. Ham, C. J. Nielsen, S. Pullen, and J. N. H. Reek. Supramolecular Coordination Cages for Artificial Photosynthesis and Synthetic Photocatalysis. *Chemical Reviews*, 123(9):5225–5261, May 2023.

[170] A. Aster, F. Zinna, C. Rumble, J. Lacour, and E. Vauthey. Singlet Fission in a Flexible Bichromophore with Structural and Dynamic Control. *Journal of the American Chemical Society*, 143(5):2361–2371, February 2021.

[171] E. Kumarasamy, S. N. Sanders, M. J. Y. Tayebjee, A. Asadpoordarvish, T. J. H. Hele, E. G. Fuemmeler, A. B. Pun, L. M. Yablon, J. Z. Low, D. W. Paley, J. C. Dean, B. Choi, G. D. Sc-

holes, M. L. Steigerwald, N. Ananth, D. R. McCamey, M. Y. Sfeir, and L. M. Campos. Tuning Singlet Fission in π-Bridge-π Chromophores. *Journal of the American Chemical Society*, 139(36):12488–12494, September 2017.

[172] M. H. Shaw, J. Twilton, and D. W. C. MacMillan. Photoredox Catalysis in Organic Chemistry. *The Journal of Organic Chemistry*, 81(16):6898–6926, August 2016.

[173] S. Fukuzumi and K. Ohkubo. Organic synthetic transformations using organic dyes as photoredox catalysts. *Org. Biomol. Chem.*, 12(32):6059–6071, 2014.

[174] X. Zhao, Y. Hou, L. Liu, and J. Zhao. Triplet Photosensitizers Showing Strong Absorption of Visible Light and Long-Lived Triplet Excited States and Application in Photocatalysis: A Mini Review. *Energy & Fuels*, 35(23):18942–18956, December 2021.

[175] C. K. Prier, D. A. Rankic, and D. W. C. MacMillan. Visible Light Photoredox Catalysis with Transition Metal Complexes: Applications in Organic Synthesis. *Chemical Reviews*, 113(7):5322–5363, July 2013.

[176] N. A. Romero and D. A. Nicewicz. Organic Photoredox Catalysis. *Chemical Reviews*, 116(17):10075–10166, September 2016.

[177] P. Bharmoria, H. Bildirir, and K. Moth-Poulsen. Triplet–triplet annihilation based near infrared to visible molecular photon upconversion. *Chemical Society Reviews*, 49(18):6529–6554, 2020.

[178] W. Wu, H. Guo, W. Wu, S. Ji, and J. Zhao. Organic Triplet Sensitizer Library Derived from a Single Chromophore (BODIPY) with Long-Lived Triplet Excited State for Triplet–Triplet Annihilation Based Upconversion. *The Journal of Organic Chemistry*, 76(17):7056–7064, September 2011.

[179] H. A. Collins, M. Khurana, E. H. Moriyama, A. Mariampillai, E. Dahlstedt, M. Balaz, M. K. Kuimova, M. Drobizhev, V. X. D. Yang, D. Phillips, A. Rebane, B. C. Wilson, and H. L. Anderson. Blood-vessel closure using photosensitizers engineered for two-photon excitation. *Nature Photonics*, 2(7):420–424, July 2008.

[180] R. Prieto-Montero, A. Prieto-Castañeda, R. Sola-Llano, A. R. Agarrabeitia, D. García-Fresnadillo, I. López-Arbeloa, A. Villanueva, M. J. Ortiz, S. De La Moya, and V. Martínez-Martínez. Exploring BODIPY Derivatives as Singlet Oxygen Photosensitizers for PDT. *Photochemistry and Photobiology*, 96(3):458–477, May 2020.

[181] X. Zhang, Z. Wang, Y. Hou, Y. Yan, J. Zhao, and B. Dick. Recent development of heavy-atom-free triplet photosensitizers: molecular structure design, photophysics and application. *Journal of Materials Chemistry C*, 9(36):11944–11973, 2021.

[182] H. Uoyama, K. Goushi, K. Shizu, H. Nomura, and C. Adachi. Highly efficient organic light-emitting diodes from delayed fluorescence. *Nature*, 492(7428):234–238, December 2012.

[183] F. B. Dias, T. J. Penfold, and A. P. Monkman. Photophysics of thermally activated delayed fluorescence molecules. *Methods and Applications in Fluorescence*, 5(1):012001, March 2017.

[184] K. J. Fallon, E. M. Churchill, S. N. Sanders, J. Shee, J. L. Weber, R. Meir, S. Jockusch, D. R. Reichman, M. Y. Sfeir, D. N. Congreve, and L. M. Campos. Molecular Engineering

of Chromophores to Enable Triplet–Triplet Annihilation Upconversion. *Journal of the American Chemical Society*, 142(47):19917–19925, November 2020.

[185] M. Kasha. Collisional Perturbation of Spin-Orbital Coupling and the Mechanism of Fluorescence Quenching. A Visual Demonstration of the Perturbation. *The Journal of Chemical Physics*, 20(1):71–74, January 1952.

[186] A. P. Marchetti and D. R. Kearns. Investigation of Singlet-Triplet Transitions by the Phosphorescence Excitation Method. IV. The Singlet-Triplet Absorption Spectra of Aromatic Hydrocarbons. *Journal of the American Chemical Society*, 89(4):768–777, February 1967.

[187] G. G. Giachino and D. R. Kearns. Nature of the External Heavy-Atom Effect on Radiative and Nonradiative Singlet–Triplet Transitions. *The Journal of Chemical Physics*, 52(6):2964–2974, March 1970.

[188] E. M. Kober and T. J. Meyer. Concerning the absorption spectra of the ions M(bpy)32+ (M = Fe, Ru, Os; bpy = 2,2'-bipyridine). *Inorganic Chemistry*, 21(11):3967–3977, November 1982.

[189] G. B. Shaw, D. J. Styers-Barnett, E. Z. Gannon, J. C. Granger, and J. M. Papanikolas. Interligand Electron Transfer Dynamics in [Os(bpy) $_3$] $^{2+}$: Exploring the Excited State Potential Surfaces with Femtosecond Spectroscopy. *The Journal of Physical Chemistry A*, 108(23):4998–5006, June 2004.

[190] A. B. Maurer and G. J. Meyer. Stark Spectroscopic Evidence that a Spin Change Accompanies Light Absorption in Transition Metal Polypyridyl Complexes. *Journal of the American Chemical Society*, 142(15):6847–6851, April 2020.

[191] N. Sinha and O. S. Wenger. Photoactive Metal-to-Ligand Charge Transfer Excited States in 3d ^{6} Complexes with Cr ^{0} , Mn ^{i} , Fe ^{ii} , and Co ^{iii}. *Journal of the American Chemical Society*, 145(9):4903–4920, March 2023.

[192] G. Malouf and P. C. Ford. Photochemistry of the ruthenium(II) ammine complexes, Ru(NH3)5(py-X)2+. Variation of systemic parameters to modify photochemical reactivities. *Journal of the American Chemical Society*, 99(22):7213–7221, October 1977.

[193] M. A. Filatov, S. Karuthedath, P. M. Polestshuk, H. Savoie, K. J. Flanagan, C. Sy, E. Sitte, M. Telitchko, F. Laquai, R. W. Boyle, and M. O. Senge. Generation of Triplet Excited States via Photoinduced Electron Transfer in *meso* -anthra-BODIPY: Fluorogenic Response toward Singlet Oxygen in Solution and in Vitro. *Journal of the American Chemical Society*, 139(18):6282–6285, May 2017.

[194] M. A. Filatov, S. Karuthedath, P. M. Polestshuk, S. Callaghan, K. J. Flanagan, T. Wiesner, F. Laquai, and M. O. Senge. BODIPY-Pyrene and Perylene Dyads as Heavy-Atom-Free Singlet Oxygen Sensitizers. *ChemPhotoChem*, 2(7):606–615, July 2018.

[195] A. A. Buglak, A. Charisiadis, A. Sheehan, C. J. Kingsbury, M. O. Senge, and M. A. Filatov. Quantitative Structure-Property Relationship Modelling for the Prediction of Singlet Oxygen Generation by Heavy-Atom-Free BODIPY Photosensitizers**. *Chemistry – A European Journal*, 27(38):9934–9947, July 2021.

[196] Z. Wang and J. Zhao. Bodipy–Anthracene Dyads as Triplet Photosensitizers: Effect of Chromophore Orientation on Triplet-State Formation Efficiency and Application in

Triplet–Triplet Annihilation Upconversion. *Organic Letters*, 19(17):4492–4495, September 2017.

[197] M. A. Filatov, S. Karuthedath, P. M. Polestshuk, S. Callaghan, K. J. Flanagan, M. Telitchko, T. Wiesner, F. Laquai, and M. O. Senge. Control of triplet state generation in heavy atom-free BODIPY–anthracene dyads by media polarity and structural factors. *Physical Chemistry Chemical Physics*, 20(12):8016–8031, 2018.

[198] A. M. Brouwer. Standards for photoluminescence quantum yield measurements in solution (IUPAC Technical Report). *Pure and Applied Chemistry*, 83(12):2213–2228, August 2011.

[199] J. V. Caspar and T. J. Meyer. Application of the energy gap law to nonradiative, excited-state decay. *The Journal of Physical Chemistry*, 87(6):952–957, March 1983.

[200] S. De Boer and D. A. Wiersma. Dephasing-induced damping of superradiant emission in J-aggregates. *Chemical Physics Letters*, 165(1):45–53, January 1990.

[201] J. Moll, S. Daehne, J. R. Durrant, and D. A. Wiersma. Optical dynamics of excitons in J aggregates of a carbocyanine dye. *The Journal of Chemical Physics*, 102(16):6362–6370, April 1995.